Sequestration of Arsenic and Molybdenum during the Neutralization of Uranium Mill Wastes: Key Lake Mill, Saskatchewan, Canada

A Thesis

Submitted to the College of Graduate Studies and Research

in Partial Fulfillment of the Requirements

for the Degree of Masters of Science

in the

Department of Geological Sciences

University of Saskatchewan, Saskatoon, SK., Canada

By

Jocelyn S. Bissonnette

PERMISSION TO USE

In presenting this thesis in partial fulfillment of the requirements for a Postgraduate degree from the University of Saskatchewan, I agree that the Libraries of this University may make it freely available for inspection. I further agree that permission for copying of this thesis in any manner, in whole or in part, for scholarly purposes may be granted by the professor or professors who supervised my thesis work or, in their absence, by the Head of the Department or the Dean of the College in which my thesis work was done. It is understood that any copying or publication or use of this thesis or parts thereof for financial gain shall not be allowed without my written permission. It is also understood that due recognition shall be given to me and to the University of Saskatchewan in any scholarly use which may be made of any material in my thesis.

DISCLAIMER

Reference in this thesis to any specific commercial products, process, or service by trade name, trademark, manufacturer, or otherwise, does not constitute or imply its endorsement, recommendation, or favoring by the University of Saskatchewan. The views and opinions of the author expressed herein do not state or reflect those of the University of Saskatchewan, and shall not be used for advertising or product endorsement purposes.

Requests for permission to copy or to make other uses of materials in this thesis in whole or part should be addressed to:

Head of the Department of Geological Sciences
114 Science Place
University of Saskatchewan
Saskatoon, Saskatchewan S7N 5E2 Canada

OR

Dean: College of Graduate Studies and Research
University of Saskatchewan
107 Administration Place
Saskatoon, Saskatchewan S7N 5A2 Canada

ABSTRACT

The As- and Mo- bearing secondary mineral phases formed during the neutralization of uranium mill wastes were studied for a variety of ore blends including current and future ore sources at the Key Lake milling operation, northern Saskatchewan, Canada. A lab-scale plant model was employed to characterize secondary precipitates obtained during the mill waste neutralization process. Three scenarios of ore blends were processed through the lab-scale plant to produce mill waste solutions for neutralization before combination into final tailings. Slurry samples (n = 12) were collected from the secondary precipitates formed during the neutralization of mill wastes (raffinate) by precipitation with $Ca(OH)_2$ (slaked lime) from pH 1.5 to 10.5. Synchrotron based X-ray absorption spectroscopy of mill and lab-scale plant precipitates showed arsenate adsorbed to ferrihydrite was the dominant As mineral phase regardless of pH or sample blend (53-77%), with fractional contributions from ferric arsenates, and adsorption to aluminum phases ($AlOHSO_4$, $As(OH)_3$ and hydrotalcite). Molybdate adsorbed to ferrihydrite was the dominant Mo mineral phase, regardless of pH or sample blend, with fractional contribution decreasing with increasing pH, and minor contributions from calcium molybdate, ferric molybdate and nickel molybdate. These results were used in geochemical modelling to predict the source terms for these mineral phases in tailings facilities. Sequestration of As and Mo in the model showed solubility was controlled by adsorption to both Fe and Al oxide surfaces as well as by direct precipitation with other dissolved constituents (Ni, Ca and SO_4).The models developed pH profiles of mineral phase precipitation to explain the solubility of As, Mo, Fe, Al, Mg and Ni during sequestration from pH 1.5 to 10.5 that were consistent regardless of ore blend used in simulations. Since adsorption of anions to the surface of ferrihydrite has been shown to slow conversion to crystalline forms of Fe oxides (goethite and hematite) and sequestration of arsenate effectively controls As solubility at high pH (pH >10), As-bearing mineral phases are expected to be stable for thousands of years. With adsorption as well as direct precipitation considered, Mo phases though effectively sequestering below pH 8, became unstable and released Mo back into the tailings porewater (pH >10), as predicted by the thermodynamic model. Historical data obtained from as-discharged tailings as well as previously published U mill tailings studies agree with these findings.

ACKNOWLEDGEMENTS

Many deserve acknowledgement of their support during my research and studies at the University of Saskatchewan. This document would not exist without the collaborative effort of the following individuals.

First I must thank my supervisor Dr. Jim Hendry for coaxing a reluctant student into taking on this challenge. Your enthusiasm and support throughout this endeavor was clear. And second, my co-supervisor Dr. Brett Moldovan for providing on-site support at Key Lake operation and a wealth of mill chemistry knowledge in the uranium milling process.

I am extremely grateful to committee member Dr. Joseph Essilfie-Dughan for his mentorship and tutoring through many courses, labs, geochemical models and XAFS analysis. Your knowledge and patience was abundant throughout the entirety of my studies.

I thank the participation of my final committee member Tom Kotzer for support and mineralogy expertise. And I acknowledge assistance received from Fina Nelson, J. Fan, Erin Schmeling, Tom Bonli and Brian Novakowski with lab analysis and instrumentation in Geological Sciences at the University of Saskatchewan.

I am grateful to Arthur Lieu for designing and constructing the model that was used to process the lab-scale plant scenarios. And to students: Kelsey Lutz, Samson Bwaya, Jared Robertson and Matt Cleavely for their assistance running the model.

I must thank my long-suffering husband, Adam for taking on full-time parenting roles and for always encouraging me to continue. As well, my son Oliver and the new baby due to arrive very soon, for providing inspiration after each long day.

I acknowledge Cameco Corporation and NSERC for their financial support. And the synchrotron staff: Dr. Ning Chen, Dr. W. Chen and Dr. Jinru Lin for their assistance with data collection and analysis on the HXMA beamline at the Canadian Light Source, Saskatoon, Canada

TABLE OF CONTENTS

LIST OF FIGURES

LIST OF TABLES

1.0 Introduction

1.1 Overview

Mining and milling activities generate excessive volumes of waste materials, such as waste rock piles and tailings that hold contaminants of concern. Tailings management facilities must be engineered and monitored to ensure that the long-term stability of these contaminants are effectively managed to protect the surrounding environment. Uranium (U) mining and milling accounts for an estimated one billion tons of tailings from 4000 U mines globally (IAEA, 2004). In Canada, U mining operations are required to "demonstrate that they have made adequate provision for the protection of human health and the environment from any releases of contaminants of potential concern" (CSA, 2015). This includes demonstrating the stability of secondary mineral phases that precipitate during the mill effluent treatment process and ultimately contribute to the final tailings. The U milling process leaches untargeted elements of concern (EOC; e.g., arsenic and molybdenum) that occur at elevated concentrations within the ore bodies and must be removed from the raffinate through neutralization of mill waste solutions before combination with other waste streams for deposition in tailings facilities. The long term fate of these EOCs (~10,000 years) within the tailings facility must be determined for the protection of local surface and ground water bodies from potential contamination. Characterizing the precipitates formed during the neutralization of mining wastes contributes to the understanding of the long-term stability of these tailing facilities.

Arsenic (As) and molybdenum (Mo) are naturally occurring elements however, when present at elevated concentrations in groundwater and surface waters, can be hazardous to human and ecological health. Arsenic, a known toxin, has also been identified as a carcinogen due to exposure from contaminated drinking water (U.S. EPA, 1998; Harvey et al., 2002). Molybdenum, though essential for animal nutrition, has also been identified as a potential toxin at elevated concentrations (Barceloux, 1999; Fitzgerald et al., 2008). Because the toxicity and bioavailability of these EOCs (As and Mo) are a function of the chemical form or speciation, it is necessary to identify the As- and Mo-bearing mineral species in the tailings.

The Key Lake U mill is located in the Athabasca Basin in northern Saskatchewan, Canada. This region is one of the most favorable regions in the world for U mining with ore grades up to 21 % (w/w) U_3O_8 (Essilfie-Dughan et al., 2013; Jamieson and Frost, 1997). As a result, Key Lake is one of the largest U producing operations in the world at 8.69 million kg of U_3O_8 (2014 production). Based on available reserves and resources, the Key Lake mill is expected to continue operating until 2035. For the operation to continue the mill must ensure the geochemical performance of tailings meets or exceeds regulatory requirements for environmental protection. Regulations stipulated by the Canadian Nuclear Safety Commission (CNSC) demand certainty on geochemical controls out to 10,000 years for tailings facilities (CNSC, 2012). This necessitates detailed speciation information as well as characterization of mineralogical controls for these potential contaminants. Although the characteristics of the final tailings at Key Lake have been well described through numerous studies on the speciation of EOCs in the Deilmann Tailings Management Facility (DTMF) (Essilfie-Dughan and Hendry, 2011; Essilfie-Dughan et al., 2013, 2012; Gomez et al., 2013; Robertson et al., 2015, 2014; Shaw et al., 2011), the evolution of the secondary mineral phases of EOCs that form during the neutralization of mill waste in the bulk-neutralization (BN) circuit remains poorly understood. Characterizing these BN precipitates will aid in predicting source terms for elements contained in the tailings facility and in understanding the impact of future ore sources on the long-term stability of these precipitates.

1.2 Research Objectives

The goal of this study is to improve our understanding of the geochemical controls on As and Mo in the production of U mill tailings at the Key Lake mill. The objectives are to: i) characterize the As- and Mo-bearing secondary precipitates formed during the neutralization of mill wastes, ii) use these mineral phases as inputs in geochemical models to develop a solubility profile for precipitate formation in the effluent treatment process termed bulk neutralization (BN) with increasing pH, iii) investigate the impact of altering the hydrometallurgical processes and chemical parameters (i.e., ore used) on the removal of As and Mo by precipitation with lime from Fe-, Mg-, and Al-rich raffinate solutions, and iv) predict the long-term stability of the formed secondary mineral phases once combined with other waste streams for deposition in the tailings facility. These objectives were part of a larger, ongoing investigation into the long-term stability of EOCs in the DTMF at Key Lake using a lab-scale plant (LSP) model of the entire mill process, from the grinding circuit through to tailings generation and discharge. The LSP model was also used to investigate the effect

that future ore blends could have on the long-term stability of tailings. The portion of the investigation described in this thesis used a variety of blends from McArthur River and Millennium ore bodies processed through the LSP to characterize the secondary precipitates formed in the BN circuit. This was an important step in understanding the final tailings by characterizing the precipitates formed at each pH stage in the BN circuit and predicting their stability once combined with other waste streams for deposition as final tailings.

To meet the objectives in this study, inductively coupled plasma-mass spectrometry (ICP-MS), X-ray diffraction (XRD), scanning electron microscope (SEM) and X-ray absorption spectroscopy (XAS) were used to characterize the precipitates from the various sections of the BN system to aid in understanding the evolution of the secondary mineral phases of As and Mo with pH during the neutralization process. ICP-MS was used to determine the total chemistry profiles of the elements as a function of pH, in aqueous and solids samples, to provide input values for geochemical modeling. XRD and SEM were used to determine the predominant mineral phases precipitating with respect to pH that may serve to control As and Mo solubility. The element-specific synchrotron-based XAS was used to determine the chemical form (oxidation state and coordination environment) of the EOCs precipitating with respect to set pH in the BN system. Previous studies (Essilfie-Dughan and Hendry, 2011; Essilfie-Dughan et al., 2013, 2011; Moldovan et al., 2003) have shown that X-ray absorption near edges spectra (XANES) portion of XAS can be insightful in identifying oxidation state and chemical form of trace elements (e.g., As and Mo) in complex environmental systems such as U tailings, whereas extended X-ray absorption fine structure (EXAFS) portion can provide quantitative information on the coordination environments (type ligand, coordination number and bond lengths) for these samples. The aqueous chemical profiles over the pH range 1-11 and characterization of associated secondary precipitates were then used as inputs into the geochemical modelling programs Geochemist's Workbench and PHREEQCI to gain a better understanding of the solubility of As- and Mo-bearing secondary precipitates within the Key Lake bulk neutralization (BN) circuit. The characterization of the precipitated mineral phases of As and Mo in the BN system will aid in the understanding of their evolution with pH during the neutralization process and ultimately the long-term stability of these EOCs in the environment.

1.3 Literature Review

1.3.1 Arsenic

Arsenic is common to air, water, soil and all living tissues. It ranks 20th in abundance in the earth's crust, 14th in seawater and 12th in the human body (Eisler, 1988). Arsenic is released naturally to the environment through processes such as weathering, ash from volcanic activity, marine sedimentary rocks, and geothermal and hydrothermal sources (Korte and Fernando, 1991; Smedley and Kinniburgh, 2002; Wang and Mulligan, 2006). The anthropogenic sources of As include non-ferrous metal mining and smelting operations, fossil-fuel processing and combustion, use of pesticides and wood preservatives, disposal of domestic and industrial wastes, and mine tailings and effluents (Cullen and Reimer, 1989; Korte and Fernando, 1991; Smedley and Kinniburgh, 2002; Wang and Mulligan, 2006). The major natural inputs into water systems come from weathering of arsenic bearing minerals, mainly sulfides such as orpiment (As_2S_3) and realgar (As_4S_4), or from emissions of volcanism, wildfires and volatilization. Anthropogenic sources range from mining and smelting to medical uses, agriculture and waste incineration. Arsenic is found associated with iron, aluminum, manganese, (hydro)oxides, clays, sulfates, phosphates and carbonates in soils and sediments (Foster, 2003; Wang and Mulligan, 2006).

Tailings from uranium and gold mines are known for their high arsenic concentrations (Paktunc et al., 2004; Pichler et al., 2001). Arsenic has caused increased anxiety following studies from contaminated water supplies showing high correlation to cancers and arsenicosis in places such as Bangladesh (Harvey et al., 2002; Ngai, 2002). Elevated health risks arise due to its ability to readily dissolve in water, where 0.01 mg/L of dissolved inorganic forms are harmful to humans and content above 60 mg/L may be fatal (Wang and Mulligan, 2006; WHO, 1993). This has compelled the Canadian Environmental Protection Act (CEPA) to list arsenic in Group 1 of the Priority Substances List as natural weathering combined with anthropogenic sources have attributed to elevated concentrations in the Canadian environment (Wang and Mulligan, 2006).

The toxicity of arsenic is well documented. Evidence of carcinogenesis and arsenicosis in humans is clear (U.S. EPA, 1998; Harvey et al., 2002), however, evidence of these effects is scarce among other mammals (Eisler, 1988). Similarly, episodes of poisoning are either acute or subacute, and chronic cases of arsenosis are rarely encountered in non-human species (Eisler, 1988) though acute and chronic toxicity thresholds have been measured in freshwater benthic species (Liber et al.,

2011). Typically, As is shown to biodiminish through marine organisms in water systems, but there is evidence that it can accumulate with increasing trophic levels relative to uncontaminated food webs (Chen and Folt, 2000).

Arsenic exists most frequently in the oxidation states -3, 0, +3, +5, though the formal oxidation state of +2 is also possible in As_4S_4, which features As-As bonds allowing for a total valency of +3. Speciation of As is very important in groundwater systems as solubility, mobility, bioavailability and toxicity depends upon oxidation state (Korte and Fernando, 1991; Masscheleyn, 1991). In most groundwaters, arsenic is found primarily as arsenite (As^{3+}) and arsenate (As^{5+}), with arsenite being generally more toxic and mobile than the oxidized form (Cullen and Reimer, 1989; Korte and Fernando, 1991). Arsenite is reported to be more acutely toxic than arsenate and several hundred times as toxic as methylated arsenicals (CCME, 1999; Goldberg, 2002; Korte and Fernando, 1991; Morrison et al., 1989). Oxidation state and pH also play a role in As mobility. Arsenite shows the highest mobility through aqueous and soil systems, except in high pH soil systems where it is more tightly bound (Goldberg, 2002; Korte and Fernando, 1991). The Eh-pH diagram for the As-O-H system shows the variation of protonation with change in pH for aqueous arsenic species (Figure 1-1).

Both arsenite and arsenate are triprotic weak acids, gaining or losing a proton from pH 2-12 in solution (Korte and Fernando, 1991). The tetrahedral shape of these molecules and lone pair of electrons allow them to behave similarly to phosphates, which are found in the same group of the periodic table. Equilibrium reactions for protonation of arsenite (AsO_3^{3-}) and arsenate (AsO_4^{3-}) molecules in aqueous media are shown in Table 1-1.

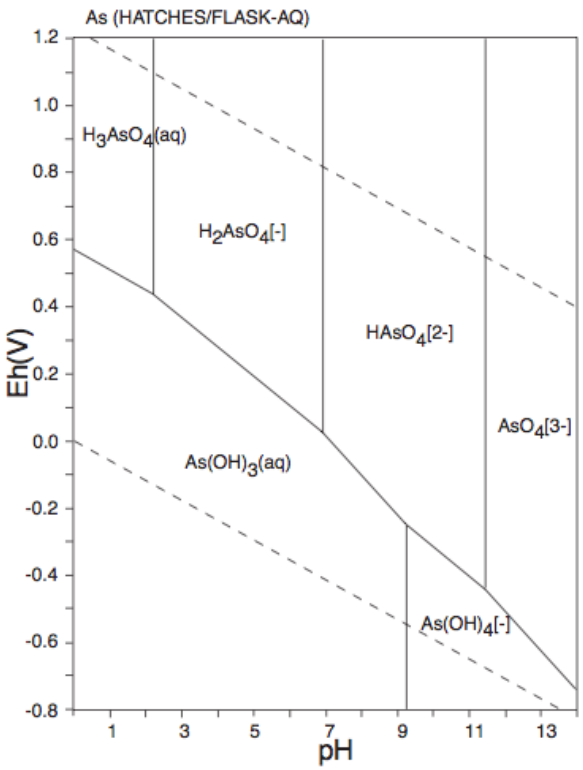

Figure 1-1. Eh-pH diagrams of the system As-O-H for aqueous systems typical of freshwater. $\sum As = 10^{-10}$, 298.15K, 10^5 Pa. (Takeno, 2005)

Table 1-1. Equilibrium reactions for arsenite and arsenate aqueous protonation

Reaction	Log K	Reference
$H^+ + H_2AsO_3^- = H_3AsO_3^0$	9.17 [a], 9.23[b]	(Nordstrom and Archer, 2003)[a]
$H^+ + HAsO_3^{2-} = H_2AsO_3^-$	14.1 [a]	(Wagman et al., 1982)[b]
$H^+ + AsO_3^{3-} = HAsO_3^{2-}$	15.0 [a]	(Whiting, 1992)[c]
$H^+ + H_2AsO_4^- = H_3AsO_4^0$	2.30 [a], 2.24[c]	
$H^+ + HAsO_4^{2-} = H_2AsO_4^-$	6.99 [a]	
$H^+ + AsO_4^{3-} = HAsO_4^{2-}$	11.8 [a]	

This wide range of aqueous speciation creates an extensive capability for both forms of arsenic to react with other ions present in solution. In natural water the dominant control on arsenic is direct precipitation or surface adsorption to hydrous ferric oxides (Fuller et al., 1993). In soils, adsorption to or co-precipitation of arsenate with iron and aluminum oxides and clay minerals is a dominant

control (Goldberg, 2002; Paktunc et al., 2004). Greater concentrations of phosphates, bicarbonates, silicates and organic matter may enhance desorption of arsenic due to competition for adsorption sites (Smedley and Kinniburgh, 2002). Requirements for water treatment of As-rich wells in areas such as Bangladesh and other southeastern Asian countries have motivated research on As removal by aeration of Fe-rich water to precipitate Fe oxyhydroxide and coprecipitate As from solution (Nickson et al., 2000; Pierce and Moore, 1980). As a result, arsenic complexes have been extensively studied in aqueous media. Many of these studies focus on precipitation reactions with magnesium, aluminum, nickel and iron as well as adsorption to hydrous ferric hydroxides and aluminum hydroxides.

Arsenic is known to have an affinity for Fe oxide materials, and has been found to associate with ferrihydrite (HFO) colloids even in the presence of competing ions such as PO_4^{2-}, SiO_4^{4-}, and CO_3^{2-} in soil effluent (Fritzsche et al., 2011). It is commonly associated with iron (hydr)oxide mineral phases in oxic systems by coprecipitation (Ford, 2002; Fritzsche et al., 2011; Fuller et al., 1993) or by forming inner-sphere complexes at surface bonding sites (Manning et al., 1998; Waychunas et al., 1993). This is significant as coprecipitated arsenic has been shown to disrupt the growth of ferrihydrite nuclei in more extended structures such as goethite and hematite by poisoning the surface (Das et al., 2014, 2011; Ford, 2002; Waychunas et al., 1993).

A dominant control on arsenic has been reported as adsorption to ferrihydrite in an inner-sphere bidentate ligand complexed to the iron oxyhydroxyl octahedral corners (Fuller et al., 1993; Moldovan and Hendry, 2005; Moldovan et al., 2008, 2003; Waychunas et al., 1993). Other studies have attributed the control on arsenic to the formation of ferric arsenates such as scorodite ($FeAsO_4 \bullet 2H_2O$) and amorphous ferric arsenate mineral phases ($FeAsO_4$), with only residual aqueous species controlled by adsorption to hydrous ferric oxides (Chen et al., 2009; Jia et al., 2005; Langmuir et al., 2006, 1999; Mahoney et al., 2007).

The sorption of arsenic on hydrous ferric oxides has been extensively studied. The typical sorption behavior of anions is exhibited by arsenate and arsenite, with the variable protonation as a function of pH that decreases sorption at pH values above the zero point charge of the oxide surface (Waychunas et al., 1993; Wilkie and Hering, 1996). By integrating theoretical surface speciation of arsenate with an extended triple-layer model (ETLM) of surface complexation, three reactions forming inner-sphere arsenate surface species were found to be consistent with adsorption envelop,

adsorption isotherm, proton surface titration and proton co-adsoprtion of arsenate on hydrous ferric oxides (ferrihydrite) and aluminum oxide analogues shown in Reactions 1.1-1.3 (Fukushi and Sverjensky, 2007).

$$2 >SOH + H_3AsO_4^0 = (>SO)_2AsO_2^- + H^+ + 2H_2O \quad (1.1)$$

$$2 >SOH + H_3AsO_4^0 = (>SO)_2AsOOH + 2H_2O \quad (1.2)$$

$$>SOH + H_3AsO_4^0 = >SOAsO_2^{2-} + 2H^+ + H_2O \quad (1.3)$$

Arsenate is generally more effectively removed by ferrihydrite than arsenite, though more needs to be considered for these reactions such as Fe/As ratios, pH and the presence of individual species versus mixtures (Twidwell et al., 2005). As discussed earlier, the presence of associated ions such as phosphate, sulfate, carbonate, and dissolved organic species must also be considered as their interaction with the surface may influence arsenic removal and the relative long-term stability.

1.3.2 Molybdenum

Molybdenum is a naturally occurring trace element with an average abundance of 1.5 ppm in the earth's crust (Das et al., 2007; Essilfie-Dughan et al., 2011). It is a refractory metallic element used primarily as an alloying agent in steel, cast iron and super-alloys to enhance strength and resistance for the manufacture of aircraft and weapons, electrode materials and as a catalyst in petroleum refining. The many properties exhibited by molybdenum are also utilized in chemical applications such as lubricants, pigments and catalyst (USGS, 2013). Activities contributing to Mo contamination in biota include the combustion of fossil fuels, smelting, and mining and milling (e.g. steel, copper and uranium) (Heinrich et al., 2010; Morris and Fitzgerald, 2008).

Molybdenum can exist in a wide range of oxidation states, from -2 to +6, with the most common species in the form of +4, +5 and +6 (Barceloux, 1999). Pure metallic forms are not found in geological deposits, but various mineral forms exist such as molybdenite (MoS_2) and jordisite (amorphous MoS_2) often associated with uranium and arsenic (Barceloux, 1999). Though it is an essential micronutrient to living organism, it can be toxic at high concentrations, causing high uric acid levels in humans (Mendel, 2005; Vyskocil and Viau, 1999). The toxicity to various mammals, fish and amphibians is well documented (Das et al., 2007; Eisler, 1989; U.S. Department of the Interior, 1998). In aquatic systems, fish and amphibians measured a toxicity threshold of 0.12 mg/L

and 0.96 mg/L respectively (U.S. Department of the Interior, 1998). Aquatic organisms show great resistance to Mo, as algae and invertebrates have recorded high bioconcentration without apparent harm; however, there is insufficient evidence to postulate the hazard potential to consumers of aquatic organisms which have accumulated Mo (Eisler, 1989). Pore water concentrations have been well correlated to sediment toxicity for freshwater benthic organisms, with lowest-observed-effect concentrations (LOECs) > 1488 mg/L for some species (Liber et al., 2011).

Previous studies at the Key Lake mill found that the predominate speciation in the mill appeared as the oxyanion molybdate (MoO_4^{2-}), with molybdenum existing in the highest valence state (Mo^{6+}) throughout the mill process (Lieu et al., 2010). Core samples from the Key Lake DTMF analyzed for the Mo K-edge x-ray adsorption near edge spectroscopy (XANES) indicated Mo remained as molybdate in the DTMF after deposition as tailings (Essilfie-Dughan et al., 2011). The pH dependence of species stability is shown in the Eh-pH diagram for aqueous molybdenum species (Figure 1-2).

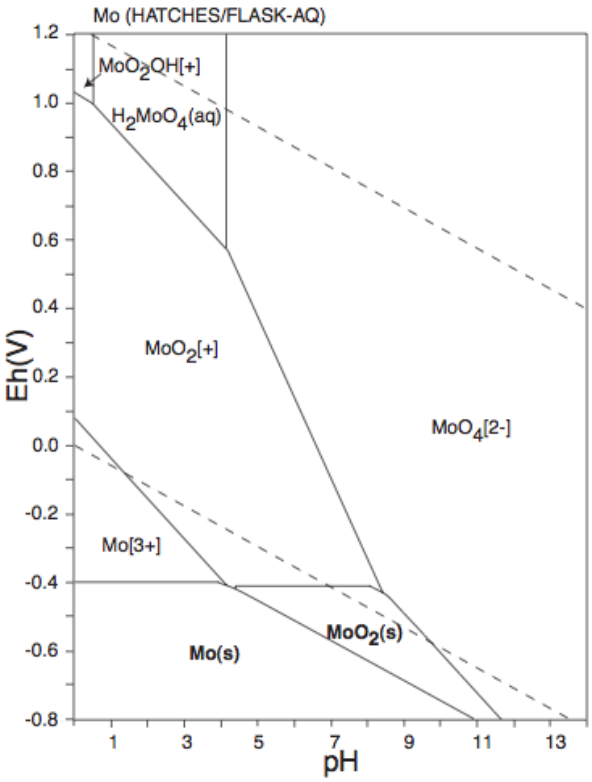

Figure 1-2. Eh-pH diagrams of the system Mo-O-H for aqueous systems typical of freshwater. $\sum Mo = 10^{-10}$, 298.15K, 10^5 Pa. (Takeno, 2005)

Molybdenum species have been found in bench-scale experiments to be effectively removed from the mill wastes by reaction with ferric iron and lime ($Ca(OH)_2$) at pH 3.5 and forming iron molybdate and calcium molybdate precipitates (Lieu et al., 2010). When these precipitates are collected in a low pH range thickener (pH 3.5-4.2) and then neutralized to pH 6-7, the precipitates are encapsulated with gypsum ($CaSO_4 \bullet 2H_2O$) to increase stability. Refer to Table 1-2 for the relevant equations to describe these reactions.

Table 1-2. Precipitation Reactions for Molybdate in the Key Lake Circuit

Reaction	**Reference**
$MoO_4^{2-} + 2H^+ \rightarrow H_2MoO_4$	(Lieu et al., 2010)
$3H_2MoO_4 + 2Fe(OH)_3 \rightarrow Fe_2(MoO_4)_3 + 6H_2O$	
$H_2MoO_4 + Ca(OH)_2 \rightarrow CaMoO_4 + 2H_2O$	

Molybdate species found in core samples from the DTMF exist as $NiMoO_4$ and $CaMoO_4$ as well as molybdate adsorbed onto ferrihydrite (Essilfie-Dughan et al., 2011). The dominant species were distinguished in the DTMF to vary according the Ni/Mo and Fe/Mo ratio found at each sample depth. Subsequently, tailings at depths with higher Ni/Mo ratios were dominated by $NiMoO_4$, and those found at depths with higher Fe/Mo were dominated by molybdate adsorbed to ferrihydrite. Geochemical aging studies completed at Key Lake indicated that the molybdate precipitates formed from the reactions in Table 1-2 are thermodynamically stable in the mill tailings (Lieu et al., 2010).

1.3.3 Hydrous Ferric (Hydr)oxides

Evidence of adsorption of the EOCs highlighted in this study (As and Mo) to hydrous ferric (hydr)oxides in uranium mill tailings demonstrates the importance of Fe mineral phases on the control of EOCs in the secondary precipitates formed during the Key Lake BN process. Hydrous ferric oxides (ferrihydrite) are important sorbants in aquatic systems due to their wide occurrence, tendency to nucleate and grow on the surface of other phases, important redox capabilities, and relatively high reactivity (Waychunas et al., 2005). These properties make them useful for immobilizing contaminants in groundwater systems, wastewater treatments, and drinking water

due to their high surface area and strong affinity for ions, depending upon solution composition and pH (Stipp et al., 2002; Wilkie and Hering, 1996).

The structure of ferrihydrite is critical to determining the uptake of contaminants and colloidal stability. Often characterized as an amorphous material due to the large surface area, ferrihydrite is more accurately describes as a nano-crystalline or colloidal material (Fritzsche et al., 2011; Waychunas et al., 2005). These materials are named according to their structure in X-ray diffraction as either 2-line or 6-line ferrihydrite, relating to the number of broad peaks present in the spectra. Thus the two broad peaks found for ferrihydrite in classical XRD patterns lead to the term of 2-line ferrihydrite (2-line Fh). When formed at temperatures less than 125 ^{0}C by rapid hydrolysis under oxidizing conditions, it exists as poorly crystalline 2-line Fh (Dzombak and Morel, 1990; Moldovan and Hendry, 2005; Pichler et al., 2001). Surface complexation models have successfully described the adsorption of both cations and anions, with a wide range of adsorption constants derived for the two-layer model (Dzombak and Morel, 1990; Wilkie and Hering, 1996). The amphoteric nature of ferrihydrite allows the acid-base chemistry of the surface and adsorption of anions to be described with the adsorption site of 0.2 mole sites/mole Fe, and for cations an adsorption of 0.005 mole sites/mole Fe (Dzombak and Morel, 1990). Thus, an understanding how dissolved species influence the structure of ferrihydrite precipitates is essential to characterizing the mineral species of EOCs that form during neutralization.

1.3.4 Amorphous Aluminum hydroxides

Recently, adsorption to amorphous aluminum hydroxides and hydrotalcite-like layered double hydroxides (HT-LDHs) has been considered with respect to the uptake of anions (AsO_4^{2-} and MoO_4^{2-}) in solution (Arai et al., 2001; Goldberg, 2002; Paikaray et al., 2013) and possible applications to U mill wastes (Gomez et al., 2013; Robertson et al., 2015). Amorphous aluminum hydroxide precipitates during the neutralization of Al-bearing acidic solutions in the pH range of 5-9 with potential adsorption of arsenates beginning at pH 5 and maximum loading reported from pH 7-8 (Arai et al., 2001; Goldberg, 2002; Moldovan and Hendry, 2005). Aluminum oxides such as gibbsite may play a role in EOC retention as the aluminol functional groups serve as dynamic sinks for various oxyanions and correlate with As^{+5} retention in waters and soils (Arai et al., 2001).

Absorption envelope studies have observed that As^{+5} adsorption decreases with increasing pH on amorphous aluminum hydroxides and is sensitive to ionic changes at pH 3.5-10 (Arai et al., 2001).

XAS analysis indicates inner-sphere bidentate-binuclear complexes are predominantly formed for the As^{+5} oxyanion, similar to that for ferrihydrite (Arai et al., 2001; Kappen and Webb, 2013; Moldovan and Hendry, 2005; Moldovan et al., 2003). Direct precipitation of anions (AsO_4^{2-}) as mineral phases may also occur in addition to adsorption, as in the formation of scorodite ($FeAsO_4 \bullet 2H_2O$). In the case of scorodite-mansfieldite solid solution compounds ($Fe_{1-x}Al_xAsO_4 \bullet 2H_2O$), an increase in Al fraction in the scorodite structure may cause destabilization and subsequent release of As (Le Berre et al., 2007).

Mg/Al- and Mg/Fe-hydrotalcites may also serve as important sorbants in neutralized acidic wastes. Characterization of U mill precipitates has discovered these precipitates in the high pH (>pH 8) region of the U mill circuit and found association of As and Mo with the surfaces (Gomez et al., 2013; Robertson et al., 2015, 2014). Arsenates have a higher affinity for hydrotalcites (HT-LDHs) than molybdates, with greater uptake efficiencies reported for Fe containing HT-LDHs from pH 6 to 8 (Paikaray et al., 2013). Thus, these precipitates would have the greatest impact on contaminants at high pH values (pH 6-10).

1.4 The Uranium Milling Process

1.4.1 The Key Lake mill

The Key Lake operation is located in northern Saskatchewan, Canada (57°11'N, 105°34'W) where open-pit mining occurred at the site from 1982 to 1997. The mill began production in 1983, using ore from the Gaertner and Deilmann pits until stockpiles were consumed in 1999 (Janz et al., 2014). Deposition of tailings in the Deilmann tailings management facility (DTMF) has occurred since 1996, after the mined-out pit was converted into an in-pit tailings facility (Bharadwaj and Moldovan, 2005). Since 1999, the Key Lake mill has processed ore from the McArthur River deposit, located approximately 80 km north of the facility (Bharadwaj and Moldovan, 2005). These U ores are some of the highest grades found in the world. Details of the site characteristics of the DTMF have been previously published (Shaw et al., 2011).

Currently, high grade ore originating from the McArthur River mining operation (14-18% U_3O_8) is blended with various low-grade U ore (<0.5% U_3O_8) present at the Key Lake site to achieve the desired leach feed grade (4% U_3O_8). These ground ore sources are mixed with water in the Key Lake mill to produce a slurry of approximately 50% solids, 45-50% which pass a sieve of 75um

grain size. The resulting 4% U_3O_8 slurry is leached using 94% sulfuric acid (H_2SO_4), 92% oxygen to maintain strong oxidizing conditions (Eh maintained > 600mV) and steam (reaction temperature maintained at 60ºC) to maintain strong oxidizing conditions and solubilize the targeted U from the host ore. This acidic leachate reports to the counter current decantation process, where the U-bearing solution is separated from the leach residues. The U-bearing leach solution containing other untargeted impurities such as As and Mo reports to solvent extraction where tertiary amines are used to purify and concentrate the U in solution. The resulting uranium-rich solution is further purified in a precipitation circuit and then calcined for the U_3O_8 final product. The barren waste stream from the solvent extraction process (raffinate) that contains non-uranium dissolved elements such as arsenic and molybdenum reports to the bulk neutralization (BN) process where secondary mineral phases are formed before combination with leached residues in the final tailings (

Figure 1-3).

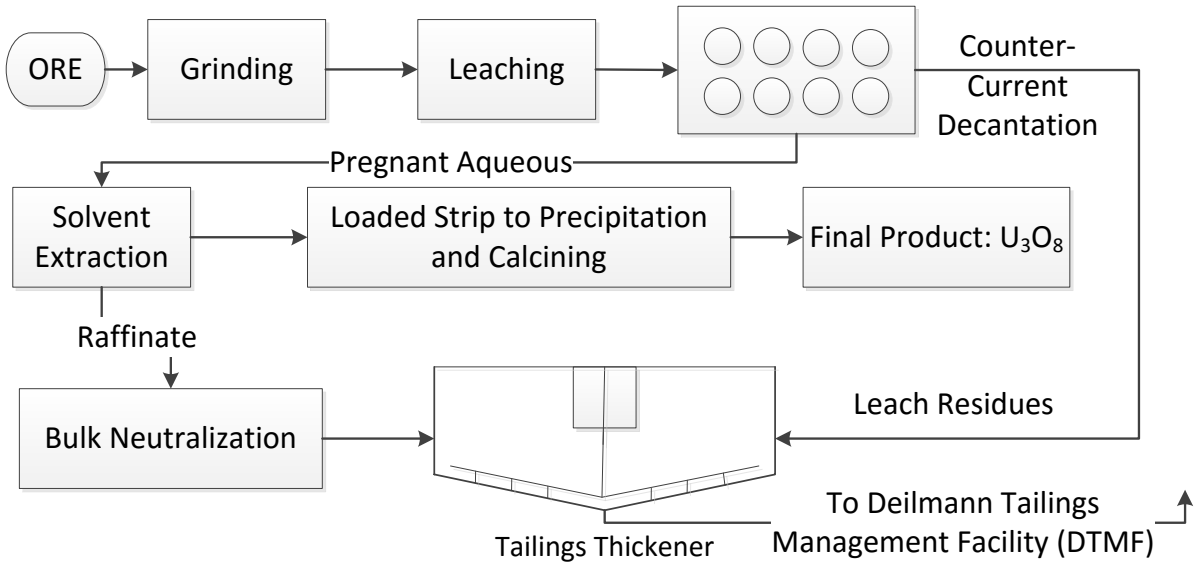

Figure 1-3. High Level Overview of the Key Lake milling process.

1.4.2 The Key Lake Bulk Neutralization (BN) process

The BN circuit at Key Lake operation is designed to consistently produce clean mill effluent which meets regulatory requirements and produce a geochemically stable precipitate which exhibits long-term stability within the tailings facility. The BN circuit treats multiple waste streams including

raffinate and contaminated water (reservoir 1 and reservoir 2) to produce: i) treated effluent for discharge to downstream receptors and ii) secondary precipitates that make up a portion of the total mill tailings for deposition in the DTMF. The BN circuit serves to control the environmental impact of EOCs by neutralizing the waste feed solutions with $Ca(OH)_2$ at incremental pH values (pH 1.5, 3.5-4.2, 6.5, 9.2). The major impurities in the raffinate include calcium (Ca), magnesium (Mg), sodium (Na), sulphate (SO_4) and chloride (Cl); while elements of concern include: selenium (Se), molybdenum (Mo), arsenic (As), nickel (Ni), uranium (U), radium (Ra), ammonium (NH_4^+) and organic components (Lieu, et al., 2010). The formation of secondary As-, Mo-, Al- and Fe-bearing mineral phases serve to control EOC aqueous concentrations at very low levels in the tailings pore water.

The Key Lake BN circuit uses a series of four neutralization tanks (Pachucas) and two thickeners to advance the neutralized solution and precipitates via gravity flow (Figure 1-4).

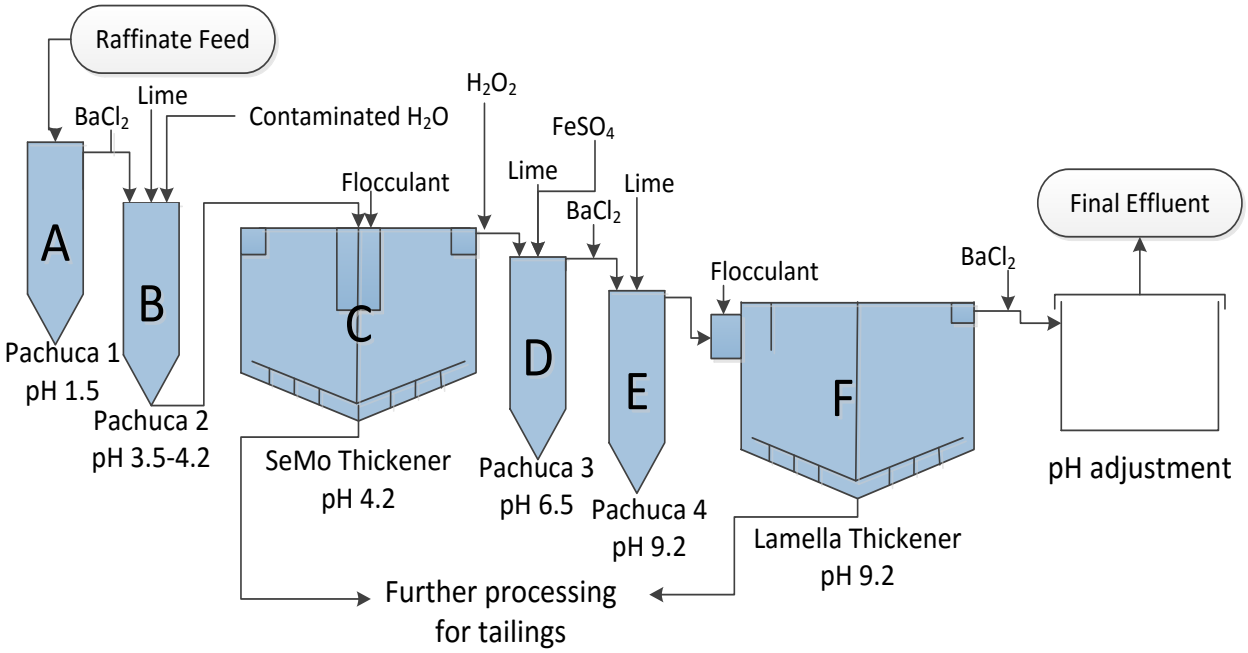

Figure 1-4. Process flow diagram of Key Lake Bulk Neutralization circuit. A = Pachuca 1 (pH 1.4) B = Pachuca 2 (pH 3.5-4.2) C = SeMo Thickener (pH 3.5-4.2) D = Pachuca 3 (pH 6.5) E = Pachuca 4 (pH 9.2) F = Lamella Thickener (pH 9.2).

The raffinate feed solution is continuously pumped (75 m^3/hr) to Pachuca 1 at pH 1-1.5 and the overflow mixed with other contaminated water streams (225 m^3/hr) in Pachuca 2. Lime ($Ca(OH)_2$)

addition begins to the target pH range of 3.5 to 4.2, along with $BaCl_2$ in Pachuca 2. Pachuca 2 slurry is pumped to the SeMo thickener where secondary mineral phase precipitation occurs until the slurry thickens to 30% solids with addition of flocculant. The thickener supernatant overflows into Pachuca 3 where additional $Ca(OH)_2$ increases the pH to 6.5, which again overflow to Pachuca 4 at a target pH of 9.2. The trace-metal precipitates found in the high pH range are in the form of hydroxides (Ni, Cu, Pb and Zn) or co-precipitation with ferrihydrite (As) (Lieu et al., 2010). These are captured when the overflow of Pachuca 4 enters the Lamella thickener at pH 9.2. The overflow from the Lamella thickener reports to further pH adjustment in three-stage reactor tanks with H_2SO_4 and clarification in the radium-removal thickener to achieve the final regulatory limits before release to the environment as effluent. The underflows from both the SeMo and Lamella thickeners are combined with solids from the leach residues of counter-current decantation in the final tailings tank, then thickened and adjusted to the final pH target of 10.5 before deposition into the DTMF. Mineralogical and geochemical characterization of solids from each thickener is crucial to understanding the evolution of the mineral phases observed in the DTMF.

1.4.3 The lab-scale plant (LSP) model

The bulk neutralization circuit of the LSP model was designed to processes the raffinate solution generated by three scenarios of leached ore blends through a model 1:310,000 the size of the Key Lake mill (Figure 1-5).

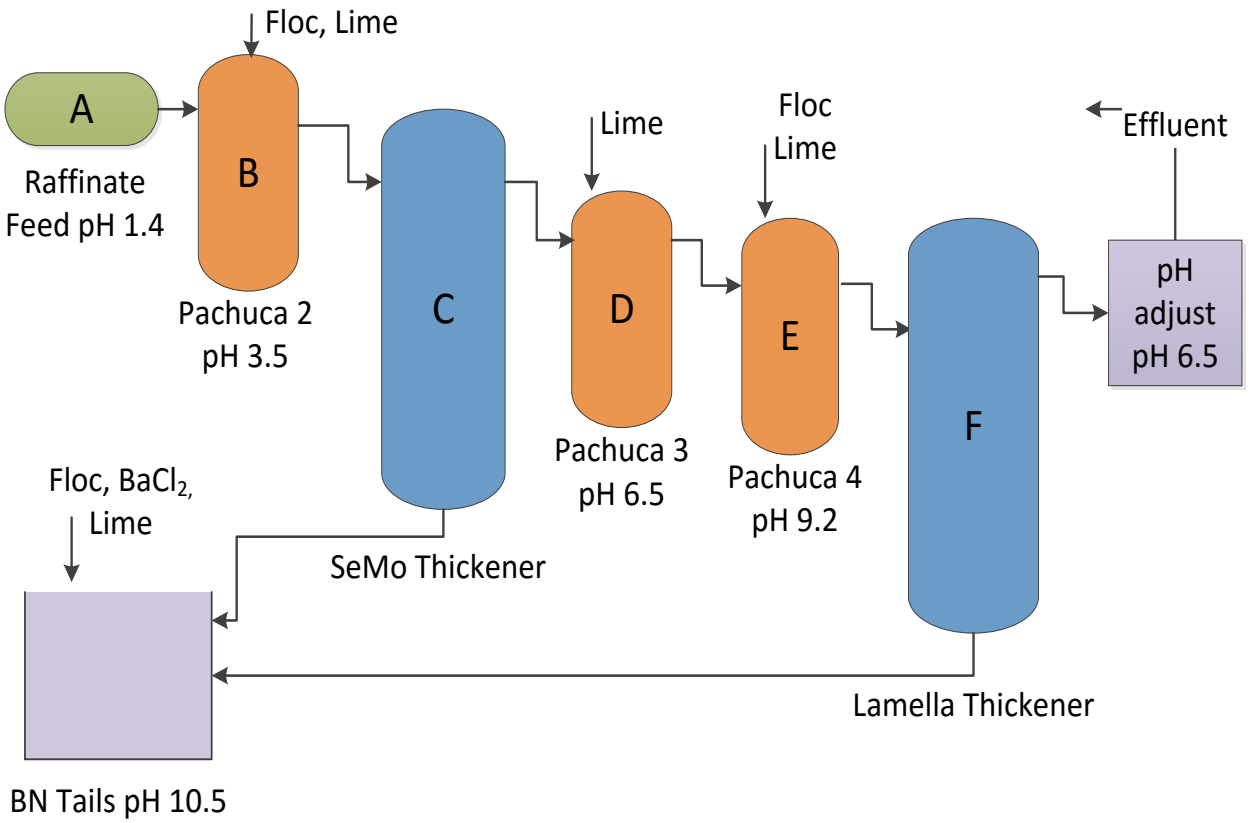

Figure 1-5. Flow diagram of LSP model of the Key Lake Bulk Neutralization Circuit. A = Pachuca 1 (pH 1.4) B = Pachuca 2 (pH 3.5) C = SeMo Thickener (pH 3.5-4.2) D = Pachuca 3 (pH 6.5) E = Pachuca 4 (pH 9.2) F = Lamella Thickener (pH 9.2)

Pumps were used to feed the raffinate, $BaCl_2$ and $Ca(OH)_2$ solutions during neutralization, while pH values were monitored to ensure set points were reached at each Pachuca. Pachuca 2 was left in batch mode for 1.2 hours to the achieve pH set point, and the process was allowed to gravity flow into each reaction vessel at 14.5 mL/min for a total retention time of approximately 31 hours. Samples were collected at each thickener (C and F in Figure 1-5) and the aqueous and solids phases were separated and preserved for analysis.

Proper identification of mineral phases of As and Mo in the precipitates formed in this LSP model will aide in determining the source chemistry for potential contaminants that exist in the discharged tailings. Because the long-term migration of metals and metalloids from tailing facilities to adjacent groundwater systems is of concern, accurately identified mineral phases will ultimately assist in mill design and reduce the impact of tailings facilities on groundwater systems after decommissioning.

1.5 References

Arai, Y., Elzinga, E.J., Sparks, D.L., 2001. X-ray absorption spectroscopic investigation of arsenite and arsenate adsorption at the aluminum oxide-water interface. J. Colloid Interface Sci. 235, 80–88. doi:10.1006/jcis.2000.7249

Barceloux, D.G., 1999. Molybdenum 37, 231–237.

Bharadwaj, B., Moldovan, B.J., 2005. Cameco Corporation - the Key Lake uranium mill: current status and vision for the future, in: International Atomic Energy Agency (IAEA), Proceedings of an International Symposium: Uranium Production and Raw Materials for the Nuclear Fuel Cycle - Supply and Demand, Economics, the Environment and Energy Security. pp. 205–212.

CCME, 1999. Canadian Sediment Quality Guidelines for the Protection of Aquatic Life - Arsenic. In: Canadian environmental quality guidelines, Canadian Council of Ministers of the Environment. Winnipeg.

Chen, C.Y., Folt, C.L., 2000. Bioaccumulation and diminution of arsenic and lead in a freshwater foodweb: RN - Environ. Sci. Technol., v. 34, p. 3878-3884. Environ. Sci. Technol. 34, 3878–3884.

Chen, N., Jiang, D.T., Cutler, J., Kotzer, T., Jia, Y.F., Demopoulos, G.P., Rowson, J.W., 2009. Structural characterization of poorly-crystalline scorodite, iron(III)–arsenate co-precipitates and uranium mill neutralized raffinate solids using X-ray absorption fine structure spectroscopy. Geochim. Cosmochim. Acta 73, 3260–3276. doi:10.1016/j.gca.2009.02.019

CNSC, 2012. Management of uranium mine waste rock and mill tailings, in: Regulatory Document RD/GD-370, Canadian Nuclear Safety Commission, Ottawa. doi:Regulatory Document RD/GD-370

CSA, 2015. CSA Group Standard N288.7-15: Groundwater protection programs at Class I nuclear facilities and uranium mines and mills. Toronto: Canada.

Cullen, W.R., Reimer, K.J., 1989. Arsenic speciation in the environment. Chem. Rev. 89, 713–764. doi:10.1021/cr00094a002

Das, A.K., Chakraborty, R., Cervera, M.L., de la Guardia, M., 2007. A review on molybdenum determination in solid geological samples. Talanta 71, 987–1000. doi:10.1016/j.talanta.2006.07.017

Das, S., Essilfie-Dughan, J., Hendry, M.J., 2014. Arsenate partitioning from ferrihydrite to hematite : Spectroscopic evidence. Am. Mineral. 99, 749–754.

Das, S., Hendry, M.J., Essilfie-Dughan, J., 2011. Transformation of two-line ferrihydrite to goethite and hematite as a function of pH and temperature. Environ. Sci. Technol. 45, 268–275. doi:10.1021/es101903y

Dzombak, D.A., Morel, F.M.., 1990. Surface Complexation Modeling: Hydrous Ferric Oxide. Wiley-Interscience, New York.

Eisler, R., 1989. Molybdenum hazards to fish, wildlife, and invertebrates: a synoptic review. U.S. Fish Wildl. Serv. Biolocial Reprod. 85, 61.

Eisler, R., 1988. Arsenic hazards to fish, wildlife, and invertebrates: A synoptic review, Contaminant Hazard Reviews. Report No.12: U.S. Fish and Wildlife Service.

Essilfie-Dughan, J., Hendry, M.J., 2011. Speciation of Selenium in Uranium Mine Tailings using XAS and EMPA: A Fact Sheet Report for Cameco Corporation. Cameco Corporation, Saskatoon.

Essilfie-Dughan, J., Hendry, M.J., Warner, J., Kotzer, T., 2013. Arsenic and iron speciation in uranium mine tailings using X-ray absorption spectroscopy. Appl. Geochemistry 28, 11–18. doi:10.1016/j.apgeochem.2012.10.022

Essilfie-Dughan, J., Hendry, M.J., Warner, J., Kotzer, T., 2012. Microscale mineralogical characterization of As, Fe, and Ni in uranium mine tailings. Geochim. Cosmochim. Acta 96, 336–352. doi:10.1016/j.gca.2012.08.005

Essilfie-Dughan, J., Pickering, I.J., Hendry, M.J., George, G.N., Kotzer, T., 2011. Molybdenum speciation in uranium mine tailings using X-ray absorption spectroscopy. Environ. Sci. Technol. 45, 455–60. doi:10.1021/es102954b

Fitzgerald, D., Ph, D., Nicholson, R., Regoli, L., 2008. Environmental management criteria for molybdenum and selenium: a review relavant to the mining industry, in: British Columbia Mine Reclamation Symposium.

Ford, R.G., 2002. Rates of hydrous ferric oxide crystallization and the influence on coprecipitated arsenate. Environ. Sci. Technol. 36, 2459–63.

Foster, A., 2003. Spectroscopic investigations of arsenic species in solid phases, in: Welch, A., Stollenwer, K. (Eds.), Arsenic in Groundwater: Geochemistry and Occurance. Kluwer Academic Publishers, Boston, pp. 27–65.

Fritzsche, A., Rennert, T., Totsche, K.U., 2011. Arsenic strongly associates with ferrihydrite colloids formed in a soil effluent. Environ. Pollut. 159, 1398–1405. doi:10.1016/j.envpol.2011.01.001

Fukushi, K., Sverjensky, D. a., 2007. A predictive model (ETLM) for arsenate adsorption and surface speciation on oxides consistent with spectroscopic and theoretical molecular evidence. Geochim. Cosmochim. Acta 71, 3717–3745. doi:10.1016/j.gca.2007.05.018

Fuller, C.C., Davis, J.A., Waychunas, G.A., 1993. Surface chemistry of ferrihydrite : Part 2. Kinetics of arsenate adsorption and coprecipitation. Geochim. Cosmochim. Acta 58(10), 2271-2282.

Goldberg, S., 2002. Competitive adsorption of arsenate and arsenite on oxides and clay minerals. Soil Sci. Soc. Am. J. 66, 413. doi:10.2136/sssaj2002.0413

Gomez, M.A., Hendry, M.J., Koshinsky, J., Essilfie-Dughan, J., Paikaray, S., Chen, J., 2013. Mineralogical controls on aluminum and magnesium in uranium mill tailings: Key Lake, Saskatchewan, Canada. Environ. Sci. Technol. 47, 7883–7891. doi:10.1021/es400658f

Harvey, C.F., Swartz, C.H., Badruzzaman, A.B.M., Keon-Blute, N., Yu, W., Ali, M.A., Jay, J., Beckie, R., Niedan, V., Brabander, D., Oates, P.M., Ashfaque, K.N., Islam, S., Hemond, H.F., Ahmed, M.F.,

2002. Arsenic mobility and groundwater extraction in Bangladesh. Science 298, 1602–1606. doi:10.1126/science.1076978

Heinrich, G., Kyser, K., Chipley, D., Lam, E., 2010. The determination of selenium and molybdenum distribution in uranium ore and mill solids, in: Lam, E.K., Rowson, J.W., Ozberk, E. (Eds.), Proceedings of the 3rd International Conference on Uranium (Uranium 2010). Canadian Institute of Mining, Metallurgy and Petroleum, Westmont, p. 609.

IAEA, 2004. The Long Term Stabilization of Uranium Mill Tailings: IAEA TECDOC-1403. Vienna.

Jamieson, B.W., Frost, S.E., 1997. The McArthur River project: high grad uranium mining, in: 22nd Annual International Symposium of the Uranium Institute. The Uranium Institute, London, England.

Janz, D.M., Liber, K., Pickering, I.J., Wiramanaden, C.I., Weech, S. a, Gallego-Gallegos, M., Driessnack, M.K., Franz, E.D., Goertzen, M.M., Phibbs, J., Tse, J.J., Himbeault, K.T., Robertson, E.L., Burnett-Seidel, C., England, K., Gent, A., 2014. Integrative assessment of selenium speciation, biogeochemistry, and distribution in a northern coldwater ecosystem. Integr. Environ. Assess. Manag. 10, 543–54. doi:10.1002/ieam.1560

Jia, Y., Demopolous, G.P., Chen, N., Cutler, J., 2005. Coprecipitation of As(V) with Fe(III) in sulfate media: solubility and speciation of arsenic, in: Reddy, R.G., Ramachandran, V.S. (Eds.), Arsenic Metallurgy. 2005 TMS Annual Meeting, San Fransisco, pp. 137–148.

Kappen, P., Webb, J., 2013. An EXAFS study of arsenic bonding on amorphous aluminium hydroxide. Appl. Geochemistry 31, 79–83. doi:10.1016/j.apgeochem.2012.12.007

Korte, N.E., Fernando, Q., 1991. A review of arsenic (III) in groundwater. Crit. Rev. Environ. Control 21, 1–39.

Langmuir, D., Mahoney, J., MacDonald, A., Rowson, J., 1999. Predicting arsenic concentrations in the porewaters of buried uranium mill tailings. Geochim. Cosmochim. Acta 63, 3379–3394. doi:10.1016/S0016-7037(99)00259-8

Langmuir, D., Mahoney, J., Rowson, J., 2006. Solubility products of amorphous ferric arsenate and crystalline scorodite ($FeAsO_4 \cdot 2H_2O$) and their application to arsenic behavior in buried mine tailings. Geochim. Cosmochim. Acta 70, 2942–2956. doi:10.1016/j.gca.2006.03.006

Le Berre, J.F., Cheng, T.C., Gauvin, R., Demopoulos, G.P., 2007. Hydrothermal synthesis and stability evaluation of iron (III)-aluminum (III) arsenate solid solutions. Metall. Mater. Trans. B Process Metall. Mater. Process. Sci. 38, 159–166. doi:10.1007/s11663-007-9032-7

Liber, K., Doig, L.E., White-Sobey, S.L., 2011. Toxicity of uranium, molybdenum, nickel, and arsenic to Hyalella azteca and Chironomus dilutus in water-only and spiked-sediment toxicity tests. Ecotoxicol. Environ. Saf. 74, 1171–1179. doi:10.1016/j.ecoenv.2011.02.014

Lieu, A., Zheng, J., Moldovan, B., Ko, K., Jarvi, J., Saruchera, T., Bergbusch, P., Paulsen, K., Tremblay, M., Bharadwaj, B., 2010. Selenium and molybdenum removal from contaminated mill process effluent: Cameco Key Lake Operation, in: Lam, E.K., Rowson, J.W., Ozberk, E. (Eds.), Proceedings

of the 3rd International Conference on Uranium (Uranium 2010). Canadian Institute of Mining, Metallurgy and Petroleum, Westmont, pp. 749–759.

Mahoney, J., Slaughter, M., Langmuir, D., Rowson, J., 2007. Control of As and Ni releases from a uranium mill tailings neutralization circuit: Solution chemistry, mineralogy and geochemical modeling of laboratory study results. Appl. Geochemistry 22, 2758–2776. doi:10.1016/j.apgeochem.2007.06.021

Manning, B. a., Fendorf, S.E., Goldberg, S., 1998. Surface Structures and Stability of Arsenic(III) on Goethite: Spectroscopic Evidence for Inner-Sphere Complexes. Environ. Sci. Technol. 32, 2383–2388. doi:10.1021/es9802201

Masscheleyn, P.H., Delaune, R.D., Patrick W.H.Jr., 1991. Effect of redox potential and pH on arsenic speciation and solubility in a contaminated soil. Environ. Sci. Technol. 25(8) 1414–1419.

Mendel, R.R., 2005. Molybdenum: biological activity and metabolism. Dalt. Trans. 21, 3404–3409.

Moldovan, B.I., Hendry, M.J., 2005. Characterizing and quantilying controls on arsenic solubility over a pH range of 1-11 in a uranium mill-scale experiment. Environ. Sci. Technol. 39, 4913–4920.

Moldovan, B.J., Jiang, D.T., Hendry, M.J., 2003. Mineralogical characterization of arsenic in uranium mine tailings precipitated from iron-rich hydrometallurgical solutions. Environ. Sci. Technol. 37, 873–879.

Moldovan, B.J., Hendry, M.J., Harrington, G.A., 2008. The arsenic source term for an in-pit uranium mine tailings facility and its long-term impact on the regional groundwater. Appl. Geochemistry 23, 1437–1450. doi:10.1016/j.apgeochem.2007.12.037

Morris, N., Fitzgerald, D., 2008. A Review of Environmental Management Criteria for Selenium and Molybdenum, MEND Report 10.1.1. Brampton.

Morrison, G.M.P., Batley, G.E., Florence, T.M., 1989. Metal speciation and toxicity. Chem. Britian 25, 791–794.

Ngai, T.K.K., 2002. Arsenic Speciation and Evaluation of an Adsorption Media in Rupandehi and Nawalparasi Districcts of Nepal. Massachusetts Institute of Technology.

Nickson, R.T., McArthur, J.M., Ravenscroft, P., Burgess, W.G., Ahmed, K.M., 2000. Mechanism of arsenic release to groundwater, Bangladesh and West Bengal. Appl. Geochemistry 15, 403–413. doi:10.1016/S0883-2927(99)00086-4

Nordstrom, D.K., Archer, D.G., 2003. Arsenic thermodynamic data and environmental geochemistry, in: Arsenic in Groundwater: Geochemistry and Occurance. Kluwer Academic Publishers, Dordrecht, pp. 1–25.

Paikaray, S., Hendry, M.J., Essilfie-Dughan, J., 2013. Controls on arsenate, molybdate, and selenate uptake by hydrotalcite-like layered double hydroxides. Chem. Geol. 345, 130–138. doi:10.1016/j.chemgeo.2013.02.015

Paktunc, D., Foster, A., Heald, S., Laflamme, G., 2004. Speciation and characterization of arsenic in gold ores and cyanidation tailings using X-ray absorption spectroscopy. Geochim. Cosmochim. Acta 68, 969–983. doi:10.1016/j.gca.2003.07.013

Pichler, T., Hendry, M.J., Hall, G.E.M., 2001. The mineralogy of arsenic in uranium mine tailings at the Rabbit Lake In-pit Facility, northern Saskatchewan, Canada. Environ. Geol. 40, 495–506.

Pierce, M., Moore, C., 1980. Absorption of amorphous iron hydroxide from dilute aqueous solution. Environ. Sci. Technol. 14, 214–216.

Robertson, J., Hendry, M.J., Essilfie-Dughan, J., Chen, J., 2015. Precipitation of aluminum and magnesium secondary minerals from uranium mill raffinate (pH 1.0-10.5) and their controls on aqueous contaminants. Appl. Geochem. *in press*. doi:10.1016/j.apgeochem.2015.09.002

Robertson, J., Shacklock, K., Frey, R., Gomez, M. a., Essilfie-Dughan, J., Hendry, M.J., 2014. Modeling the Key Lake uranium mill's bulk neutralization process using a pilot-scale model. Hydrometallurgy 149, 210–219. doi:10.1016/j.hydromet.2014.08.010

Shaw, S.A., Hendry, M.J., Wallschläger, D., Kotzer, T., Essilfie-Dughan, J., 2011. Distribution, characterization, and geochemical controls of elements of concern in uranium mine tailings, Key Lake, Saskatchewan, Canada. Appl. Geochem. 26, 2044–2056. doi:10.1016/j.apgeochem.2011.07.002

Smedley, P.., Kinniburgh, D.., 2002. A review of the source, behaviour and distribution of arsenic in natural waters. Appl. Geochem. 17, 517–568. doi:10.1016/S0883-2927(02)00018-5

Stipp, S.L.S., Hansen, M., Kristensen, R., Jr, M.F.H., Bennedsen, L., 2002. Behaviour of Fe-oxides relevant to contaminant uptake in the environment. Chem. Geol. 190, 321–337.

Takeno, N., 2005. Atlas of Eh-pH diagrams. Intercomparison of thermodynamic databases: Geological Survey of Japan. Open File Report No.419.

Twidwell, L.G., Robins, R.G., Hohn, J.W., 2005. The removal of arsenic from aqueous solution by coprecipitation with iron (III), in: Reddy, R.G., Ramachandran, V.S. (Eds.), Arsenic Metallurgy. 2005 TMS Annual Meeting, San Fransisco.

U.S. Department of the Interior, 1998. National Irrigation Water Quality Program Information Report No. 3: Guidelines for Interpretation of the Bilogical Effects of Selected Constituents in Biota, Water, and Sediment: Molybdenum. Washington.

US EPA, 1998. Research plan for arsenic in drinking water: EPA/600/R-98/042, in: U.S. Environmental Protection Agency. Office of Research and Development: National Centre for Environmental Assessment, Cincinnati.

USGS, 2013. USGS Minerals Information: Molybdenum [WWW Document]. URL http://minerals.usgs.gov/minerals/pubs/commodity/molybdenum/

Vyskocil, A., Viau, C., 1999. Assessment of molybdenum toxicity in humans. J. Appl. Toxicol. 19, 185–192.

Wagman, D.D., Evans, W.H., Parker, V.B., Schumm, R.H., Halow, I., Bailey, S.M., Churney, K.L., Nuttall, R.L., 1982. The NBS Tables of Chemical Thermodynamic Properties. J. Phys. Chem. Ref. Data 11, 1–407.

Wang, S., Mulligan, C.N., 2006. Occurrence of arsenic contamination in Canada: sources, behavior and distribution. Sci. Total Environ. 366, 701–21. doi:10.1016/j.scitotenv.2005.09.005

Waychunas, G. a., Kim, C.S., Banfield, J.F., 2005. Nanoparticulate Iron Oxide Minerals in Soils and Sediments: Unique Properties and Contaminant Scavenging Mechanisms. J. Nanoparticle Res. 7, 409–433. doi:10.1007/s11051-005-6931-x

Waychunas, G.A., Rea, B.A., Fuller, C.C., Davis, J.A., 1993. Surface chemistry of ferrihydrite: Part 1. EXAFS studies of the geometry of coprecipitated and adsorbed arsenate. Geochim. Cosmochim. Acta 57, 2251–2269. doi:10.1016/0016-7037(93)90567-G

Whiting, K.S., 1992. The Thermodynamics and Geochemistry of Arsenic with Application to Subsurface Waters at the Sharon Steel Superfund Site at Midvale, Utah. Colorado School of Mines, Colorado.

WHO, 1993. Guidelines for Canadian Drinking Water Quality: Water Treatment Principles and Applications: a Manual for the Production of Drinking Water. World Health Organization, Geneva.

Wilkie, J.A., Hering, J.G., 1996. Adsorption of arsenic onto hydrous ferric oxide: effects of adsorbate/adsorbent ratios and co-occuring solutes. Colloids Surf. A Physicochem. Eng. Asp. 107, 97–110.

2.0 Sequestration of As and Mo in Uranium Mill Precipitates (pH 1.0-9.2): an XAS Study

2.1 Abstract

As- and Mo- bearing secondary mineral phases formed during the neutralization of uranium mill wastes require characterization. Previous studies indicate that arsenate and molybdate adsorbed to ferrihydrite are dominant controls in the tailings materials. A lab-scale plant mill was employed to characterize secondary precipitates from a variety of ore blends. Through total elemental analysis of precipitates and As and Mo K-edge X-ray absorption spectroscopy, different ratios of contributing phases were determined for each pH stage (4.2, 6.5, and 9.2) of the neutralization process. Overall, arsenate adsorbed to ferrihydrite was the dominant As mineral phase regardless of pH or sample blend (53-77%), with fractional contribution from ferric arsenates, and adsorption to aluminum phases ($AlOHSO_4$, $Al(OH)_3$ and hydrotalcite). Molybdate adsorbed to ferrihydrite was the dominant Mo mineral phase, regardless of pH or sample blend, with fractional contribution decreasing with increasing pH, and minor contributions from calcium molybdate, ferric molybdate and nickel molybdate. The characterization of these phases in the secondary precipitates provides further understanding of the contributing mineral species in tailing facilities.

2.2 Introduction

Arsenic (As) and molybdenum (Mo) are naturally occurring elements but, when present at elevated concentrations in groundwater and surface waters, both can be a hazard to heath. As a result, regulatory limits and guidelines have been established for drinking water (Mo=70 µg/L, As=10 µg/L; WHO, 1993a, 1993b), the protection of aquatic life in freshwater (Mo=73 µg/L, As=5 µg/L; CCME, 2007, 1999a, 1999b, 1997), and freshwater quality (chronic As=150 µg/L, acute As=340 µg/L; US EPA, 1995). Natural water quality criteria have not been published for Mo by the US EPA due to rare occurrences of elevated concentrations, though a groundwater standard for inactive uranium sites has been proposed (Mo=100 µg/L; US EPA, 1987).

A major anthropogenic source of Mo and As contamination in surface and ground waters is tailings generated by mining (Cutler et al., 2003; Donahue et al., 2000; Essilfie-Dughan et al., 2012, 2011; Heinrich et al., 2010; Langmuir et al., 2006, 1999; Lieu et al., 2015; Mahoney et al., 2007, 2005;

Moldovan et al., 2003, 2008; Robertson et al., 2014; 2015, Shaw et al., 2011). Uranium (U) ores mined in northern Saskatchewan, Canada from deposits such as Cigar Lake, McClean Lake, Rabbit Lake, McArthur River, and Key Lake often contain elevated concentrations of As and Mo (Bharadwaj and Moldovan, 2005; Langmuir et al., 1999; Lieu et al., 2010). Subsequently, the acidic solution (pH <1.0) remaining after U solubilisation and extraction (termed raffinate) contains elevated concentrations of dissolved As and Mo. As part of tailings production, this raffinate solution is neutralized with slaked lime and the resulting precipitates are combined with the neutralized leach residues. The neutralization process involves a series of pH steps under oxic conditions during which As and Mo are sequestered in geochemically stable precipitates, resulting in regulatory compliant mill effluent. These precipitates are then combined with other residues from the leaching process and discharged into a mill tailings facility as tailings.

The geochemistry of As in U-mill tailings has been well studied. Ferric arsenates (a precursor to scorodite mineral phases) control As in the solid phase when precipitated from a two stage (pH 4 and 7.5) continuous bulk neutralization circuit at low Fe/As ratios (Fe/As < 5) with high settling retention times (90 min) (Chen et al., 2009; Cutler et al., 2003; Jia et al., 2006, 2005; Langmuir et al., 2006, 1999; Mahoney et al., 2007, 2005). Arsenate adsorbed to ferrihydrite controls As in the solid phase when co-precipitated in a four stage (pH 4.2, 6.5, 9.2, and 11) rapid and continuous bulk neutralization circuit at high Fe/As ratios (Fe/As > 5) with shorter settling times (< 30 min) (Essilfie-Dughan et al., 2013, 2012, 2011; Moldovan and Hendry, 2005; Moldovan et al., 2008, 2003; Pichler et al., 2001; Shaw et al., 2011). Important distinguishing characteristics between these two As sequestration mechanisms include the Fe/As molar ratio, pH, and retention times (Jia et al., 2007; Mahoney et al., 2007; Moldovan et al., 2003; Twidwell et al., 2005). Ferric arsenates form at acidic pH values (pH 2-4) and have also been reported as surface precipitates on ferrihydrite (Jia et al., 2007, 2006; Moldovan and Hendry, 2005). For Fe/As ratios near two, mixtures of poorly crystalline ferric arsenate and ferrihydrite are reported to co-exist; as the molar ratios increase above 4-8, however, the major phase becomes ferrihydrite with arsenate adsorbed to the surface (Jia et al., 2006). Ferrihydrite begins to form above pH 3.2 with the optimal precipitation range for arsenate (As^{5+}) adsorption between pH 4 and 6; this is most effective at Fe/As molar ratios ≥ 4-7 (Dixit and Hering, 2003; Moldovan and Hendry, 2005; Twidwell et al., 2005). Attenuation of effective pH has been reported when co-precipitated anions become adsorbed to the surface (AsO_4^{2-}, MoO_4^{2-}, $Al(OH)_4^-$), which has been shown to disrupt the growth

of ferrihydrite into more extended structures such as goethite and hematite (Ford, 2002; Jia et al., 2007; Twidwell et al., 2005; Waychunas et al., 1993).

Because arsenic strongly absorbs on and co-precipitates with iron oxides in waters and soils (ferrihydrite, hematite, and goethite), many studies have characterized this behaviour (Das et al., 2014a, 2014b; Dixit and Hering, 2003; Ford, 2002; Fritzsche et al., 2011; Fukushi and Sverjensky, 2007; Gomez et al., 2013b; Twidwell et al., 2005; Waychunas et al., 2005; Wilkie and Hering, 1996). In the U mining sector, X-ray absorption spectroscopy (XAS) of As in tailings from the Key Lake Deilmann tailings management facility (DTMF) and the Rabbit Lake in-pit tailings management facility (RLTMF) at Cameco's northern Saskatchewan mining operations show the As is predominantly adsorbed to ferrihydrite through inner-sphere bidentate linkages (Essilfie-Dughan et al., 2013; Moldovan et al., 2003). Results from sequential extraction experiments performed on DTMF samples in conjunction with thermodynamic modeling support conclusions that ferrihydrite is the dominant solubility control on aqueous As concentrations (Shaw et al., 2011). Similar studies on tailings at the McClean Lake Tailings Management Facility observed As associated as a mixture of amorphous ferric arsenates and adsorbed arsenates that were pH dependent (Chen et al., 2009; Cutler et al., 2003; Mahoney et al., 2007).

The characterization of Mo sequestration has been based on the knowledge that nanoparticle iron oxides (ferrihydrite) can serve as control for other elements of concern (EOCs; Mo, Se, Ni) during co-precipitation due to their high sorption capacities for metal and anion contaminants (Stipp et al., 2002; Waychunas et al., 2005). As such, ferrihydrite has been shown to also play a significant role in controlling the solubility of Mo in the DTMF (Essilfie-Dughan et al., 2011, 2012; Shaw et al., 2011). An XAS study of Mo in the DTMF identified $NiMoO_4$ and $CaMoO_4$ as well as Mo adsorbed onto ferrihydrite as phases responsible for solubility control of Mo in the tailings (Essilfie-Dughan et al., 2011).

Recently, adsorption to amorphous aluminum hydroxides and hydrotalcite-like layered double hydroxides (HT-LDHs) has been considered with respect to the uptake of anions (AsO_4^{2-} and MoO_4^{2-}) in solution (Arai et al., 2001; Goldberg, 2002; Paikaray et al., 2013) and possible applications to U mill wastes (Gomez et al., 2013a; Robertson et al., 2015). Greater uptake affinities have been reported for As than Mo when precipitated with MgFe-SO_4 hydrotalcites, over those formed with MgAl-CO_3, and have a high affinity for adsorption over the pH range 6 to 8

(Paikaray and Hendry, 2013; Paikaray et al., 2013). Amorphous aluminum hydroxides precipitate over a pH range of 5 to 9 with adsorption of arsenates beginning at pH 5 and maximum loading reported from pH 7 to 8 (Arai et al., 2001; Goldberg, 2002; Moldovan and Hendry, 2005). Thus, these precipitates would have the greatest impact on contaminants at high pH values (pH 6-10).

Although the sequestration of EOCs (As and Mo) in the DTMF are well characterized, the evolution of secondary mineral controls on EOCs during the progressive neutralization of raffinate wastes remains poorly understood. To date, studies by Robertson et al. (2014, 2015) and De Klerk et al. (2012) have characterized the evolution of As and Mo within lab-scale U mill neutralization circuits. Robertson et al. (2014, 2015) used synthetic raffinate in a continuous flow lab-scale model of the Key Lake process to show that ferrihydrite precipitated in the mill process contains Al and may best be described as aluminous ferrihydrite. Robertson et al. (2015) used extraction experiments to show that the As and Mo were associated with both the Al-doped ferrihydrite and Mg-Al and Mg-Al-Fe HTLCs. De Klerk et al. (2012) compared batch versus bench-scale continuous circuit lime neutralization to determine the role of process and chemical parameters on the removal of As with ferric ions between one, two, and three stage neutralization systems. They concluded that the lowest residual arsenate concentrations were obtained using a two stage (pH 4 and 8) co-precipitation circuit, where co-precipitates consisted of a mixture of gypsum, poorly crystalline ferric arsenate, and (arsenate-bearing) ferrihydrite (De Klerk, 2008; De Klerk et al., 2012)). Aluminum was also found to be a suitable equimolar substitute for a portion of the ferric ion in this study.

Overall, the evolution of As- and Mo- bearing secondary mineral phases formed during the neutralization of uranium mill wastes, before combination into the final tailings, remain largely uncharacterized. Based on this, the objectives of the current study were to: i) characterize the As- and Mo-bearing secondary precipitates that form during raffinate neutralization (pH 1 to 9.2), ii) determine what effect different mill feed materials (ores) have on the formation of the precipitates that serve to control EOCs in the tailings, and iii) predict the long-term stability of As- and Mo-bearing mineral phases in the secondary precipitates that will contribute to the final mill tailings. Characterizing these secondary mill neutralization precipitates will aid in predicting source terms for As and Mo in the tailings facilities and in understanding the impact of future ore sources on the long-term stability of these precipitates.

The study was conducted using a unique laboratory-scale model of the KL mill using current and future ore blends. In all cases, samples of solids precipitated over various incremental pH ranges during the neutralization process in the mill model were analyzed using inductively coupled plasma-mass spectrometry (ICP-MS), x-ray diffraction (XRD), scanning electron microscope (SEM) and x-ray absorption spectroscopy (XAS) to characterize the precipitates formed and ultimately determine the evolution of the secondary mineral phases controlling As and Mo. ICP-MS was used to quantify the bulk chemistry of elements in the solids while XRD and SEM was used to identify possible Fe and Al mineral phases that may control As and Mo in the solids. Finally, XAS was used to quantify the ratio of As- and Mo- bearing mineral phases based on model compounds chosen for comparison and to discover oxidation state, coordination and geometry of the As and Mo environments. This is, to the authors' knowledge, the first time a continuous flow lab-scale model of a U mill circuit has been used to characterize the precipitated mineral phases containing As and Mo from actual ore blends intended for U mill production.

2.3 Materials and Methods

2.3.1 Site Description and Bulk Neutralization Process

The Key Lake mill is located in northern Saskatchewan, Canada (57°11'N, 105°34'W) and is currently one of the largest U mills in the world, producing 7.37 M kg U in 2014 (Cameco, 2014). This mill processes the McArthur River deposit that contains high grade ore (average concentration 15.8% U_3O_8 by weight) and must be blended with low-grade materials to acceptable mill grades (feed grade of 4% U_3O_8) prior to milling (Hossain, 2014; Lieu et al., 2015). The low grade ore sources contribute the most to As and Mo concentrations found in the tailings (Hossain, 2014). The historical development of the Key Lake mill and a description of previously mined reserves up to 25 % U_3O_8 by weight are presented in detail elsewhere (Bharadwaj and Moldovan, 2005).

The Key Lake mill uses H_2SO_4 (94% vol/vol), oxygen (93% vol/vol), and steam (target temperature 60 °C) to leach U from the crushed ore slurry. This acidic leachate (free acid = 40 g/L) reports to the counter current decantation process, where the U-bearing solution is separated from leach residues (Bharadwaj and Moldovan, 2005; Lieu et al., 2010). The U-bearing solution containing dissolved As and Mo reports to solvent extraction where tertiary amines are used to purify and concentrate the U in solution. The purified U solution continues on to the yellowcake precipitation process, while the U-barren waste solution (raffinate) containing As and Mo (As ~

200 mg/L, Mo ~ 2 mg/L) reports to the mill effluent treatment process called bulk neutralization (BN).

The BN circuit (Figure 2-1) treats multiple mill process-based waste streams (e.g., raffinate and contaminated water streams from the site's tailings management activities). The raffinate flows through four reaction vessels (Pachucas). In each Pachuca (labeled A, B, D, and E), slaked lime ($Ca(OH)_2$) is added to increase the pH from 1.5 to 4.2 to 6.5 to 9.2 and precipitate As- and Mo-bearing mineral phases from solution. In addition to slaked lime, $BaCl_2$ is added at points B, E, and F to remove Ra-226 from the effluent (Figure 2-1). Two thickeners are located at strategic process locations to allow solids to settle with addition of flocculant at pH 4.2 (C; SeMo thickener) and pH 9.2 (F; Lamella thickener).

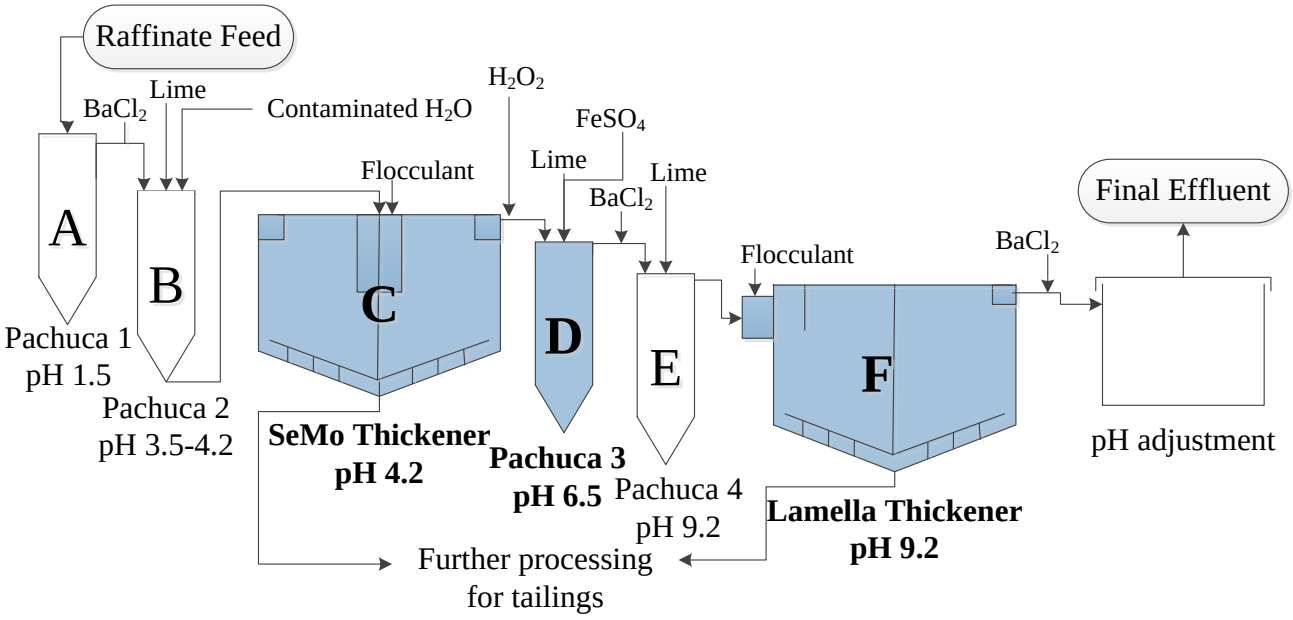

Figure 2-1. Block flow diagram of the Key Lake bulk neutralization (BN) circuit showing sample points A through F. Slurry samples from positions C (SeMo Thickener pH; 4.2), D (Pachuca 3; pH 6.5), and F (Lamella Thickener; pH 9.2) were chosen for comparative analysis.

2.3.2 Sampling the Lab-scale Plant Mill

To replicate the current Key Lake tailings production process at the laboratory scale, three U-feed blends were created from an ore deposit currently being mined (McA) and a potential ore deposit, Millennium (MLM), being considered for future milling. The purpose of using a variety of ore

blends was to determine if the sinks for As and Mo would remain the same, regardless of starting material. The first was created from 100 % McA ore (scenario one: S1), a second that combined 75 % McA ore and 25 % representative core material from the MLM (scenario two; S2), and the third from 100% MLM ore (scenario three; S3) (Appendix A). The ore blends were processed through a unique continuous-flow lab-scale model of the Key Lake mill. The entire lab-scale model—from ore grinding to tailings—was validated and shown to replicate the Key Lake milling process with respect to current mill performance targets and effluent quality (Lieu et al., 2015).

The lab-scale BN circuit was constructed at 1/311,600 scale of the Key Lake mill (Figure 2-1). Slurry samples were collected from each thickener in the lab-scale BN circuit, C (SeMo thickener; pH 4.2), and F (Lamella thickener; pH 9.2), as well as the reaction vessel D (Pachuca 3; pH 6.5). The Key Lake BN circuit was also sampled from actual process slurries in the same locations to provide a baseline for comparison to the lab-scale plant study. Four sets of slurry samples (n=12) were vacuum filtered through commercially available 6 μm filter paper at standard temperature and pressure. Filtered solids were dried at ambient conditions then stored at 4°C until analysis.

2.3.3 ICP-MS

ICP-MS was used for bulk elemental analysis of both solution and solid phases. Solution samples were preserved with 0.5% HNO_3 before analysis. Solid samples were digested in a four acid leach (HCl, HNO_3, $HClO_4$, HF) (Donallson, 1981) in the Key Lake chemistry laboratory as well as in the Aqueous and Environmental Laboratory (AEL), Department of Geological Sciences, University of Saskatchewan using a two acid leach (HNO_3, HF) for comparison (Longerich et al., 1990; Stefanova et al., 2003). Bulk elemental analysis on all samples was performed using Agilent 7500cx and 7700 instruments equipped with an ASX–500 series sample changer (RSD ±10%) at the Key Lake chemistry laboratory and a Perkin-Elmer NexION 300D instrument (RSD ±10%) at the University of Saskatchewan.

2.3.4 XAS

X-ray absorption spectroscopy (XAS) analysis was conducted using the Hard X-ray Microanalysis beamline (HXMA-06ID-1) at the Canadian Light Source (CLS), a third generation synchrotron facility operating at an electron energy of 2.9 GeV and injection current of 250 mA. Approximately 200 mg of dried sample was loaded onto Teflon® holders contained by triple layers of Kapton tape due to the radioactive nature of the samples. Two-line ferrihydrite was prepared from $FeCl_3$ (J.T.

Baker) at the University of Saskatchewan according to the methods of Schwertmann and Cornell (1991) with slight modifications as per Jia et al., (2007) and Das et al., (2014b) and confirmed using X-ray diffraction (XRD) and BET surface area analyses (Appendix C). As and Mo adsorbed to 2-line ferrihydrite (As(V)_ferrihydrite, As(III)_ferrihydrite, and Mo_Ferrihydrite) were prepared using 0.1 M NaCl as the electrolyte at three different pH values to achieve target molar ratios using known methods (Dixit and Hering, 2003; Raven et al., 1998) (Appendix D). Commercially purchased reference compounds $Ca_3(AsO_4)_2$ (Alfa AESAR), $NaAsO_2$, As_2O_3, MoO_2, $NiMoO_4$, $CaMoO_4$, and $FeMoO_4$ (Sigma Aldrich) were diluted with boron nitride and loaded onto same holders, while synthesized sorption standards were prepared in the same way as samples. Previously characterized scorodite, amorphous ferric arsenate (am-$FeAsO_4$), and yukonite were prepared in the same way as purchased compounds (Essilfie-Dughan et al., 2013; Moldovan et al., 2003). Spectra from previously characterized arsenate adsorbed to aluminum phases (hydrotalcite, $Al(OH)_3$ and $AlOHSO_4$) were used for comparison (Paikaray and Hendry, 2014; Robertson et al., 2015). All standards and samples were stored at -17 °C following preparation and immediately cooled with liquid nitrogen before analysis to prevent potential changes in oxidation state. Arsenic K-edge XAS spectra were collected in a cryostat from -200 to +800 eV of the edge (11867 eV) using gold (Au) foil for simultaneous calibration measurement. Molybdenum K-edge XAS spectra were collected from -200 to +200 eV the adsorption edge (20000 eV) using Mo foil for simultaneous calibration measurement. Cryostat equipment under helium gas was monitored to ensure the temperature remained below -20 °C for all standards and samples. XAS data for reference compounds were collected in transmission mode, whereas the samples and sorption standards were collected in fluorescence mode using a Canberra 32-element detector. X-ray absorption near edge structure (XANES) and extended X-ray absorption fine structure (EXAFS) analyses were carried out together for As samples; only XANES data were collected for Mo samples due to low concentrations and time constraints.

Data were analyzed using IFFEFIT, with data reduction performed using ATHENA and EXAFS analysis performed using ARTEMIS (Newville, 2001; Ravel and Newville, 2005). Principal component analysis (PCA) followed by target transform with reference compounds was used to identify and quantify the reference compounds most likely to make up the complex precipitates in our study. Based on the results of the PCA and Target Transform, linear combination fitting (LCF)

analysis was applied to determine the fraction of each Mo species present by fitting reference compounds best matched to sample spectra using normalized μ(E) data in the energy range from -20 to 30 eV. LCF with As K-edge spectra best matched by target transforms were performed from 1-12 $Å^{-1}$ in k^2 weighted $\chi(k)$ space. The residuals (R-factor) and the total values represent the goodness of fit. Smaller values for R-factors provide a measure of best fit for each calculation and the totals when unconstrained can provide a measure of the goodness of fit by fractional amounts summing to 1.00. Data reduction included the standard procedures of energy calibration, multiple scan averaging, background and spline subtraction, normalization, and extraction of EXAFS. Known phases from the crystallographic databases of absorption coefficients and anomalous scattering factors were used as the input data for ab initio, multiple scattering, and phase and amplitude functions generated with FEFF version 6 in the IFFEFIT package (Ravel, 2001; Rehr, 1995). An input file was generated from running the ATOMS code using reported structure and scattering parameters for scorodite (Ravel, 2001). With the amplitudes and phases, EXAFS fit analysis with the crystalline scorodite structural data obtained the interatomic distance (R), Debye-Waller parameter (σ^2), and threshold energy (E_o). The coordination numbers (CN) and amplitude functions were fixed during the fitting process, and structural data obtained from scorodite data were used as guiding values for analysis of samples.

2.4 Results and Discussion

2.4.1 Characterization of BN precipitates

The evolution of the As, Mo, Fe, Mg, and Al concentrations was evaluated for all three scenarios in the model mill and for the Key Lake BN mill (Figure 2-2). Most elements were removed from solution early in the BN process. Average removals for As, Mo, Fe, and Al were 99.9, 98.0, 91, and 91%, respectively, by pH 4.2 (SeMo thickener); removal of Fe and Al were near complete (99.6 and 99.4%, respectively) by pH of 6.5 (Pachuca 3). The removal of Mg was notable different, with only 80.8% removed from solution by pH 6.5 (Pachuca 3) but 98.8 % by pH 9.2 (Lamella thickener). These observations are consistent with previous work that reports complete As removal (99.9-100%) and near complete Mo removal (95.5-99.6 %) from the solution phase in a similar U mill bulk neutralization circuit by pH 4 (Robertson et al., 2014). The mill is designed to sequester the majority of As- and Mo- bearing minerals at the low pH stage of the circuit in the first thickener (C; SeMo Thickener) by pumping the solids away to further tailings treatment where the initial

formation of ferrihydrite, $FeAsO_4$, and $CaMoO_4$ complexes begins (Lieu et al., 2010; Parkhurst and Appelo, 2013, 1999).

Raffinate (mg/L)	KL	S1	S2	S3
As	210	195	223	47.7
Mo	2.23	3.08	6.10	1.34
Fe	2429	4062	5628	1311
Al	3277	3167	5076	1108
Mg	2270	2792	4438	553
Ca	797	1267	1286	504

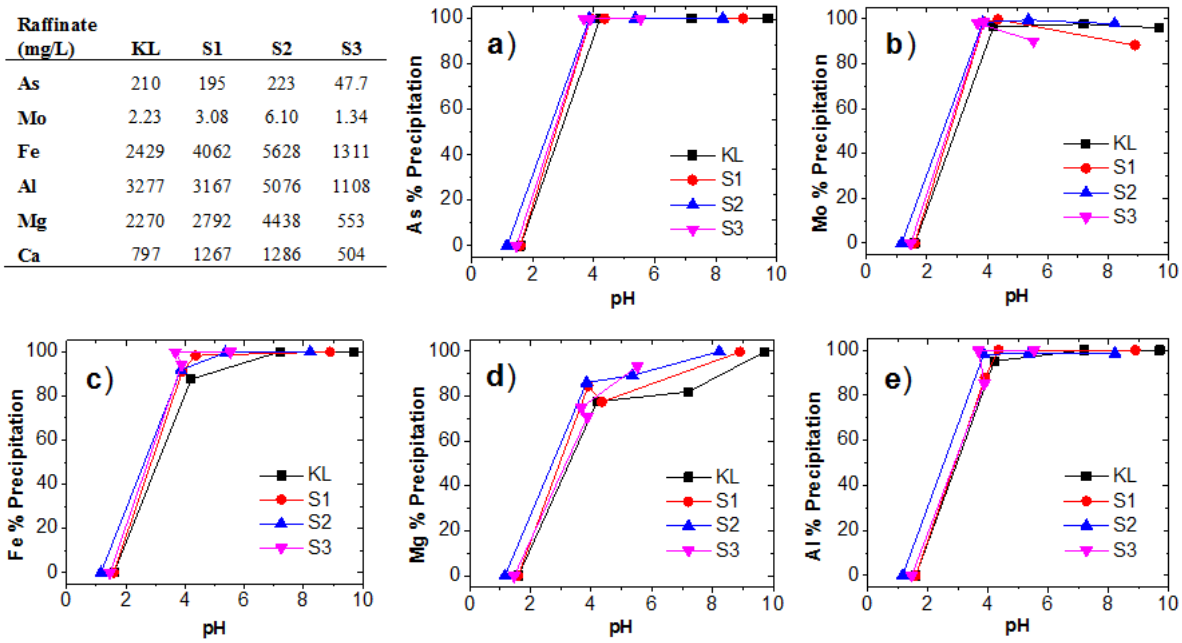

Figure 2-2. Raffinate concentrations of As, Mo, Fe, Al, Mg, and Ca before neutralization and % precipitation with respect to solution pH of a) As, b) Mo, c) Fe, d) Mg, and e) Al for Key Lake (KL) and scenario 1 (S1), scenario 2 (S2), and scenario 3 (S3) samples

Results of elemental analysis of the precipitates with increasing pH are consistent with the elemental mass lost from the raffinate during neutralization. As and Mo concentrations in the solid phase were greatest in the first stage of the neutralization circuit (2,630 to 3,010 µg/g and 152 to 331 µg/g, respectively) where neutralized slurries were allowed to settle in the SeMo thickener and are removed for further processing before combination in the final tailings tank (pH 4.2; Table 2-1). The presence of lower As and Mo concentrations (11.8 to 25.6 µg/g) at higher pH stages (pH 6.5 and 9.2) indicate precipitation of As- and Mo- bearing mineral phases continues to occur but the contribution to the total in the final tailings is minimal (< 2%) as most have been removed from the circuit in the SeMo thickener (C; pH 4.2).

The Fe/As and Fe/Mo molar ratios for all samples were greater than those reported in U tailings studies where molybdate and arsenate adsorbed to ferrihydrite were the dominant mineral phases

(Chen et al., 2009; Essilfie-Dughan et al., 2011; De Klerk, 2008; Langmuir et al., 1999; Moldovan et al., 2003). The solids elemental data presented in Table 2-1 show the Mg/Fe molar ratios (1.65 to 2.87) favor the formation of Mg-Al-Fe HTLCs over Mg-Al HTLCs (Mg/Al ratios: 0.46 to 1.39) and indicate Mg-Al-Fe HTLCs are most likely to exist at pH 9.2 (Gomez et al., 2014; Paikaray and Hendry, 2014; Robertson et al., 2014).

The presence of amorphous Fe and Al phases in the SeMo thickener (pH 4.2) solids and the presence of HTLCs in the lamella thickener (pH 9.2) solids was confirmed by XRD and SEM analysis (Appendix C). Due to the lack of crystallinity in the SeMo solids, it is unclear if these precipitates include an Al mineral phase ($AlOHSO_4$ or $Al(OH)_3$) or if it is predominantly ferrihydrite (doped with Al), as previously described (Gomez et al., 2013a; Robertson et al., 2015, 2014). Similarly, the type of HTLC compound is difficult to ascertain because the difference between Mg-Al-Fe and Mg-Al HTLCs cannot be determined by XRD alone (Paikaray and Hendry, 2014). Thus, evidence of a variety of mineral phases in the precipitates led to the selection of model compounds included in XAS analysis.

Table 2-1. Elemental concentrations of As, Mo, Fe, Mg, and Al and molar ratios of Fe/As, Fe/Mo, Mg/Al, and Mg/Fe in solid phases of Key Lake and LSP samples for scenario 1 (S1), scenario 2 (S2), and scenario 3 (S3).

Sample	pH	As (µg/g)	Mo (µg/g)	Fe (µg/g)	Mg (µg/g)	Al (µg/g)	Fe/As (M)	Fe/Mo (M)	Mg/Al (M)	Mg/Fe (M)
Key Lake (KL)										
SeMo	4.2	2634	219	29550	2289	63914	13.1	231	0.04	0.18
Pachuca 3	6.5	482	19.2	52697	16224	48812	25.1	555	0.05	0.06
Lamella	9.2	556	11.8	40719	50767	40588	28.1	292	0.03	0.04
Scenario 1 (S1)										
SeMo	4.2	2634	152	49250	1498	28382	531	4710	0.37	0.71
Pachuca 3	6.5	482	30.4	27315	3897	50106	75.9	1540	0.09	0.33
Lamella	9.2	556	16.3	37236	26600	52455	106	775	0.03	0.21
Scenario 2 (S2)										
SeMo	4.2	1951	146	35028	2065	51039	24.1	412	0.04	0.14
Pachuca 3	6.5	232	36.8	44152	6651	81295	255	2058	0.07	0.35
Lamella	9.2	119	13.1	31997	39597	56704	360	4190	0.78	2.85
Scenario 3 (S3)										
SeMo	4.2	2688	331	56410	989	34406	688	5920	1.39	2.87
Pachuca 3	6.5	332	58.2	26268	2408	89122	89.6	3910	0.56	1.65
Lamella	9.2	393	25.6	32456	32880	79654	111	2180	0.46	2.33

Source: ICP-MS data.

2.4.2 XANES and EXAFS analysis of As K-edge spectra

Comparison of the As^{3+} and As^{5+} reference compound spectra indicate that arsenate (As^{+5}) was the dominant form of arsenic in the BN precipitates, regardless of pH or sample blend (Figure 2-3). The energy position of maximum absorbance (the pre-edge) for As K-edge shifts to higher energy with increased oxidation state over a 10 eV interval starting at the adsorption edge at approximately 11,860 eV, was consistent with As^{5+} for all samples. This finding agrees with results obtained from comparison of XANES reference standards to tailings samples from the DTMF and RLTMF as well as geochemical modeling of mill waste neutralization by Essilfie-Dughan et al. (2013) and Moldovan et al. (2003).

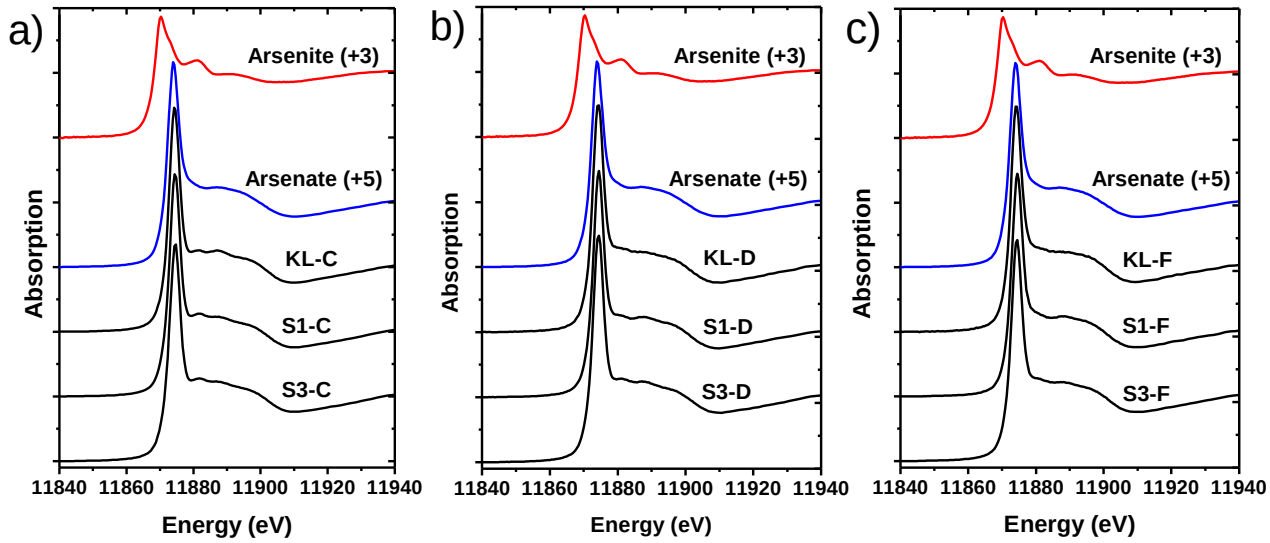

Figure 2-3. As K-edge XANES from bulk solid analysis indicate the redox state of solids from Key Lake (KL), scenario 1 (S1), and scenario 3 (S3): a) SeMo thickener (C; pH 4.2) b) Pachuca 3 (D; pH 6.5), and c) Lamella thickener (F; pH 9.2) with $NaAsO_2$ (As^{3+}) and arsenate adsorbed to ferrihydrite (As^{5+}) standards.

Previous studies on tailings samples from the DTMF successfully determined the dominant As, Fe and Mo mineral phases using XAS, followed by PCA and LCF (Essilfie-Dughan et al., 2013, 2011). In our study, PCA of As K-edge EXAFS with samples (n = 9) determined that the spectra are comprised of contributions from three components (Figure 2-4).

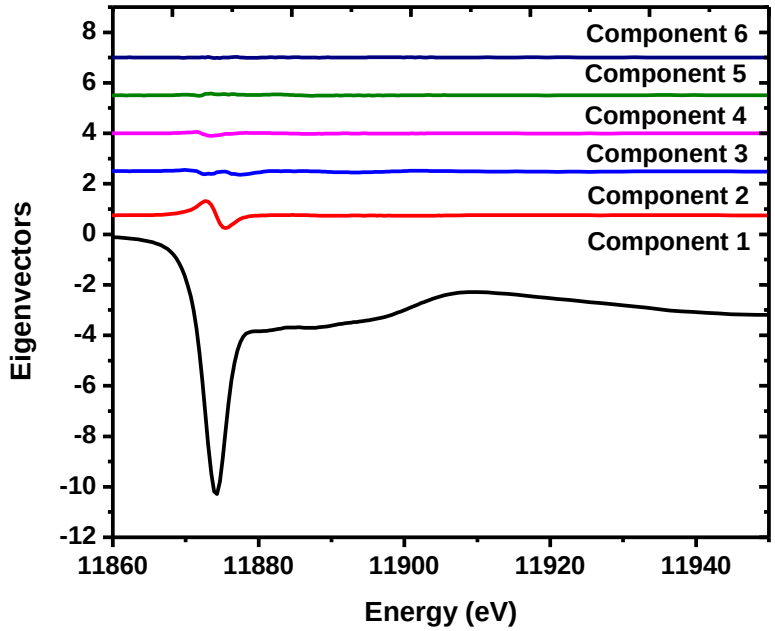

Figure 2-4. Results of principal component analysis (PCA) of the set of As K-edge spectra. Analysis using Athena's suite of programs, shown with Eigenvectors, indicates that normalized u(E) data from -20 to 80 (eV) can be made up of two major components and up to two minor components.

Target transforms of the normalized data were compared to a range of reference compounds analyzed (arsenate adsorbed to aluminum hydroxide sulfate ($AlOHSO_4$), amorphous aluminum hydroxide ($As\_Al(OH)_3$), hydrotalcite (As_HTLC), ferrihydrite (As_Ferrihydrite); ferric arsenate ($FeAsO_4$), $Ca_3(AsO4)_2$, scorodite, yukonite, arsenite adsorbed to ferrihydrite, and $NaAsO_2$) (Figure 2-5a). The transform data indicated the standards that most closely matched the spectra are As_Ferr, $FeAsO_4$, and $AlOHSO_4$ at pH 4.2, As-Ferr, $FeAsO_4$, and $As\_Al(OH)_3$ at pH 6.5, and As_Ferr, $As\_Al(OH)_3$ and As_HTLC at pH 9.5 (data not included). Because the formation of crystalline scorodite was considered thermodynamically unfavourable in the lab-scale mill conditions, it was not used as a standard in the subsequent LCF analysis (Chen et al., 2009; Langmuir et al., 2006; Moldovan and Hendry, 2005). Results of the LCF of SeMo thickener samples from scenario 1 (S1-C, pH 4.2) is shown with spectra denoting the fractional contributions of the components used to generate the fitted spectrum (Figure 2-5b).

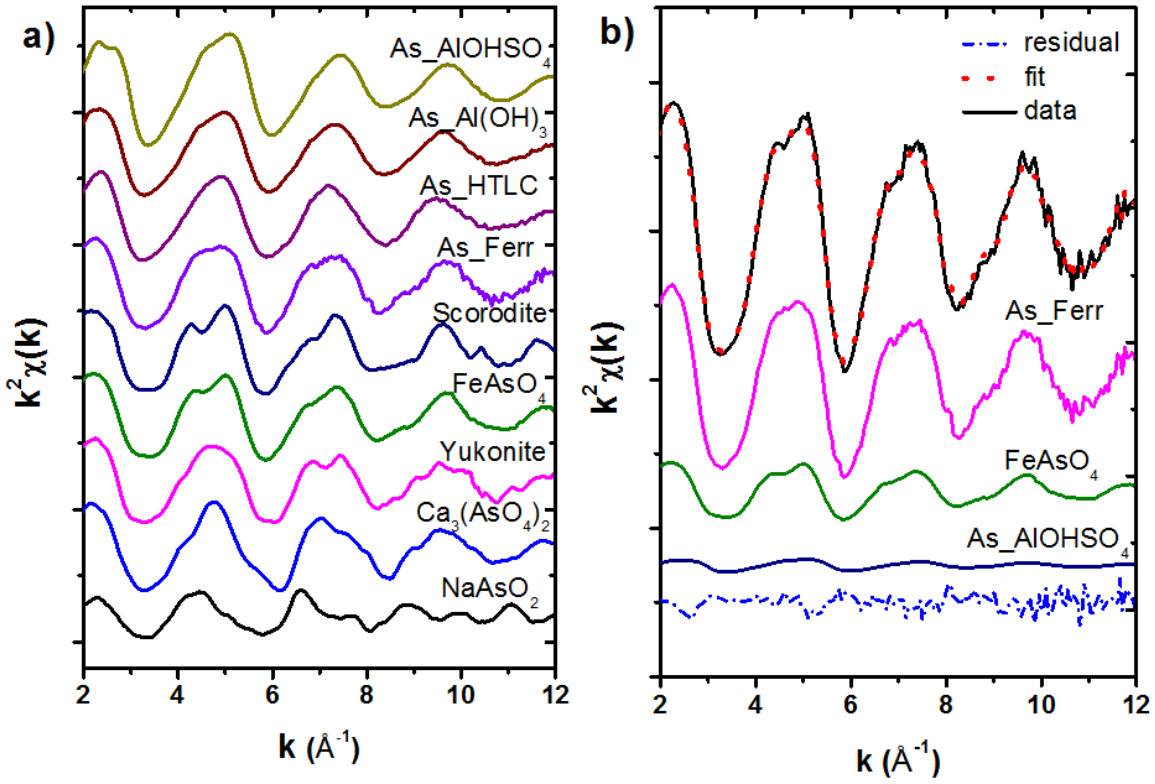

Figure 2-5. a) As K-edge EXAFS spectra of As model compounds. b) Experimental and linear combination fits (solid lines represent data, dotted red lines optimal fit and dash-dot blue lines represent calculated residual) for sample S1-C (SeMo thickener pH 4.2) along with spectra denoting fraction contributions of components used to general the linear combination fit.

LCF confirmed samples had the greatest contributions (53–76%) of arsenate adsorbed to ferrihydrite (As_Ferr) for all samples regardless of pH or sample blend, with minor contributions from ferric arsenate ($FeAsO_4$) and arsenate adsorbed to aluminum hydroxide sulfate (As_AlOHSO_4), aluminum hydroxide ($As\_Al(OH)_3$) and hydrotalcite phases (As_HTLC) (Table 2-2). This can be explained by the solubility profiles of these mineral phases (Chen et al., 2009; Langmuir et al., 2006; Moldovan et al., 2003; Paikaray et al., 2013; Paktunc and Bruggeman, 2010; Robertson et al., 2015). Solubility factors dictate $FeAsO_4$ will control As solely at the pH state of the SeMo thickener (pH 4.2) and LCF indicates it contributes less (23-26%) than the dominant As_Ferr phase (71-73%) in the total ratio of solids at this pH (Table 2-2). As well, As_AlOHSO_4 only contributed to the low stage (pH 4.2) at low ratios (3-4%) as predicted by documented

solubility profiles (Robertson et al., 2015, 2014) (Table 2-2). In the middle pH stage (Pachuca 3, pH 6.5) As_Ferr remained the dominant mineral phase (66-77%) with minor contributions from $FeAsO_4$ (<1- 8%) and As_$Al(OH)_3$ (15-34%). As_HTLC and As_$Al(OH)_3$ were included at pH 9.2 (Lamella thickener) as their formation is more thermodynamically favourable at this pH (Paikaray and Hendry, 2014; Robertson et al., 2015, 2014) and its inclusion improved the calculated R- factors (Table 2-2). Based on LCF values for As minerals at pH 9.2, As_HTLC and As_$Al(OH)_3$ remained minor mineral phases (<1-24%) and (17-47%) respectively, and As_Ferr remained the dominant phase (53-74%) in the Lamella thickener.

Table 2-2. Type and fractional amounts of As species in precipitates obtained from LCF of Key Lake (KL) and LSP samples for scenario 1 (S1) and scenario 3 (S3) in k^2 weighted chi space (k-range 1-12) for sample locations as indicated (see Fig. 2-1). Expressed as a fractional amount ± the estimated standard deviation as calculated by Athena.

	Linear Combination Fitting*					**Goodness-of-fit**	
Sample	As_Ferr	$FeAsO_4$	As_$AlOHSO_4$	As_$Al(OH)_3$	As_HTLC	Total	R-factor
	Key Lake (KL)						
C (pH 4.2)	0.72 (0.11)	0.24 (0.11)	0.04 (0.16)			1.00	0.0126
D (pH 6.5)	0.76 (0.00)	0.00 (0.12)		0.24 (0.14)		1.00	0.0312
F (pH 9.2)	0.59 (0.12)			0.17 (0.14)	0.24 (0.12)	1.00	0.0494
	Scenario 1 (S1)						
C (pH 4.2)	0.73 (0.06)	0.23 (0.06)	0.04 (0.08)			1.00	0.0262
D (pH 6.5)	0.77 (0.06)	0.08 (0.07)		0.15 (0.09)		1.00	0.0139
F (pH 9.2)	0.53 (0.00)			0.47 (0.00)	0.00 (0.0)	1.00	0.0350
	Scenario 3 (S3)						
C (pH 4.2)	0.71 (0.05)	0.26 (0.05)	0.03 (0.07)			1.00	0.0083
D (pH 6.5)	0.66 (0.00)	0.00 (0.00)		0.34 (0.05)		1.00	0.0253
F (pH 9.2)	0.74 (0.03)			0.20 (0.07)	0.06 (0.06)	1.00	0.0115

* Fit using the choice of reference compounds: arsenate adsorbed to ferrihydrite (As_Ferr), ferric arsenate ($FeAsO_4$), arsenate adsorbed to aluminum hydroxide sulfate (As_$AlOHSO_4$), aluminum hydroxide (As_$Al(OH)_3$) and hydrotalcites (As_HTLC). Phases were included at pH range most thermodynamically favourable to form and where inclusion improved the R-factors (goodness of fit).

The As k^3-weighted $\chi(\kappa)$ space spectra and the corresponding Fourier transformed (FT) EXAFS using the Hanning window (k range = 3-12.5, with phase correction) are shown in Figure 2-6. In the *k*-space spectra, the region indicated by arrows was observed to broaden and flatten out with increasing pH. The feature appears as a split peak in samples from the SeMo thickener (pH 4.2), begins to broaden in samples from Pachuca 3 (pH 6.5), and then completely plateaus in samples from the Lamella thickener (pH 9.2). The same feature is present in the scorodite reference standard, begins to broaden in ferric arsenate ($FeAsO_4$), and then completely plateaus for arsenate adsorbed to ferrihydrite (As_Ferr), consistent with previously published EXAFS studies (Chen et al., 2009; Das et al., 2014b; Moldovan et al., 2003; Paktunc et al., 2004). Moldovan et al. (2003) attributes these fine structure differences between scorodite and arsenic ferrihydrite to backscattering from second neighbour Fe ions in a mono- or bi-dentate arsenate complex on the ferrihydrite surface. Since the arsenate adsorbed to aluminum hydroxide sulfate (As_AlOHSO_4), aluminum hydroxide ($As\_Al(OH)_3$) and hydrotalcites (As_HTLC) standards contributed low ratios (<47 %) to the total precipitates by LCF analysis, they were not included in subsequent EXAFS fits.

Fit analysis of the As EXAFS spectra of scorodite, ferric arsenate, and arsenate adsorbed to ferrihydrite and hydrotalcite indicated CNs and bond lengths are consistent with previous reports, within measurement errors (Das et al., 2014a, 2014b; Fuller et al., 1993; Jia et al., 2006, 2005; Moldovan et al., 2003; Paikaray and Hendry, 2014; Paktunc et al., 2008). Samples from pH 4.2 and 6.5 are shown for comparison (Table 3). Phase correction was included to eliminate R-shifts and asymmetric peaks typical of transform peaks where phase correction is neglected (Cotelesage et al., 2012). Data for the first shell (As-O), with a CN of 4 and bond lengths of 1.68-1.69 ± 0.02 Å, arise from interactions within the AsO_4 tetrahedron and are the same for standards and samples. The consistent interatomic distances indicate that the AsO_4 tetrahedron remains relatively rigid, regardless of the compound to which it is bound. Samples collected from the final Lamella thickener (KL-F, S1P-F, and S3P-F) were not included in EXAFS fitting calculations due to poor scan quality at low As concentrations and the ratio of fractional components < 70% for any one reference compound (Table 2-2).

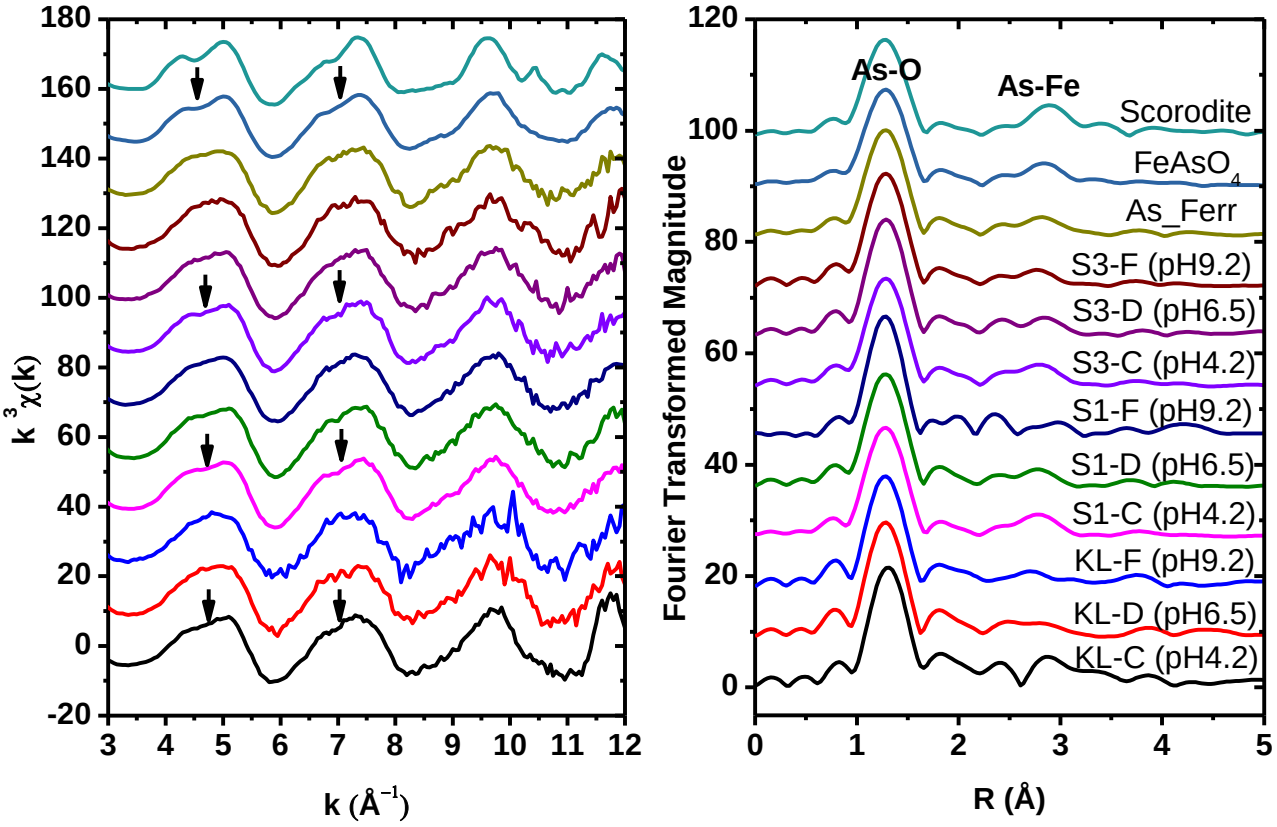

Figure 2-6. As K-edge k^3- weighted EXAFS spectra and Fourier transform (FT) (k range of 3 to 12.5) for three As standards well matched by target transforms of principal component analysis, off-set for illustrative purposes. See Figure 2-1 for sample locations. Arrows indicate the flattening and broadening of the marked feature with increasing pH.

Table 2-3. Arsenic K-edge fitting results of selected reference compounds and Key Lake (KL), scenario 1 (S1), and scenario 3 (S3) samples (see Fig. 2-1 for sample locations). Coordination number (CN), interatomic distance (R), Debye-Waller parameter (σ^2) and threshold energy (E_o) were determined using IFEFFIT with FEFF fitting theoretical phase and amplitude functions.

Sample	**As-O shell**				**As-O multiple scattering**				**As-Fe shell**			
	N	*R*(Å)	σ^2(Å^2)	E_o	*N*	*R*(Å)	σ^2(Å^2)	E_o	*N*	*R*(Å)	σ^2(Å^2)	E_o
Scorodite	4.0	1.69	0.0031	4.72	12.0	3.21	0.0057	4.72	3.0	3.35	0.0072	4.72
					1.0	3.39			1.0	3.39		
					2.0	3.49						
					2.0	3.37	0.0072					
amFeAsO$_4$[a]	4.0	1.69	0.0030	5.06	12.0	3.22	0.0031	5.06	3.0	3.32	0.0088	5.06
					1.0	3.43			1.0	3.36		
					4.0	3.33	0.0088					
As_Ferrihydrite	4.0	1.69	0.0022	5.35	12.0	3.24	0.0075	5.35	2.0	3.30	0.0053	5.35
					1.0	3.43						
					4.0	3.31	0.0053					
KL-C (pH 4.2)	4.0	1.68	0.0013	5.56	12.0	3.26	0.0032	5.56	2.0	3.31	0.0053	5.56
					1.0	3.44			1.0	3.35		
					4.0	3.32	0.0053					
KL-D (pH 6.5)	4.0	1.69	0.0017	6.74	12.0	3.24	0.0023	6.74	1.5	3.30	0.0073	6.74
					1.0	3.42			1.0	3.34		
					4.0	3.32	0.0073					
S1-C (pH 4.2)	4.0	1.69	0.0020	5.84	12.0	3.22	0.0022	5.84	1.8	3.30	0.0067	5.84
					1.0	3.40			1.0	3.34		
					4.0	3.31	0.0067					
S1-D (pH 6.5)	4.0	1.68	0.0019	5.39	4.0	3.20	0.0018	5.39	2.0	3.30	0.0062	5.39
					1.0	3.39						
					2.0	3.49						
S3-C (pH 4.2)	4.0	1.68	0.0021	5.46	12.0	3.21	0.0073	5.46	2.0	3.29	0.0067	5.46

					2.0	3.39			1.0	3.33		
					2.0	3.50						
					2.0	3.31	0.0067					
S3-D (pH 6.5)	4.0	1.68	0.0016	6.67	12.0	3.20	0.0041	6.74	2.0	3.30	0.0081	6.74
					1.0	3.38			1.0	3.34		
					2.0	3.49						

The amplitude reduction factor was constrained to 0.9, while the Debye-Waller parameter (σ^2) was allowed to float during the fitting process. Threshold energy (E_o) was allowed to float but all variables constrained to equal in each fit. The measurement uncertainties of the interatomic distances (R) and coordination number (CN) are 0.02 Å and ± 20%, respectively (Cotelesage et al., 2012). Samples collected from the final Lamella thickener (pH 9) are not included due to low As concentrations and the minimal contribution to As mineral phases at this pH stage.

[a] FeAsO4 – ferric arsenate

[b] As_Ferrihydrite – arsenate adsorbed to ferrihydrite

[c] As_Hydrotalcite – arsenate adsorbed to hydrotalcite

The second set of peaks from 3.29 to 3.39 Å (corrected for phase shift) show the As-Fe and As-Al interactions of the second shell of atoms as well as multiple scattering effects. Additional multiple scattering was included from 3.20 to 3.50 Å where appropriate to the fit. The results of the fits for the second shell indicate scorodite has two backscattering (As-Fe) effects with bond distances of 3.35 and 3.39 ± 0.02 Å and CNs of 3.0 and 1.0, respectively. Similarly, ferric arsenate has two (As-Fe) bond distances of 3.32 and 3.36 ± 0.02 Å with CNs of 3.0 and 1.0, respectively. Arsenate adsorbed to ferrihydrite was fit with a single (As-Fe) bond distance of 3.30 ± 0.02 Å and a CN of 2.0. The results of sample fitting indicate the interatomic distances of the first (As-Fe) shell range from 3.29 to 3.31 ± 0.02 Å and CNs of 1.5 to 2.0 in all pH 4.2 and 6.5 samples. These compare best to those for arsenate adsorbed to ferrihydrite in bidentate binuclear coordination, though the extended distances (3.31 ± 0.02 Å) could be attributed to contribution from amorphous ferric arsenate (Chen et al., 2009; Essilfie-Dughan et al., 2013; Moldovan et al., 2003; Waychunas et al., 1993) or Al substitution in the ferrihydrite structure (Adra, et al., 2013). Waychunas et al. (1993) report arsenate adsorbed to ferrihydrite bond distances for an idealized bidentate geometry at 3.28 Å, and freshly co-precipitated samples with shorter distances from 3.24-3.27 ± 0.02 Å. Chen et al. (2009) report distances for poorly crystalline scorodites of 3.33 ± 0.02 Å with average CNs of 3.2. The distances and coordination numbers measured in our study are within error of the idealized arsenate adsorbed to ferrihydrite (Waychunas et al., 1993) and align with those reported for neutralized raffinate samples at the Rabbit Lake U mill (Moldovan et al., 2003).

The second As-Fe interaction present in all samples except S1-D (Pachuca 3, pH 6.5) were characterized by bond distances ranging from 3.33-3.35 ± 0.02 Å and a CN of 1.0, matching those from the ferric arsenate reference standard and literature values for poorly crystalline scorodite (Chen et al., 2009), sometimes referred to as amorphous ferric arsenate. LCF from these samples indicated the solids could be represented by a contribution of <1 to 26 % of ferric arsenate, whereas sample S1-D (Pachuca 3, pH 6.5) had minor contributions from $FeAsO_4$ (8%) and $As\_Al(OH)_3$ (15%), and the highest contribution of As_Ferr (77%) (Table 2-2). As well, the bond lengths (3.30 ± 0.02 Å) and coordination numbers (1.5 ± 0.3) for the first shell of sample S1-D agreed well with those reported for arsenate adsorbed to ferrihydrite in bidentate-binuclear coordination (Das et al., 2014b; Fuller et al., 1993; Jia et al., 2005; Moldovan et al., 2003; Waychunas et al., 1993). The As K-edge k^3-weighted EXAFS and FT using the Hanning window (k range = 3 to 12.5, R range = 1 to 3.2) for sample S1-D and As_Ferr are shown in Figure 2-7.

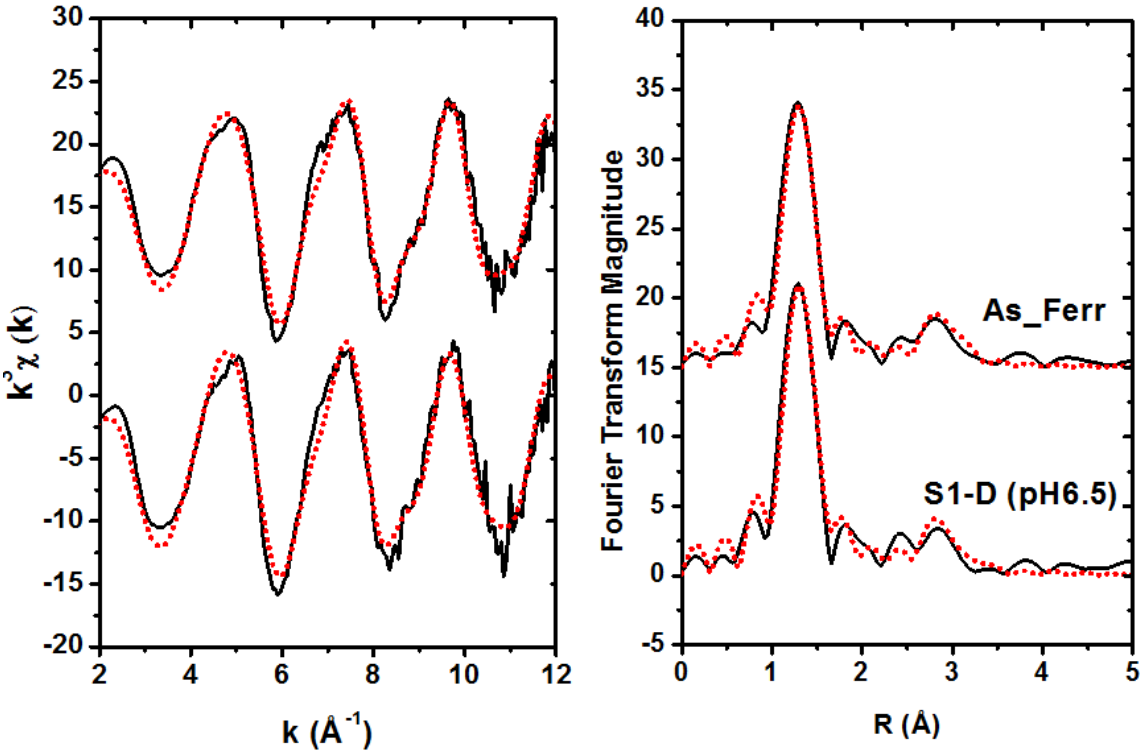

Figure 2-7. As K-edge k3-weighted EXAFS spectra and Fourier transform (FT) using Hanning window in the k range of 3 to 12.5 and R range of 1 to 3.2 comparing fits for Pachuca 3 sample at pH 6.5 (S1D) and arsenate adsorbed to ferrihydrite (As_Ferr) standard. Data is shown with a solid black line and the calculated fit with a red dotted line.

The fits of the As_Ferr reference standard and sample S1-D are in good agreement, and differed by 0.02 Å for the ferric arsenate and 0.05 Å for the scorodite reference standards. Given results from LCF and the similarity of ferric arsenate and arsenate adsorbed on ferrihydrite bond lengths, there are likely contributions from both at both the pH 4.2 and 6.5 stages. However, because both ferric arsenate and arsenate adsorbed to aluminum phases contributed in such minor amounts, fitting these phases was unsuccessful. From the results of the LCF of EXAFS in k^2-weighted chi space, the agreement to the As_Ferr reference standard in this study, and the bond lengths consistent with previously reported values for arsenate adsorbed to ferrihydrite; we determined that ferrihydrite is the dominant mineral control for As regardless of pH or sample blend considered in this study. This finding is important because when co-precipitated, adsorption of arsenate to the surface of ferrihydrite will slow the transformation of this iron oxide to more

crystalline forms, such as goethite and hematite, thus stabilizing the arsenate-ferrihydrite structure (Das et al., 2014a, 2014b, 2011; Ford, 2002).

2.4.3 XANES analysis of Mo K-edge spectra

Comparison of XANES data to the energy shift of the reference compounds confirmed the dominant form of Mo in the samples is Mo (+6), regardless of pH or sample blend (Figure 2-8). This finding was supported by geochemical modeling of mill waste neutralization (PHREEQCI: data not presented) and pH/Eh diagrams for soluble Mo species (Parkhurst and Appelo, 2013, 1999; Takeno, 2005). The pre-edge feature in Mo (+6) compounds at approximately 19995 eV but absent in Mo (+4) compounds provides a strong indication of oxidation state (Figure 2-8). This peak observed in the $NiMoO_4$ (Mo+6) model compound and absent in MoO_2 (Mo +4) is attributed to dipole forbidden $1s \rightarrow 4d$ transitions that gain intensity due to admixing of the 4d levels with p orbitals in Mo environments without a centre of symmetry (Essilfie-Dughan et al., 2011; Wharton et al., 2003).

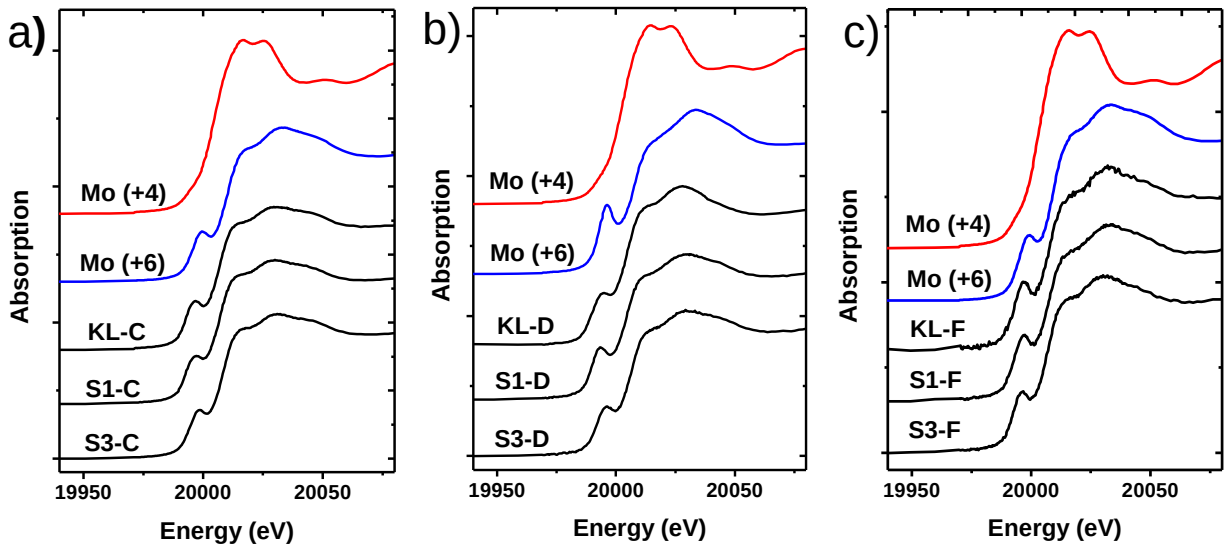

Figure 2-8. Mo K-edge XANES of bulk solid analysis indicate the redox state of solids from Key Lake (KL), Scenario 1 (S1), and Scenario 3 (S3): a) SeMo thickener (C; pH 4.2) b) Pachuca 3 (D; pH 6.5), and c) Lamella thickener (F; pH 9.2) samples with MoO_4 (Mo^{4+}) and $NiMoO_4$ (Mo^{6+}) standards.

Using a similar approach to that employed for the As K-edge EXAFS, PCA of Mo K-edge XANES determined the samples consisted of one major and three minor components, illustrated by plotting the calculated Eigenvectors (Figure 2-9).

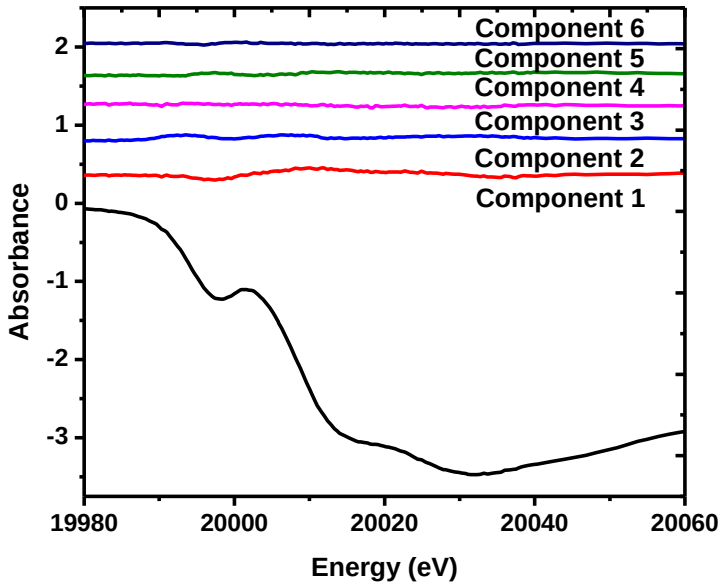

Figure 2-9. Results of principal component analysis (PCA) of the set of Mo K-edge spectra. Analysis using Athena's suite of programs, shown with Eigenvectors, indicates that normalized u(E) data from -20 to 80 (eV) can be made up of two major components and up to two minor components.

Target transforms of PCA with samples (n = 9) against each reference compound showed the best matches were molybdate adsorbed to ferrihydrite (Mo_Ferr), $NiMoO_4$ $CaMoO_4$, and $Fe_2(MoO_4)_3$ (data not included). LCF indicates samples at each pH stage can be made of varying ratios of the four reference compounds best matched by target transforms (Mo_Ferr, $Fe_2(MoO_4)_3$, $NiMoO_4$, $CaMoO_4$) of PCA, illustrated using superimposed data for scenario 1 (Figure 2-10). The precipitates in the Lamella thickener (pH 9.2) in scenario 1 best matched a combination of only Mo_Ferr and $NiMoO_4$ mineral phases (Figure 2-10a). Comparison of the sample spectra with the calculated fits for scenario 1 indicates the best fits occur at the pH 9.2 stage (S1-F); the fit for the pH 4.2 stage (S1-C) had the greatest residual (Figure 2-10b). The signal for the S1 pH 9.2 sample is dominated by Mo_Ferr (69%) with the remainder constituting $NiMoO_4$.

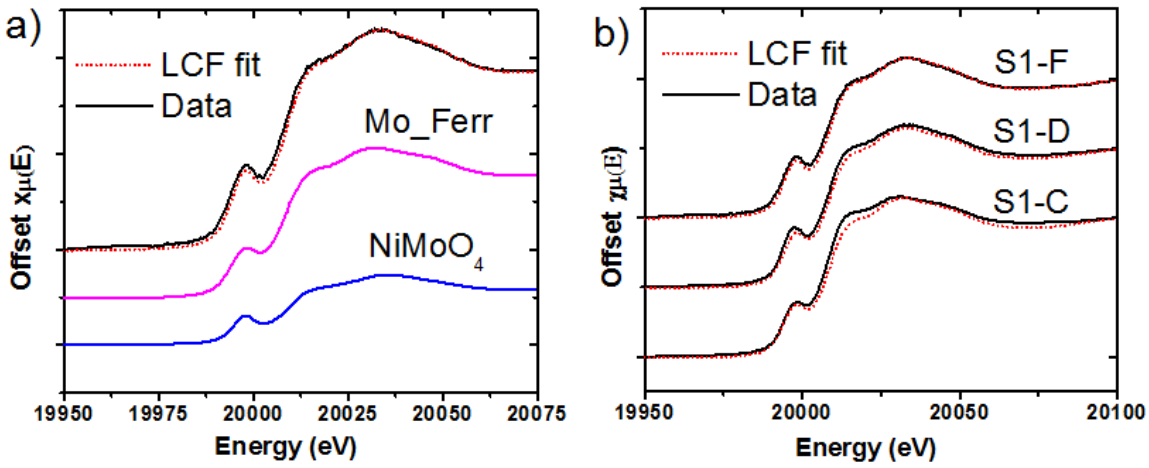

Figure 2-10. Linear combination fitting (LCF) for scenario 1 (S1) from Mo XANES spectra with reference compounds molybdate adsorbed to ferrihydrite (Mo_Ferr) and $NiMoO_4$ found in **a)** Lamella thickener (pH 9.2) with ratio of components from LCF (Table 2-2) and **b)** SeMo thickener (C; pH 4.2), Pachuca 3 (D; pH 6.5), and Lamella thickener (F; pH 9.2) offset for illustrative purposes.

Overall, combinations of Mo_Ferr, $Fe_2(MoO_4)_3$, $NiMoO_4$, and $CaMoO_4$ adequately explain the spectra for all Key Lake and LSP samples, with Mo_Ferr as the dominant mineral phase and ranging from 69 to 100% of the solids (

Table 2-4). Minor phases $Fe_2(MoO_4)_3$ and $CaMoO_4$ contributed lower ratios to the solids, mainly at the low pH 4.2 and 6.5 stages (KL-C, KL-D, S1P-C, S1P-D, and S3P-C). Samples matching $NiMoO_4$ spectra displayed an increasing contribution at higher pH values, whereas Mo_Ferr displayed a decreasing contribution with increasing pH for all scenarios. This confirmed the predictions based on thermodynamic modeling and previous studies of tailings in the DTMF (Essilfie-Dughan et al., 2011; Parkhurst and Appelo, 2013, 1999). In summary, the interpretation of XANES analyses indicates the dominant mineral phase controlling Mo in the secondary precipitates was Mo_Ferr, with minor contributions from $NiMoO_4$, $Fe_2(MoO_4)_3$, and $CaMoO_4$.

Table 2-4. Linear combination fits of Mo species in precipitates obtained from Key Lake (KL) and LSP samples for scenario 1 (S1) and scenario 3 (S3) using normalized μ(E) data in the energy range from 20 to 30 (eV) expressed as a fractional amount ± the estimated standard deviation as calculated by Athena.

Sample	Linear Combination Fitting*				Goodness-of-fit	
	Mo_Ferr	$Fe_2(MoO_4)_3$	$NiMoO_4$	$CaMoO_4$	Total	R-factor
	Key Lake (KL)					
C (pH 4.2)	1.00 (0.00)	0.00 (0.12)		0.00 (0.00)	1.00	0.0107
D (pH 6.5)	1.00 (0.21)	0.00 (0.18)		0.00 (0.12)	1.00	0.0206
F (pH 9.2)	0.79 (0.24)		0.21 (0.19)	0.00 (0.14)	1.00	0.0185
	Scenario 1 (S1)					
C (pH 4.2)	0.99 (0.11)	0.01 (0.09)		0.00 (0.06)	1.00	0.0066
D (pH 6.5)	0.87 (0.14)		0.13 (0.06)		1.00	0.0048
F (pH 9.2)	0.69 (0.09)		0.31 (0.04)		1.00	0.0026
	Scenario 3 (S3)					
C (pH 4.2)	0.84 (0.08)	0.16 (0.07)		0.00 (0.04)	1.00	0.0033
D (pH 6.5)	1.00 (0.04)		0.00 (0.04)		1.00	0.0009
F (pH 9.2)	0.93 (0.07)		0.07 (0.04)		1.00	0.0010

* Fit using the choice of reference compounds: molybdate adsorbed to ferrihydrite (Mo_Ferr), $Fe_2(MoO_4)_3$ $NiMoO_4$, $CaMoO_4$, and $FeMoO_4$. Phases were included at pH range most thermodynamically favourable to form and where inclusion improved the R-factors (goodness of fit).

Thus, the dominant phase for both As and Mo control in the secondary precipitates was determined to be adsorption to ferrihydrite. Adsorption of anions to the surface of ferrihydrite has been shown to slow conversion to crystalline forms of Fe oxides, such as goethite and hematite, when co-precipitation of mineral phases occurs (Das et al., 2014a, 2014b, 2011; Ford, 2002). As such, with the current environmental conditions in the DTMF (average pH 9.7, Eh +200 mV, temperature 1-2 °C; Shaw et al., 2011) and the incorporation of anions onto the Fe-oxide surface, ferrihydrite is not expected to transform to other crystalline phases (goethite and hematite) and should remain stable in the tailings for thousands of years.

2.5 Conclusion

Arsenic (As) and molybdenum (Mo) concentrations in uranium mine wastes have the potential to adversely impact local groundwater and surface water after tailings deposition. Characterization of the As- and Mo-bearing mineral phases formed during the bulk neutralization of mill wastes is critical to determining the long-term chemical stability of elements of concern in the tailings. The

greatest elemental concentrations of As and Mo in the solid phase exist in the first pH stage of neutralization (pH 4.2) and account for 99.9 and 98.0 % removal, respectively, from the solution phase. XAS results indicate that the majority of As exists as arsenate adsorbed to ferrihydrite in the +5 oxidation state, and Mo exists primarily as molybdate adsorbed to ferrihydrite in the +6 oxidation state. Other minor contributing mineral phases to the secondary precipitates include ferric arsenate, arsenate adsorbed to aluminum hydroxide sulfate, amorphous aluminum hydroxide and hydrotalcite, nickel molybdate, calcium molybdate, and ferrous molybdate. The As- and Mo-bearing mineral phases were pH dependant: ferric arsenates, arsenate adsorbed to aluminum hydroxide sulfate, calcium molybdate, and ferrous molybdate were observed at low pH (4.2 to 6.5) and arsenate adsorbed to ferrihydrite, amorphous aluminum hydroxide and hydrotalcite at high pH (9.2). Molybdate adsorbed to ferrihydrite had a decreasing contribution and nickel molybdate an increasing contribution with increasing pH. EXAFS data confirm that arsenate adsorbed to ferrihydrite in inner sphere bidentate linkages, regardless of pH or sample blend. These findings are in keeping with previously published U mill tailings studies. Adsorption of anions to the surface of ferrihydrite is important for As and Mo sequestration because it will retard conversion to more crystalline forms of iron oxides and the subsequent release of these anions. Given the current environmental conditions in the DTMF and the incorporation of anions onto the surface of ferrihydrite these precipitates in the tailings are expected to remain stable for thousands of years.

2.6 References

Adra, A., Morin, G., Ona-Nguema, G., Menguy, N., Maillot, F., Casiot, C., Bruneel, O., Lebrun, S., Juillot, F., Brest, J., 2013. Arsenic scavenging by aluminum-substituted ferrihydrites in a circumneutral pH river impacted by acid mine drainage. Environ. Sci. Technol. 47, 12784-12792. doi:10.1021/es4020234

Arai, Y., Elzinga, E.J., Sparks, D.L., 2001. X-ray absorption spectroscopic investigation of arsenite and arsenate adsorption at the aluminum oxide-water interface. J. Colloid Interface Sci. 235, 80–88. doi:10.1006/jcis.2000.7249

Bharadwaj, B., Moldovan, B.J., 2005. Cameco Corporation - the Key Lake uranium mill: current status and vision for the future, in: International Atomic Energy Agency (IAEA), Proceedings of an International Symposium: Uranium Production and Raw Materials for the Nuclear Fuel Cycle - Supply and Demand, Economics, the Environment and Energy Security. pp. 205–212.

Cameco, 2014. Annual Report: Key Lake Operation.

CCME, 2007. Canadian Environmental Quality Guidelines, Canadian Council of Ministers of the Environment. Ottawa. URL http://www.ccme.ca/en/resources/canadian_environmental_quality_guidelines/index.html

CCME, 1999a. Canadian Sediment Quality Guidelines for the Protection of Aquatic Life - Arsenic. In: Canadian environmental quality guidelines, Canadian Council of Ministers of the Environment. Winnipeg.

CCME, 1999b. Water Quality Guidelines for the Protection of Aquatic Life - Molybdenum, Canadian Council of Ministers of the Environment. URL http://st-ts.ccme.ca/en/index.html (accessed 11-03-15)

CCME, 1997. Canadian Environmental Quality Guidelines: Arsenic. Canadian Council of Ministers of the Environment. URL http://st-ts.ccme.ca/en/index.html (accessed 11-03-15)

Chen, N., Jiang, D.T., Cutler, J., Kotzer, T., Jia, Y.F., Demopoulos, G.P., Rowson, J.W., 2009. Structural characterization of poorly-crystalline scorodite, iron(III)–arsenate co-precipitates and uranium mill neutralized raffinate solids using X-ray absorption fine structure spectroscopy. Geochim. Cosmochim. Acta 73, 3260–3276. doi:10.1016/j.gca.2009.02.019

Cotelesage, J.J.H., Pushie, M.J., Grochulski, P., Pickering, I.J., George, G.N., 2012. Metalloprotein active site structure determination: Synergy between X-ray absorption spectroscopy and X-ray crystallography. J. Inorg. Biochem. 115, 127–137. doi:10.1016/j.jinorgbio.2012.06.019

Cutler, J.N., Chen, N., Jiang, D.T., Demopoulos, G.P., Jia, Y., Rowson, J.W., 2003. The nature of arsenic in uranium mill tailings by X-ray absorption spectroscopy. J. Phys. IV 107, 337–340.

Das, S., Essilfie-Dughan, J., Hendry, M.J., 2014a. Arsenate adsorption onto hematite nanoparticles under alkaline conditions: effects of aging. J. Nanoparticle Res. 16, 1–12. doi:10.1007/s11051-014-2490-3

Das, S., Essilfie-Dughan, J., Hendry, M.J., 2014b. Arsenate partitioning from ferrihydrite to hematite : Spectroscopic evidence. Am. Mineral. 99, 749–754.

Das, S., Hendry, M.J., Essilfie-Dughan, J., 2011. Transformation of two-line ferrihydrite to goethite and hematite as a function of pH and temperature. Environ. Sci. Technol. 45, 268–275. doi:10.1021/es101903y

DeKlerk, R.J. 2008. Investigating the Continuous Circuit Coprecipitation of Arsenic (V) with Ferric Iron in Suphate Media. M.Eng. Thesis, Department o fMining and Materials, McGill Univeristy, Montreal, QC.

DeKlerk, R.J., Jia, Y., Daenzer, R., Gomez, M.A., Demopoulos, G.P., 2008. Continuous circuit coprecipitation of arsenic(V) with ferric iron by lime neutralization: process parameter effects on arsenic removal and precipitate quality. Hydrometallurgy 111-112, 65-72.

Dixit, S., Hering, J.G., 2003. Comparison of arsenic(V) and arsenic(III) sorption onto iron oxide minerals: implications for arsenic mobility. Environ. Sci. Technol. 37, 4182–9.

Donahue, R., Hendry, M.., Landine, P., 2000. Distribution of arsenic and nickel in uranium mill tailings, Rabbit Lake, Saskatchewan, Canada. Appl. Geochemistry 15, 1097–1119. doi:10.1016/S0883-2927(99)00114-6

Donallson, E.M., 1981. Methods for the Analysis of Ores, Rocks and Related Minerals, 2nd ed. CANMET: Mines Branch, Department of Energy, Mines and Resources.

Essilfie-Dughan, J., Hendry, M.J., Warner, J., Kotzer, T., 2013. Arsenic and iron speciation in uranium mine tailings using X-ray absorption spectroscopy. Appl. Geochemistry 28, 11–18. doi:10.1016/j.apgeochem.2012.10.022

Essilfie-Dughan, J., Hendry, M.J., Warner, J., Kotzer, T., 2012. Microscale mineralogical characterization of As, Fe, and Ni in uranium mine tailings. Geochim. Cosmochim. Acta 96, 336–352. doi:10.1016/j.gca.2012.08.005

Essilfie-Dughan, J., Pickering, I.J., Hendry, M.J., George, G.N., Kotzer, T., 2011. Molybdenum speciation in uranium mine tailings using X-ray absorption spectroscopy. Environ. Sci. Technol. 45, 455–60. doi:10.1021/es102954b

Ford, R.G., 2002. Rates of hydrous ferric oxide crystallization and the influence on coprecipitated arsenate. Environ. Sci. Technol. 36, 2459–63.

Fritzsche, A., Rennert, T., Totsche, K.U., 2011. Arsenic strongly associates with ferrihydrite colloids formed in a soil effluent. Environ. Pollut. 159, 1398–1405. doi:10.1016/j.envpol.2011.01.001

Fukushi, K., Sverjensky, D. a., 2007. A predictive model (ETLM) for arsenate adsorption and surface speciation on oxides consistent with spectroscopic and theoretical molecular evidence. Geochim. Cosmochim. Acta 71, 3717–3745. doi:10.1016/j.gca.2007.05.018

Fuller, C.C., Davis, J.A., Waychunas, G.A., 1993. Surface chemistry of ferrihydrite : Part 2 . Kinetics of arsenate adsorption and coprecipitation . Geochim. Cosmochim. Acta 57(10), 2271-2282.

Goldberg, S., 2002. Competitive adsorption of arsenate and arsenite on oxides and clay minerals. Soil Sci. Soc. Am. J. 66, 413. doi:10.2136/sssaj2002.0413

Gomez, M.A., Hendry, M.J., Elouatik, S., Essilfie-Dughan, J., Paikaray, S., 2014. Fe(II) (aq) uptake of Mg(II)–Al(III)/Fe(III)–SO_4/CO_3 HTLCs under alkaline conditions: adsorption and solid state transformation mechanisms. RSC Adv. 4, 54973–54988. doi:10.1039/C4RA08802F

Gomez, M.A., Hendry, M.J., Koshinsky, J., Essilfie-Dughan, J., Paikaray, S., Chen, J., 2013a. Mineralogical controls on aluminum and magnesium in uranium mill tailings: Key Lake, Saskatchewan, Canada. Environ. Sci. Technol. 47, 7883–91. doi:10.1021/es400658f

Gomez, M.A., Jim Hendry, M., Hossain, A., Das, S., Elouatik, S., 2013b. Abiotic reduction of 2-line ferrihydrite: effects on adsorbed arsenate, molybdate, and nickel. RSC Adv. 3, 25812. doi:10.1039/c3ra44769c

Heinrich, G., Kyser, K., Chipley, D., Lam, E., 2010. The determination of selenium and molybdenum distribution in uranium ore and mill solids, in: Lam, E.K., Rowson, J.W., Ozberk, E. (Eds.), Proceedings of the 3rd International Conference on Uranium (Uranium 2010). Canadian Institute of Mining, Metallurgy and Petroleum, Westmont, p. 609.

Hossain, M.A., 2014. Mineralogical Characterization of Uranium Ores, Blends and Resulting Leach Residues from Key Lake Pilot Plant, Saskatchewan, Canada. MSc Thesis, Department of Geological Sciences, University of Saskatchewan.

Jia, Y., Demopolous, G.P., Chen, N., Cutler, J., 2005. Coprecipitation of As(V) with Fe(III) in sulfate media: solubility and speciation of arsenic, in: Reddy, R.G., Ramachandran, V.S. (Eds.), Arsenic Metallurgy. 2005 TMS Annual Meeting, San Fransisco, pp. 137–148.

Jia, Y., Xu, L., Fang, Z., Demopoulos, G.P., 2006. Observation of surface precipitation of arsenate on ferrihydrite. Environ. Sci. Technol. 40, 3248–53.

Jia, Y., Xu, L., Wang, X., Demopoulos, G.P., 2007. Infrared spectroscopic and X-ray diffraction characterization of the nature of adsorbed arsenate on ferrihydrite. Geochim. Cosmochim. Acta 71, 1643–1654.

Langmuir, D., Mahoney, J., MacDonald, A., Rowson, J., 1999. Predicting arsenic concentrations in the porewaters of buried uranium mill tailings. Geochim. Cosmochim. Acta 63, 3379–3394. doi:10.1016/S0016-7037(99)00259-8

Langmuir, D., Mahoney, J., Rowson, J., 2006. Solubility products of amorphous ferric arsenate and crystalline scorodite ($FeAsO_4 \cdot 2H_2O$) and their application to arsenic behavior in buried mine tailings. Geochim. Cosmochim. Acta 70, 2942–2956. doi:10.1016/j.gca.2006.03.006

Lieu, A., Bissonnette, J., Hossain, A.M., Essilfie-Dughan, J., Moldovan, B.J., Hendry, M.J., 2015. Simulating the mineral process at the Key Lake uranium mill, northern Saskatchewan, Canada in a lab-scale plant. Submitted to Hydrometallurgy.

Lieu, A., Zheng, J., Moldovan, B., Ko, K., Jarvi, J., Saruchera, T., Bergbusch, P., Paulsen, K., Tremblay, M., Bharadwaj, B., 2010. Selenium and Molybdenum Removal from Contaminated Mill Process

Effluent: Cameco Key Lake Operation, in: Lam, E.K., Rowson, J.W., Ozberk, E. (Eds.), Proceedings of the 3rd International Conference on Uranium (Uranium 2010). Canadian Institute of Mining, Metallurgy and Petroleum, Westmont, pp. 749–759.

Longerich, H., Jenner, G., Fryer, B., Jackson, S., 1990. Inductively coupled plasma-mass spectrometric analysis of geological samples: A critical evaluation based on case studies. Chem. Geol. 83, 105–118. doi:10.1016/0009-2541(90)90143-U

Mahoney, J., Langmuir, D., Gosselin, N., Rowson, J., 2005. Arsenic readily released to pore waters from buried mill tailings. Appl. Geochemistry 20, 947–959. doi:10.1016/j.apgeochem.2004.11.012

Mahoney, J., Slaughter, M., Langmuir, D., Rowson, J., 2007. Control of As and Ni releases from a uranium mill tailings neutralization circuit: Solution chemistry, mineralogy and geochemical modeling of laboratory study results. Appl. Geochemistry 22, 2758–2776. doi:10.1016/j.apgeochem.2007.06.021

Moldovan, B.J., Hendry, M.J., 2005. Characterizing and quantilying controls on arsenic solubility over a pH range of 1-11 in a uranium mill-scale experiment. Environ. Sci. Technol. 39, 4913–4920.

Moldovan, B.J., Jiang, D.T., Hendry, M.J., 2003. Mineralogical characterization of arsenic in uranium mine tailings precipitated from iron-rich hydrometallurgical solutions. Environ. Sci. Technol. 37, 873–879.

Moldovan, B.J., Hendry, M.J., Harrington, G.A., 2008. The arsenic source term for an in-pit uranium mine tailings facility and its long-term impact on the regional groundwater. Appl. Geochemistry 23, 1437–1450. doi:10.1016/j.apgeochem.2007.12.037

Newville, M., 2001. IFEFFIT: interactive EXAFS analysis and FEFF fitting. J. Synchrotron Radiat. 8, 322–324.

Paikaray, S., Hendry, M.J., 2014. Formation and crystallization of $Mg(^{2+})$-$Fe(^{3+})$-$SO_4(^{2-})$-$CO_3(^{2-})$-type anionic clays. Appl. Clay Sci. 88-89, 111–122. doi:10.1016/j.clay.2013.11.034

Paikaray, S., Hendry, M.J., 2013. In situ incorporation of arsenic, molybdenum, and selenium during precipitation of hydrotalcite-like layered double hydroxides. Appl. Clay Sci. 77-78, 33–39. doi:10.1016/j.clay.2013.03.016

Paikaray, S., Hendry, M.J., Essilfie-Dughan, J., 2013. Controls on arsenate, molybdate, and selenate uptake by hydrotalcite-like layered double hydroxides. Chem. Geol. 345, 130–138. doi:10.1016/j.chemgeo.2013.02.015

Paktunc, D., Bruggeman, K., 2010. Solubility of nanocrystalline scorodite and amorphous ferric arsenate: Implications for stabilization of arsenic in mine wastes. Appl. Geochem. 25, 674–683. doi:10.1016/j.apgeochem.2010.01.021

Parkhurst, D.L., Appelo, C.A.J., 2013. Description of input and examples for PHREEQC version 3–A computer program for speciation, batch-reaction, one-dimensional transport, and inverse geochemical calculations: U.S. Geological Survey Techniques and Methods, book 6, chap. A43, 497p., available only at http://pubs.usgs.gov/tm/06/a43/.

Parkhurst, D.L., Appelo, C.A.J., 1999. User's guide to PHREEQC (Version 2) - A computer program for speciation, batch-reaction, one-dimensional transport, and inverse geochemical calulations. Water-Resource Investig. Rep. 99-4259.

Pichler, T., Hendry, M.J., Hall, G.E.M., 2001. The mineralogy of arsenic in uranium mine tailings at the Rabbit Lake In-pit Facility, northern Saskatchewan, Canada. Environ. Geol. 40, 495–506.

Ravel, B., 2001. ATOMS: crystallography for the X-ray absorption spectroscopist. J. Synchrotron Radiat. 8, 314–316.

Ravel, B., Newville, M., 2005. ATHENA, ARTEMIS, HEPHAESTUS: data analysis for x-ray absorption spectroscopy using IFEFFIT. J. Synchrotron Radiat. 12, 537–541.

Raven, K.P., Jain, A., Loeppert, R.H., 1998. Arsenite and arsenate adsorption on ferrihydrite: kinetics, equilibrium, and adsorption envelopes. Environ. Sci. Technol. 32, 344–349. doi:10.1021/es970421p

Rehr, J., 1995. Feff Project: Ab initio Multiple-Scattering X-ray Absorption Fine Structure and X-ray Absorption Near Edge Structure Code Copyright 1992, 1993.

Robertson, J., Hendry, M.J., Essilfie-Dughan, J., Chen, J., 2015. Precipitation of aluminum and magnesium secondary minerals from uranium mill raffinate (pH 1.0-10.5) and their controls on aqueous contaminants. Appl. Geochem. *in press*. doi:10.1016/j.apgeochem.2015.09.002

Robertson, J., Shacklock, K., Frey, R., Gomez, M.A., Essilfie-Dughan, J., Hendry, M.J., 2014. Modeling the Key Lake uranium mill's bulk neutralization process using a pilot-scale model. Hydrometallurgy 149, 210–219. doi:10.1016/j.hydromet.2014.08.010

Schwertmann, U., Cornell, R.M., 1991. Iron Oxides in the Laboratory. VCH Verlagsgesellschaft mbH & VCH Publishers, Inc, Weinheim.

Shaw, S.A., Hendry, M.J., Wallschläger, D., Kotzer, T., Essilfie-Dughan, J., 2011. Distribution, characterization, and geochemical controls of elements of concern in uranium mine tailings, Key Lake, Saskatchewan, Canada. Appl. Geochem. 26, 2044–2056. doi:10.1016/j.apgeochem.2011.07.002

Stefanova, V., Kmetov, V., Canals, a., 2003. Application of internal standardization in ICP-QMS through discrete sample introduction methodologies. J. Anal. At. Spectrom. 18, 1171. doi:10.1039/b301809a

Stipp, S.L.S., Hansen, M., Kristensen, R., Hochella Jr, M.F., Bennedsen, L., Dideriksen, K., Balic-Zunic, T., Leonard, D., Mathieu, H.-J. 2002. Behaviour of Fe-oxides relevant to contaminant uptake in the environment. Chem. Geol. 190(1-4), 321–337.

Takeno, N., 2005. Atlas of Eh-pH diagrams. Intercomparison of thermodynamic databases: Geological Survey of Japan Open File Report No.419.

Twidwell, L.G., Robins, R.G., Hohn, J.W., 2005. The removal of arsenic from aqueous solution by coprecipitation with iron (III), in: Reddy, R.G., Ramachandran, V.S. (Eds.), Arsenic Metallurgy. 2005 TMS Annual Meeting, San Fransisco.

US EPA, 1987. Standards for Remedial Actions at Inactive Uranium Processing Sites, Federal Register, 40 CFR Part 192. U.S. Environmental Protection Agency.

US EPA, 1995. Aquatic Life Criteria Table: National Recommended Water Quality Criteria [WWW Document]. Sect. 304(a) Clean Water Act. URL http://water.epa.gov/scitech/swguidance/standards/criteria/current/index.cfm (accessed 6.1.15).

Waychunas, G.A., Kim, C.S., Banfield, J.F., 2005. Nanoparticulate iron oxide minerals in soils and sediments: unique properties and contaminant scavenging mechanisms. J. Nanoparticle Res. 7, 409–433. doi:10.1007/s11051-005-6931-x

Waychunas, G.A., Rea, B.A., Fuller, C.C., Davis, J.A., 1993. Surface chemistry of ferrihydrite: Part 1. EXAFS studies of the geometry of coprecipitated and adsorbed arsenate. Geochim. Cosmochim. Acta 57, 2251–2269. doi:10.1016/0016-7037(93)90567-G

Wharton, J.A., Ross, D.H., Treacy, G.M., Wilcox, G.D., Baldwin, K.R., 2003. An EXAFS investigation of molybdate-based conversion coatings. J. Appl. Electrochem. 33, 553–561. doi:10.1023/A:1024911119051

WHO, 1993a. Guidelines for Canadian Drinking Water Quality: Water Treatment Principles and Applications: a Manual for the Production of Drinking Water. World Health Organization, Geneva.

WHO, 1993b. International Program on Chemical Safety Guidelines: Guidelines for Drinking-Water Quality, 2nd ed. World Health Organization, Geneva.

Wilkie, J.A., Hering, J.G., 1996. Adsorption of arsenic onto hydrous ferric oxide: effects of adsorbate/adsorbent ratios and co-occuring solutes. Colloids Surfaces A Physicochem. Eng. Asp. 107, 97–110.

3.0 Geochemical Modeling of As and Mo Sequestration during the Bulk Neutralization of Fe-, Al-, and Mg-rich Uranium Mill Wastes (pH 1.5-10.5)

3.1 Abstract

As and Mo are observed to be controlled by adsorption to both Fe and Al oxyhydroxide surfaces as well as by direct precipitation with other dissolved constituents (Ni, Ca and SO_4) in the U mill bulk neutralization process. These precipitated mineral phases require thermodynamic solubility characterization for predicting source terms for their stability in tailings facilities. A geochemical model describing the evolution of the pH and the precipitation/dissolution of known secondary mineral phases on the solubility of As, Mo, Fe, Al, Mg and Ni from the bulk neutralization U mill wastes was studied in a physical lab-scale model of the Key Lake U milling process. Overall, As and Mo were controlled by adsorption to ferrihydrite surfaces and were effectively removed from solution by pH 4. With adsorption as well as direct precipitation considered, As remains sequestered in the ferrihydrite and exhibits no evidence of dissolution in the tailings porewater (pH > 10). Molybdenum phases though effectively sequestering below pH 8, with 98 % removal by pH 4, became unstable and released Mo into the tailings porewater. These results are consistent with historical mill data from the Key Lake mill and previous U mill tailings studies.

3.2 Introduction

Uranium (U) milling in the Athabasca basin, in northern Saskatchewan, Canada accounts for about 15% of the world's supply of U energy (http://www.cameco.com/). The U milling process at Cameco's Key Lake operation, located in this region, produces waste effluent (raffinate) that contains elevated concentrations of elements of concern (EOCs) that include arsenic (As) and molybdenum (Mo). The possible migration of these elements from tailings facilities to local groundwater and surface water is of global concern. To reduce the concentration of these EOCs in the aqueous phase to environmentally acceptable levels, the current practice at the Key Lake mill is to neutralize the raffinate to alkaline pH resulting in the precipitation of secondary mineral phases that contain the EOCs. After the precipitation of these EOCs, the precipitated solids are discharged from the mill as tailings. Maintaining low levels of As and Mo in the tailings pore water is critical to establishing their long-term stability in the U mill tailings facilities. Since the mobility,

toxicity and bioavailability of these EOCs are a function of the chemical form or speciation, pH profiles of the aqueous species formed at each step in the raffinate neutralization process are necessary to determine the mineral phases that will be present in the resulting tailings.

The toxicity of As is well documented (Eisler, 1988; U.S. EPA, 1998; Harvey et al., 2002; Ngai, 2002; Wang and Mulligan, 2006; Liber et al., 2011) and freshwater quality guidelines established (chronic As = 150 mg/L, acute As = 340 µg/L: U.S. EPA, 1995; As = 5ug/L; CCME, 1999a, 1997) Although the toxicity levels of Mo has been measured in aquatic systems (Eisler, 1989; Das et al., 2007; Liber et al., 2011) and the protection of aquatic life in freshwater has been established in Canada (Mo = 73 µg/L; CCME, 1999b; CCME, 2007), guidelines have not been published by the US EPA due to rare occurrences, except for a proposed groundwater standard for inactive U sites (Mo = 100 µg/L; U.S. EPA, 1987). In groundwater systems, both oxidation state and pH play roles in defining As solubility, mobility and toxicity (Goldberg, 2002; Korte and Fernando, 1991; Masscheleyn, 1991). It occurs primarily as arsenite (As^{3+}) and arsenate (As^{5+}), with arsenite being more toxic and mobile than the oxidized arsenate form (Cullen and Reimer, 1989; Korte and Fernando, 1991). Though oxidation states from -2 to +6 are possible for Mo species, the most stable form in oxygenated waters is molybdate (Mo^{+6}) where the MoO_4^{2-} anion has been reported to interact weakly with suspended particulates (Das et al., 2007).

Although the mineral species in the Deilmann Tailings Management Facility (DTMF) at Key Lake operation are well characterized (Essilfie-Dughan et al., 2011; Shaw et al., 2011; Essilfie-Dughan et al., 2012; Essilfie-Dughan et al., 2013; Gomez et al., 2013; Robertson et al., 2014), As and Mo sequestration during the bulk neutralization of mill wastes remain largely undetermined. To date, studies by Gomez et al. (2013) and Essilfie-Dughan et al. (2013) used geochemical modelling to describe the sequestration of EOCs in the DTMF and Robertson et al., 2014 used geochemical modelling to describe synthetic raffinate neutralization circuits in a continuous flow lab-scale model of the Key Lake process. Geochemical modelling has not, however been used to define the evolution of As and Mo in secondary minerals in ore deposits currently being milled in the Key Lake mill and in potential future ore deposits being considered. Characterization of the evolution of the precipitation of secondary mineral phases during BN of raffinate is critical to determine the long-term stability of As- and Mo-bearing phases and the potential migration of aqueous species within the tailings facility. The objectives of this study were to: (i) identify the As- and Mo- bearing

secondary mineral phases predicted to form during the neutralization of raffinate solutions during the neutralization of U mill wastes from pH 1.5 to 10.5, (ii) develop a geochemical model that describes the solubility of As and Mo during sequestration and iii) use this model to predict long term stability of As- and Mo- bearing mineral phases in the tailings, independent of mill feed ore used.

The objectives were met by studying the solubility of As, Mo, Fe, Al, Mg and Ni in a full mill laboratory-scale plant (LSP) study at the Key Lake mill, using comparisons of geochemical models to aqueous and precipitate analysis obtained from three scenarios of ore blends and actual Key Lake mill analysis described in Section 2.0. The full LSP included each step of the mill from grinding, leaching, counter-current decantation, and solvent extraction to bulk neutralization and tailings, and was determined to be a valid representation of the Key Lake mill by comparison of mill performance indicators and effluent quality (Lieu et al., 2015). Three U ore blends were created from current and potential ore deposits being considered; McArthur River (McA) and Millennium (MLM). Each ore blend was processed through the LSP mill resulting in the generation of raffinate that was subsequently neutralized to yield precipitates that replicate those produced in the Key Lake bulk neutralization circuit. For this reason, samples were also obtained from the current Key Lake circuit for comparison. Solid and solution data were used as inputs in the geochemical modelling programs Geochemist's Workbench® and PHREEQCI for the purpose of studying the geochemical controls of each scenario in the LSP model (Bethke, 1998; Parkhurst and Appelo, 1999; Parkhurst and Appelo, 2013).

3.3 Site Description and Bulk Neutralization Process

Key Lake mill is located in northern Saskatchewan, Canada (57°11'N, 105°34'W). The mill currently processes ore from McArthur River (McA) deposits, located approximately 80 km north of Key Lake. A new deposit, Millennium (MLM), located approximately 35 km north of Key Lake and 35 km southwest of McA is being considered for mining and could also potentially be milled at the Key Lake mill in the future (Cloutier et al., 2009). These U ore deposits contain some of the highest U concentrations in the world with ore grades up to 21 % (McA) and 4.5 % (MLM) (w/w) U_3O_8, and subsequently must be blended down with low grade U-bearing ore material (0.25% U3O8) before milling (Jamieson and Frost, 1997; Cloutier et al., 2009; Essilfie-Dughan et al., 2013). The low grade U-bearing materials contribute elevated concentrations of As and Mo to the

milling process (Hossain et al., 2014). The previously mined-out open pit at Key Lake was converted to the Deilmann Tailings Management Facility (DTMF) to house the tailings generated by the mill. Details of the site characteristics of the DTMF have been previously published (Shaw et al., 2011).

The Key Lake mill uses a sulfuric acid leach process (H_2SO_4) that dissolves the host rock with oxygen and steam. This acidic leachate reports to the counter current decantation process, where the U-bearing solution is separated from the leach residue materials. This solution reports to the solvent extraction circuit where tertiary amines are used to sequester the U in solution from other dissolved elements. The sequestered U rich solution continues on to precipitation and preparation for the final product (U_3O_8), while the U barren waste (raffinate) solution containing elevated concentrations of other un-targeted elements that were dissolved in the leaching process, reports to the mill effluent treatment process called bulk neutralization (BN). Multiple waste streams such as raffinate and tailings run-off (reservoir 1 and reservoir 2) are combined in the BN circuit before treatment with $Ca(OH)_2$ (slaked lime) and $BaCl_2$ to alkaline pH. The BN process generates precipitates during the pH adjustment with lime. These precipitates are combined with other tailings materials (including leach residues) before being discharged into the DTMF.

3.4 Materials and Methods

3.4.1 Modeling the Lab-Scale Plant after the Key Lake Process

The BN LSP was created to replicate the Key Lake mill process, in a continuous flow system 1/311,059 times the original mill (Figure 3-1). Characterization of As- and Mo- bearing minerals phases in the BN circuit was completed using the LSP; that was developed to model the Key Lake process. Slurry samples were collected from sample points A to G from the BN circuit at the Key Lake mill (Figure 3-2) to provide baseline for comparison to the LSP model (Figure 3-1).

For the LSP study, three blends of ores being considered for processing through the Key Lake mill were created from the current ore being processed, McA and potential deposit, MLM which were blended down with low grade U-bearing ore. The mineralogy of these ores were characterized by Hossain (2014) and described by Lieu et al. (2015). The blends were created to determine whether different ore materials would have an impact on the formation of secondary mineral phases of EOCs that constitute the final tailings. The design and operation of the full LSP and processing of ore blended scenarios are presented in detail in Appendix A. After processing, the three ore blends

were processed through the leaching, counter-current decantation, and solvent extraction circuits, the waste solutions (raffinate, reservoir 1 and reservoir 2) were combined and processed through the BN circuit as the raffinate feed. The raffinate feed (using 7.6 L raffinate, 7.6 L reservoir 1 and 12.1 L of reservoir 2) was pumped from position A into the first reaction vessel (B) where control pumps delivered slaked lime in batch mode until the target set point of 3.5 was achieved (Figure 3-1). With the addition of flocculant and overhead stirring, continuous mode began with B overflow to the Lamella thickener (C) at a raffinate feed flow rate of 14.5 mL/min (Figure 3-1). Solids were collected in the first thickener while the overflow from C was directed to the second reaction vessel (D) that was also controlled with pH pumps to a target of pH 6.5 with lime (Figure 3-1). D overflowed to the final reaction vessel (E) set with the same to a target of pH 9.5, where the overflow was collected into the Lamella thickener (F) (Figure 3-1). Here the settling slurry was separated from the overflow that was collected at final effluent. Slurries from each thickener, C and F, were combined into the final tailings composite (G), sampled and then brought to pH 10.5 with lime and addition of $BaCl_2$ to aid the precipitation of radium (Figure 3-1).

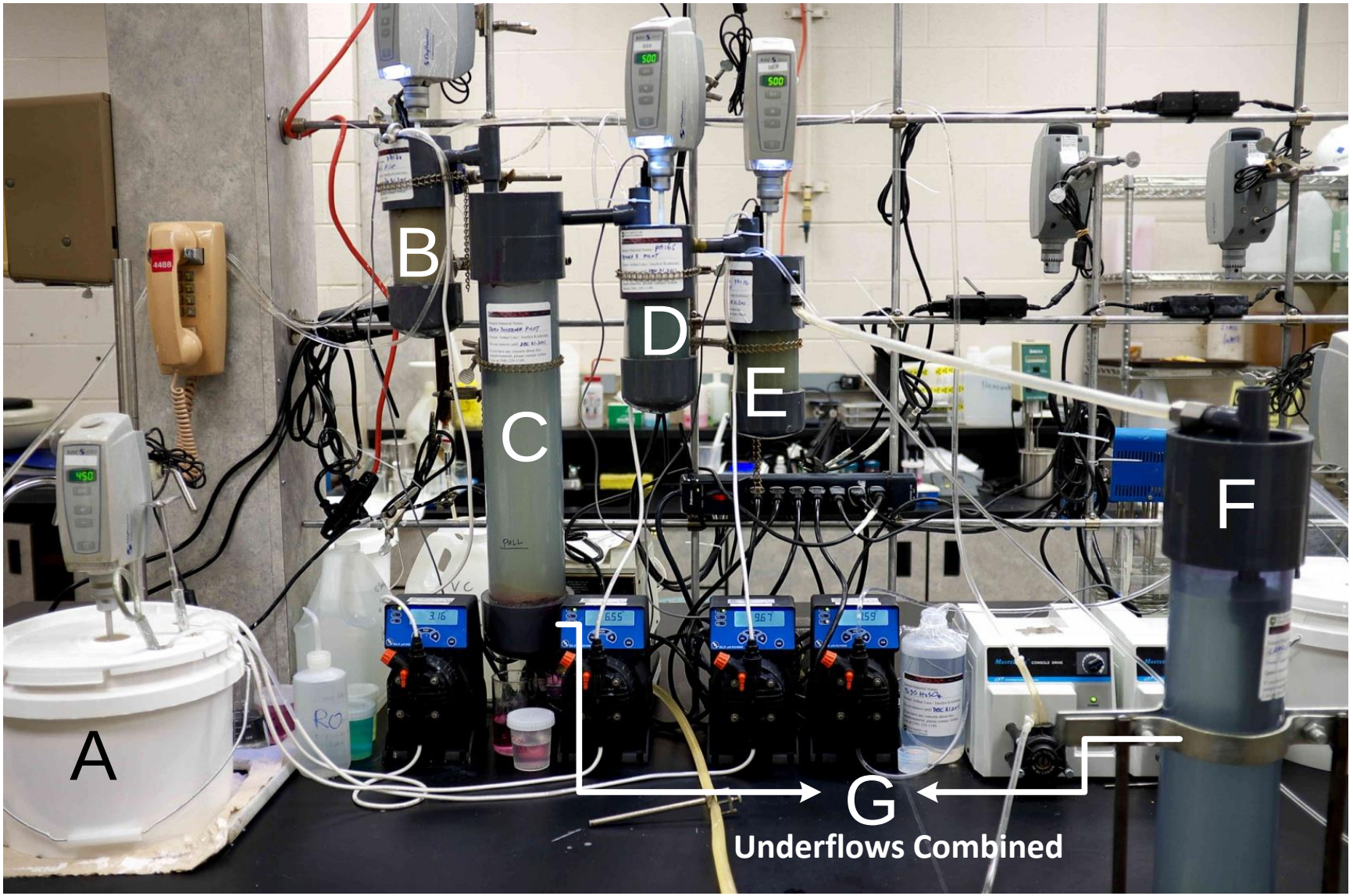

Figure 3-1. The LSP mill experiment with sample locations corresponding to Key Lake circuit (Fig. 3-2).

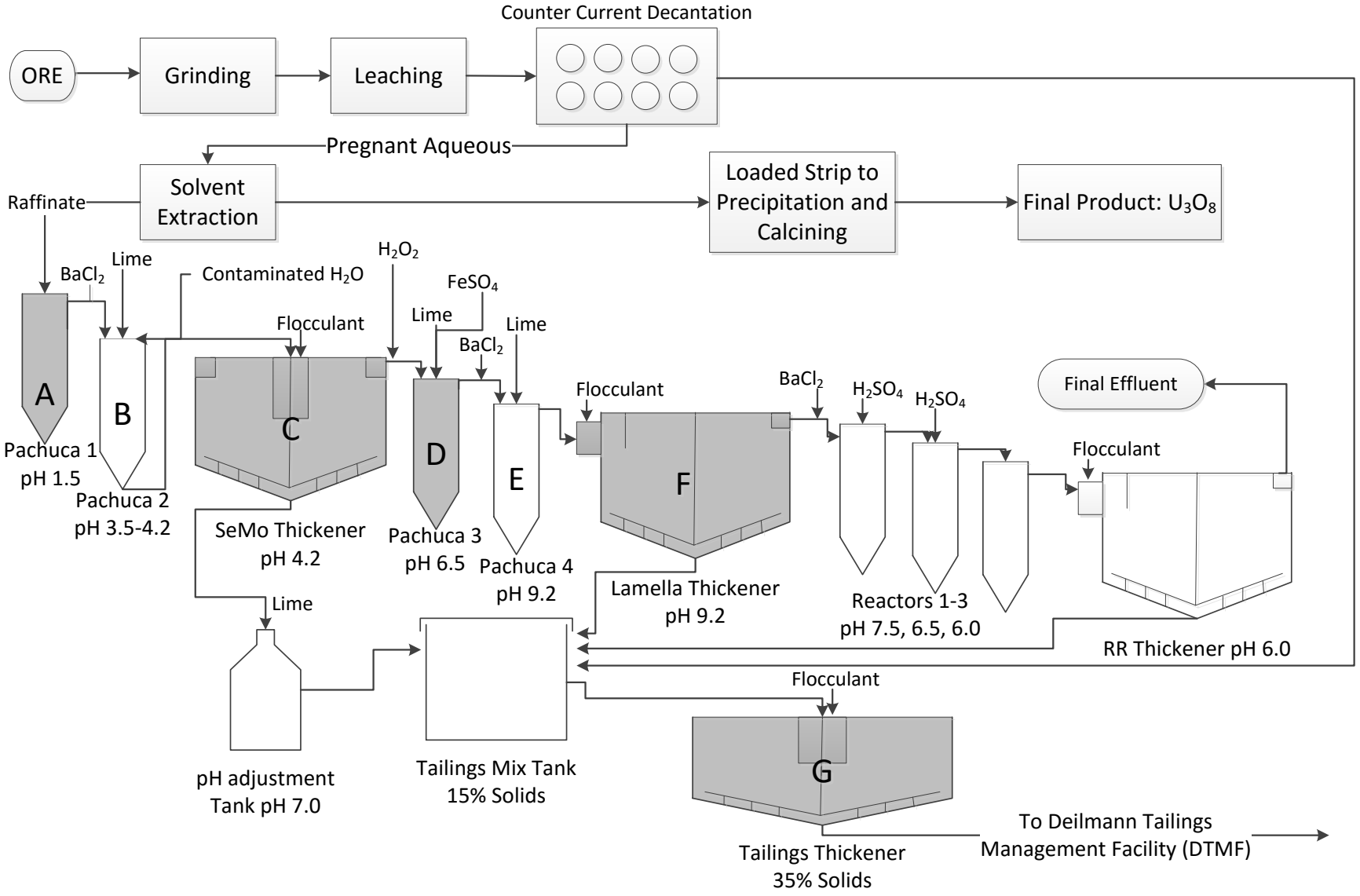

Figure 3-2. The Key Lake mill experiment with sample locations (grey-filled).

3.4.2 Sample Preparation and Solution Analysis

Slurry samples were collected from the bottom of the SeMo and Lamella thickener vessels from a valve attached to a 1.27 cm (½ inch) PVC tube for sampling. Pachuca 3 samples were collected using a syringe during stirring. Thickener samples were mixed thoroughly in a 20L pail, weighed and then 500 mL samples were collected for aqueous and solid analysis. Slurries were vacuum filtered through Watman No. 3 filter paper, with untreated solutions analyzed immediately for pH, Eh and conductivity using ASTM methods (Table 3-1) (ASTM, 1995; APHA et al., 2012a; APHA et al., 2012b; APHA et al., 2012c). The pH was measured using a Beckman Coulter Phi510 meter equipped with an epoxy gel probe and temperature (ATP) probe compensation, calibrated daily with pH 4.00±0.08, 7.00±0.14, and 10.00±0.2. Eh values were measured using a Beckman ORP (Eh) meter equipped with a KCl/AgCl electrode, calibrated weekly with a 1 g/100 mL quinhydrone standard (462±46.2 mV) standard at 25 °C, and converted to the standard hydrogen electrode. Conductivity was measured using a YSI 3200 conductivity meter equipped with a YSI 3245 platinum electrode calibrated weekly with a 10M KCl standard (1412±141.2 uS/cm). Solution samples were separated into untreated portions for anion analysis by IC and a HNO_3 treated portions for total metal analysis by ICP-MS. Solids were left to dry at ambient conditions after filtration.

3.4.2.1 IC

Ion Chromatography (IC) analyses was conducted on untreated solution samples (N = 20) at the Key Lake chemistry laboratory using a Dionex ICS-2000 equipped with an AS40 autosampler. Five-point calibration (R^2> 0.9995) was performed daily with the following dissolved anions Cl^- (MDL < 0.1± 0.01 mg/L), NO_2^-, NO_3^- (MDL < 0.01±0.02 mg/L), and SO_4^{2-} (MDL < 0.1±0.01 mg/L).

3.4.2.2 ICP-MS

Bulk elemental analysis by inductively coupled plasma mass spectrometry (ICP-MS) was performed at the Key Lake chemistry lab with duplicates sent to the Aqueous and Environmental Laboratory (AEL), Department of Geological Sciences, University of Saskatchewan for comparison. Solution samples (N = 20) were analyzed on HNO_3 treated splits. Analyses at the Key Lake chemistry lab were performed on an Agilent 7500cx and 7700 equipped with an ASX–500

series sample changer, with a relative standard deviation (RSD) of ±10%, and duplicates on a Perkin-Elmer NexION 300D (RSD ±10%) at the AEL.

3.4.3 Thermodynamic Modelling

Stability field diagrams of Fe-As, Al-As and Fe-Mo systems were created in Geochemist's Workbench® (GWB) using Eh and pH data from Key Lake and LSP analysis and activity coefficients based on solution chemistry calculations (Bethke, 1998; Moldovan and Hendry, 2005; Shaw et al., 2011). Thermodynamic modelling was used to simulate the precipitation of secondary mineral phases of Mg, Al, Fe, Ca, Ni, S and SiO_2 in the mill during a stepwise neutralization of the raffinate feed solution (pH 1.5 to 10.5 in 0.5 pH steps) with $Ca(OH)_2$. Total solution chemistry was then compared to model calculations of pH dependent neutralization experiments using PHREEQCI, version 3.1.5-9113 (Parkhurst and Appelo, 2005, 1999). Total concentrations for BN aqueous samples were used as model inputs for successive continuous flow calculations. Measured pH and Eh (as pE) were included in calculations with temperature measured from Key Lake mill (Raffinate = 47.2, Reservoir water 17.9, Pachuca 2 = 25.0, SeMo thickener 28.5, Pachuca 3 = 29.9 Pachuca 4 = 29.5 and Lamella thickener = 29.9 °C). The SO_4^- ion was used to compensate for charge imbalances until a percent error < 3 was achieved [(Cat-An)/(Cat+An)*100]. The results of the ICPMS and IC analysis of aqueous samples were used to calculate the charge balances (Equation 3-1) to determine analysis quality (Fritz, 1994).

$$\left(\frac{\sum(Z{\cdot}mc)-\sum(Z{\cdot}ma)}{\sum(Z{\cdot}mc)+\sum(Z{\cdot}ma)}\right)\times 100/_2 \qquad (3-1)$$

Where Z = molar mass, mc = molality of cation and mc = molality of anion.

The Lawrence Livermore National Laboratory (llnd) database was used with modifications as per Essilfie-Dughan et al. (2012) and Gomez et al. (2013) for simulations without equilibrium phases specified. Simulations with the modified llnl database were used to develop the modified minteq.v4 database with thermodynamic data for hydrotalcite (Rozov et al., 2010; Gomez et al., 2013), ferric arsenates (Essilfie-Dughan et al., 2012), scorodite (Dzombak and Morel, 1990; Moldovan and Hendry, 2005) amorphous scorodite, ferrihydrite (Robertson et al., 2014) and aluminum hydroxides and basaluminates (Essilfie-Dughan et al., 2012). Surface complexation site

parameters for ferrihydrite (hydrous ferric oxides, Hfo) and alumina (hydr)oxides (alumina) previously reported by Goldberg (2002), Moldovan and Hendry, (2005) and Robertson et al., (2014) were also included (Table 3-2). The calculations employed the Dzombak & Morel double diffuse layer (DDL) model with 5.34 x 10^4 m^2/mol, 0.005 site/mole strong sites and 0.2 sites/mol weak sites for adsorption to ferrihydrite, and 660 m^2/mol with 2.31 sites/nm^2 for adsorption to aluminum oxides surfaces (Goldberg, 2002; Moldovan and Hendry, 2005; Robertson et al., 2014).

Table 3-1. Thermodynamic data for species added to the modified minteq.v4 database used in PHREEQC Modeling.

Reaction	**log K**
Hydrotalcites	
$Mg_4Al_2O_{17}H_2O + 14H^+ = 2Al^{3+} + 17H_2O + 4Mg^{2+}$	75.34 [a]
$Mg_4Al(OH)10(CO_3)_{0.5}\bullet 2.5H_2O + 10H^+ = Al^{3+} + 0.5CO_3^{2-} + 4Mg^{2+} + 12.5\ H_2O$	67.5 [d]
$Mg_4Al(OH)10(SO_4)_{0.5}\bullet 2.5H_2O + 10H^+ = Al^{3+} + 0.5SO_4^{2-} + 4Mg^{2+} + 12.5\ H_2O$	66.0 [d]
Ferric Arsenate	
$Fe^{3+} + AsO_4^{3-} = FeAsO_4$	19.0 [e]
Scorodite	
$Fe^{3+} + AsO_4^{3-} + 2H_2O = FeAsO_4\bullet 2H_2O$	21.69 [b]
Amorphous Scorodite	
$Fe^{3+} + H_2AsO_4^- + 2H_2O = FeAsO_4\bullet 2H_2O + 2H^+$	4.538 [c]
Ferrihydrite	
$Fe^{3+} + 3H_2O = Fe(OH)_3(a) + 3H^+$	-3.191 [b]
Aluminum hydroxide(sulfate)	
$Al(OH)_3(a) + 3H^+ = Al^{3+} + 3H_2O$	10.8 [e]
$AlOHSO_4 + H^+ = Al^{3+} + SO_4^{2-} + H_2O$	-3.23[e]
Basaluminites	
$Al_4(OH)_{10}SO_4 + 10H^+ = 4Al^{3+} + SO_4^{2-} + 10H_2O$	22.7

[a] From HATCHES (HArweell/Nirex Thermodynamic Database for Chemical Equilibrium Studies) version NEA19
[b] From the PHREEQC database
[c] From http://thermoddem.brgm.fr/fichiers/gwb_lv1_thermodem_lvl1_no-org_15dec11.txt
[d] Rozov et al., 2010
[e] From the modified Lawrence Livermore National Library (llnl) database (Essilfie-Dughan et al., 2012)
(a) = amorphous

Table 3-2. Surface complexation adsorption constants for the adsorption of the As and Mo to ferrihydrite (Hfo) and amorphous aluminum hydroxide in the modified Minteq.v4 database.

Reaction	log K
$Hfo\_wOH + H_3AsO_3 = Hfo\_wH_2AsO_3 + H_2O$	5.41[a], (5.61)[b]
$Hfo\_sOH + H_3AsO_4 = Hfo\_sHAsO_4^- + H_2O + H^+$	2.81[c, d]
$Hfo\_wOH + H_3AsO_4 = Hfo\_wHAsO_4^- + H_2O + H^+$	2.81[c, d]
$Hfo\_sOH + H_3AsO_4 = Hfo\_sH_2AsO_4 + H_2O$	9.41[d]
$Hfo\_wOH + H_3AsO_4 = Hfo\_wH_2AsO_4 + H_2O$	9.41[d]
$Hfo\_sOH + H_3AsO_4 = Hfo\_sOHAsO_4^{3-} + 3H^+$	-10.12[c, d]
$Hfo\_wOH + H_3AsO_4 = Hfo\_wOHAsO_4^{3-} + 3H^+$	-10.12[c, d]
$Hfo\_sOH + MoO_4^{-2} + H^+ = Hfo\_sMoO_4^- + H_2O$	9.50[c,d]
$Hfo\_wOH + MoO_4^{-2} + H^+ = Hfo\_wMoO_4- + H_2O$	9.50[c,d]
$Hfo\_sOH + MoO_4^{-2} = Hfo\_sOHMoO_4^{-2}$	2.40[c,d]
$Hfo\_wOH + MoO_4^{-2} = Hfo\_wOHMoO_4^{-2}$	2.40[c,d]
$alumina\_sOH + H_3AsO_4 = alumina\_sH_2AsO_4^- + H^+ + H_2O$	2.51[b,d,e]
$alumina\_sOH + H_3AsO_4 = alumina\_sH_2AsO_4^{-2} + 2H^+ + H_2O$	-2.45[d,e]
$alumina\_sOH + H_3AsO_3 = alumina\_sH_2AsO_3 + H_2O$	2.20[b,d,e]

Source: [a]Dzombak and Morel (1990), [b]Moldovan and Hendry (2005), [c]llnl database, [d]Robertson et al. (2014), [e]Goldberg (2002).

3.5 Results and Discussion

3.5.1 Lab-Scale Plant and Mill-Scale Experiments

The calculated charge balances indicate the aqueous elemental analysis was below the acceptable water analysis level of ± 5% (Table 3-3) (Fritz, 1994). SeMo thickener and raffinate samples from scenario 1 and 3 had charge balance errors greater than this level that indicate either cations were underdetermined or anions were overdetermined, likely the latter at the low pH stage (< pH 4.0) for these aqueous samples. Concentrations of As, Mo, Fe, Al, Mg and Ni are highest in the raffinate samples, as expected for U mill waste solutions reporting to the BN circuit, with comparable pH values (pH 1.2 – 1.6) for each LSP scenario and Key Lake data. Concentration of As, Fe, Al and Ni decrease with increasing pH value for all LSP scenarios and Key Lake data, though concentrations of Mo and Al increase at high pH values (pH > 8). The increase in concentration indicate Mo- and Al- bearing mineral phases formed at low pH may become unstable at high pH and releasing these elements back into the aqueous phase. The increase in Mo concentration began in the Lamella thickener samples (pH 5.5 – 9.7) and most pronounced in the final combined tailings (Mo = 0.223 to 8.10 mg/L). The Key Lake samples yielded the highest measured Mo

concentrations in the aqueous phases of all final tailings samples tested. These high concentrations are attributed to the combination of Mo-bearing mineral phases remaining in the leach residues from the Key Lake circuit, which were not present in the combined LSP samples.

Comparison of the median pH value for the as discharged tailings porewater (pH 9.2) to samples analyzed indicates there is no significant difference between the LSP scenarios and Key Lake mill tailings samples (Table 3-4). Increased concentrations of Mo in the tailings porewater occur in the DTMF, similarly to what was observed in the LSP and Key Lake samples analysed. The mean as-discharged porewater concentrations of As, Mo, Fe, Al, Mg, Ca, Ni, Se and SO_4 and dried solid concentrations of As, Mo, Fe, Mg and Ni in the DTMF are summarized in Table 3-4. The mean Mo concentration in the porewater (7.51 mg/L) is higher than the As concentrations (0.100 mg/L), while the concentration in the solids (Mo = 55.1 µg/g) is significantly lower (As = 302 µg/g) indicating that Mo-bearing mineral phases are being solubilized at the conditions in the DTMF. XAS studies on the As- and Mo-bearing mineral phases show that adsorption to ferrihydrite a dominant control for each of these elements (Essilfie-Dughan et al., 2011; Essilfie-Dughan et al., 2013). Given As bonds via inner-sphere bidentate linkages to the ferrihydrite surface, and Mo is only able to form weaker outer sphere bonds, Mo would be expected to desorb when the solution pH attains the zero point charge of ferrihydrite (ZPC = 8.1) (Pierce and Moore, 1982; Moldovan and Hendry, 2005). Data for Se, Al and SO_4 concentrations were not available for the solid phase because they are not part of the suite of analysis currently performed at the Key Lake chemistry laboratory.

Table 3-3. Summary of aqueous analysis of the Key Lake (KL) Mill-scale and LSP scenario (S1, S2, S3) experiments with sample locations as per Figure 3-1 and Figure 3-2**.**

	pH	Eh	Cond	SO_4	Ca	K	Mg	Al	Fe	As	Mo	Ni	Charge Balance[a]
KL		(mV)	(mS/cm)	mg/L	mg/L	mg/L	mg/L	mg/L	mg/L	mg/L	mg/L	mg/L	
Raffinate (A)	1.6	596	41.0	17826[b]	797	132	2270	3277	2429	210	2.23	154	-0.805
Se-Mo (C)	4.2	475	6.12	na	478	60.1	511	163	304	0.253	0.079	37.0	na
Pachuca 3 (D)	7.2	446	4.95	na	688	64.1	411	0.431	0.320	0.006	0.052	0.191	na
Lamella (F)	9.7	411	3.09	na	612	64.1	9.25	0.937	0.032	0.010	0.090	0.019	na
Tailings (G)	9.0	412	2.73	na	470	44.8	1.15	0.068	0.017	0.280	8.81	0.087	na
S1													
Raffinate (A)	1.6	635	58.1	17938[b]	1267	502	2792	3167	4062	195	3.08	295	3.30
Se-Mo (C)	3.9	489	6.43	7080	447	69.5	434	390	367	0.129	0.043	40.6	-7.77
Pachuca 3 (D)	4.4	543	4.79	na	632	64.4	346	0.041	70.8	0.005	0.009	6.09	na
Lamella (F)	8.9	457	2.89	1633	583	60.6	9.42	3.67	0.106	0.018	0.363	0.024	-0.503
Combined (G)	9.2	382	2.36	1313	554	21.5	6.72	6.66	2.08	0.144	0.223	0.178	-0.014
S2													
Raffinate (A)	1.2	610	63.3	26292[b]	1286	177	4438	5076	5628	223	6.10	222	3.25
Se-Mo (C)	3.8	573	6.52	6232	513	68.6	580	133	440	0.093	0.090	23.3	-3.93
Pachuca 3 (D)	5.4	513	5.32	4030	776	75.3	451	0.110	20.0	0.006	0.027	0.740	-0.550
Lamella (F)	8.2	426	3.00	1664	561	73.5	5.35	6.27[c]	1.14	0.011	0.126	0.082	-1.21
Combined (G)	9.3	349	3.83	1876	706	22.0	7.10	0.061	0.051	0.056	2.13	0.020	2.68
S3													
Raffinate (A)	1.5	629	58.2	19662[b]	504	212	553	1108	1311	47.7	1.34	63.6	-10.8
Se-Mo (C)	3.9	503	4.17	4230	508	85.9	161	164	76.7	0.101	0.015	19.2	-7.69
Pachuca 3 (D)	3.7	548	4.49	na	878	85.8	139	1.65	4.12	0.049	0.026	5.12	na
Lamella (F)	5.5	507	3.11	1984	780	78.8	20.8	1.13	1.04	0.047	0.133	0.129	0.713
Combined (G)	10.0	297	2.79	1906	744	15.5	4.00	0.032	0.014	0.090	2.62	0.017	-1.22

[a] Analysis of Na, Se, Cu, Co, Zn, HCO_3, Cl, NO_2, NO_3 were completed and included in charge balance calculations, [b] Due to the high concentration of free acid in the raffinate solution (average = 13 g/L), SO_4 could not be determined by IC and was calculated from pH values, [c] outlier, inadequate sample volume for cross-check analysis, na = not available due to inadequate sample volume.

Table 3-4. Summary of as-discharged concentrations reporting to the DTMF from Jan 2010 to May 2015 (sample location G in Figure 3-2) from historical Key Lake analysis.

	units	Min	25th	Median	75th	Max	Mean	Std. dev.	n
Porewater									
pH		4.6	7.6	9.2	9.6	10.3	8.5	1.51	64
Cond	mS/cm	2.38	2.85	2.98	3.14	4.35	3.05	0.330	64
As	mg/L	0.044	0.068	0.084	0.121	0.284	0.100	0.046	64
Mo	mg/L	2.14	4.12	5.58	10.1	20.1	7.31	4.23	64
Fe	mg/L	0.014	0.047	0.148	0.385	2.61	0.305	0.430	64
Al	mg/L	0.288	1.57	3.12	4.89	10.8	3.59	2.59	64
Mg	mg/L	0.900	1.50	2.50	6.90	89.9	8.05	16.0	64
Ca	mg/L	537	580	598	628	705	604	30.7	64
Ni	mg/L	0.007	0.036	0.053	0.081	0.225	0.062	0.040	64
Se	mg/L	0.020	0.026	0.031	0.036	0.068	0.032	0.008	64
SO_4	mg/L	1558	1684	1736	1788	2274	1763	132.4	64
Dried Solids									
As	µg/g	1.50	195	269	351	883	302	174	62
Mo	µg/g	1.90	32.5	46.5	72.5	219	55.1	38.6	64
Fe	µg/g	10525	13689	14956	16735	20100	15133	2045	63
Al	µg/g	na	na	na	na	na	na	na	na
Mg	µg/g	1895	11565	12970	15200	20070	13193	2932	64
Ca	µg/g	10839	49429	54900	64133	92900	56460	13682	64
Ni	µg/g	57.0	252	338	528	1028	410	236	62
Se	µg/g	na	na	na	na	na	na	na	na
SO_4	µg/g	na	na	na	na	na	na	na	na

[a] Analysis were completed at the Key Lake chemistry laboratory for all reported values.
na= not available due to historical analysis requirements.

3.5.2 Thermodynamic Considerations

Stability field diagrams for the Fe-As (Figure 3-3a) Fe-Mo (Figure 3-3b) and Al-As (Figure 3-3c) system were created using GWB from thermodynamic data in the default database. Values of pH and Eh measured during experiment and calculated activity of raffinate feed solutions were used as inputs. The dominant oxidation states As^{+5} and Mo^{+6} was consistent throughout, regardless of pH or sample blend. The stability field diagrams suggest that in the absence of crystalline phases such as goethite, hematite, magnetite and lepidocrocite, ferrihydrite is the dominant Fe mineral phase for samples for pachuca 3, lamella and tailings samples (Figure 3-3). They also suggest that H_2MoO_4 and $FeMoO_4$ may play a role in the precipitation of Mo from the raffinate in the low pH and neutral to high pH respectively. XAS findings in Section 2.0 indicated ferric ($Fe_2(MoO_4)_3$) and calcium molybdates ($CaMoO_4$) contributed to the low pH precipitates, however neither H_2MoO_4 or $FeMoO_4$ were matched to linear combination fits of model compounds to samples analyzed. Comparison of Al phases to As speciation suggest that gibbsite is the dominant mineral phase for most Pachuca 3, Lamella and Tailings samples, while aqueous Al^{3+} exists at the low pH range for SeMo and Raffinate samples (Figure 3-3).

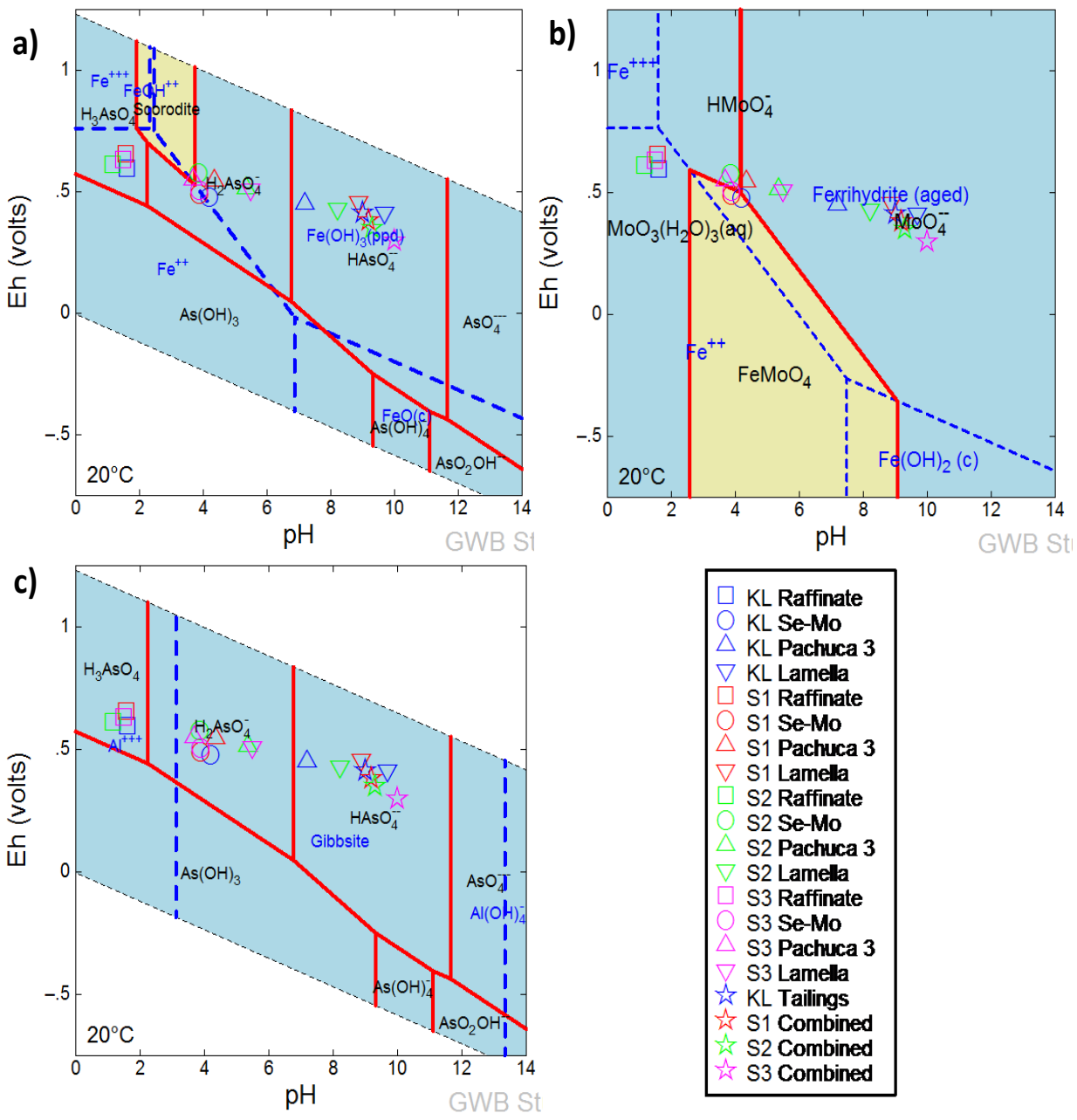

Figure 3-3. Stability field diagram for a) Fe-As b) Fe-Mo and c) Al-As system at 20 degrees C, P = 1.013 bars, using activities of Fe = 8.23e-03, As = 6.99e-04, Mo = 1.51e-05, and Al = 7.97e-03 calculated from raffinate feed solutions and actual Eh and pH values measured from Key Lake and LSP sample analysis**.**

3.5.2.1 The Fe-Al-Mg-Ca System

Geochemical modelling was conducted using analytical data in Table 3-1 for samples collected from the Key Lake mill (KL-A to KL-G) samples. The dominant mineral phases of Mg, Al, Fe, Ca, Ni, S and SiO_2 that could precipitate over the pH range 1.5 - 10.5 with addition of $Ca(OH)_2$ in 0.5 pH steps were determined by reviewing the calculated saturated indices (SI) with equilibrium phases from the modified llnl database as per Gomez et al. (2013) and Essilfie-Dughan et al. (2012). In this simulation, no equilibrium phases were specified and minerals with SI values > 0.0 were considered potential secondary mineral phases during neutralization. The dominant mineral phases predicted to form were basaluminite [$Al_4(OH)_{10}SO_4$], amorphous aluminum hydroxide [$Al(OH)_{3(am)}$], brucite [$Mg(OH)_2$], iron (oxy)hydroxides [$Fe(OH)_2$, $Fe(OH)_3$, $Fe_3(OH)_8$], ferrous molybdate [$FeMoO_4$], schwertmannite [$Fe_8O_8(OH)_6SO_4$], calcium arsenate hydroxides [$Ca_4(OH)_2(AsO_4)_2 \bullet 4H_2O$, $Ca_5(AsO_4)_3OH$], ettringite [$Ca_6Al_2(SO_4)_3(OH)_{12} \bullet 26H_2O$], gibbsite [$Al(OH)_3$], gypsum [$CaSO4 \bullet 2H_2O$], goethite [FeOOH], hematite [Fe_2O_3], amorphous silica [$SiO_2(am)$], hydrotalcite [$Mg_4Al_2O_7 \bullet 10H_2O$], and nickel mineral phases [$Ni(OH)_2$, Ni_2SiO_4, $Ni_4(OH)_6SO_4$, $NiMoO_4$]. SI values show that ferric arsenate [$FeAsO_4$] and scorodite [$FeAsO_4 \bullet 2H_2O$] were under saturated during these calculations, potentially due to the high molar ratios of Fe/As and the starting pH (>1.5) in the raffinate. Molar ratios of Fe/As ~2 and pH values <3.5 are reported for scorodite and ferric arsenate phase precipitation in U mill wastes (Langmuir et al., 2006; Mahoney et al., 2007; Paktunc and Bruggeman, 2010), which are lower than conditions measured in this study. Similarly, $CaMoO_4$ though predicted to form based on phases found in the DTMF (Essilfie-Dughan et al., 2011) was under saturated in these calculations.

XRD and XAS analysis on precipitates from the ore blend scenarios studied in Section 2.0 indicate that gypsum, ferrihydrite, ferric arsenate, amorphous aluminum hydroxides, basaluminites and hydrotalcites are the dominant mineral phases in the BN samples taken from the Key Lake mill and the LSP scenarios. These equilibrium phases and brucite ($Mg(OH)_2$), epsomite ($MgSO_4$), and $Al_4(OH)_{10}SO_4$ (to account for the decrease in Mg and Al concentrations before pH 7) were used to model the neutralization raffinate in the BN circuit. Analytical data from the Key Lake mill was used as model inputs for a step-wise addition of $Ca(OH)_2$ to pH 10.5 (every 0.1 pH units) starting with raffinate feed data for sample KL-A. Results of modeling (Figure 3-4a) show a considerable mass of gypsum precipitated from pH 1.6 - 10.5, with the majority precipitated by pH 5. The model also shows that Fe precipitated as ferrihydrite ($Fe(OH)_3$) starting at pH 3.3 and plateaued at pH 6.4

while continuing to precipitate to the terminal pH of 10.5 without becoming unstable (Figure 3-4b). Scorodite and ferric arsenate did not form in these calculations, which was unexpected based on published work in similar U mill facilities (Moldovan and Hendry, 2005; Langmuir et al., 2006; Mahoney et al., 2007; Chen et al., 2009). The precipitation of ferrihydrite and gypsum is consistent with results of Moldovan and Hendry (2005), Essilfie-Dughan et al (2012, 2013) and Gomez et al (2013).

Model results indicate Al precipitates via a variety of equilibrium phases. $AlOHSO_4$ precipitated between pH 1.8 and 4.8, where $Al_4(OH)_{10}SO_4$ became the more stable phase between pH 4.9 and 9.5 (Figure 3-4a). The results of modeling the Al phases are consistent with previous studies by Gomez et al (2013) and Robertson et al (2014). Amorphous $Al(OH)_3$ did not form until $Al_4(OH)_{10}SO_4$ was suppressed, and then began precipitating as $AlOHSO_4$ formation decreased at pH 5.8 (Figure 3-4b). At pH 8.0 Mg-Al hydrotalcite was a stable equilibrium phase and precipitated to the terminal pH of 10.5 (Figure 3-4b). The solution data from Key Lake mill was consistent with the precipitation trends of these equilibrium phases. Notably, most Mg remained in solution until precipitated as Mg-Al hydrotalcite at pH 8 (Figure 3-4c). Brucite and epsomite did not precipitate in these calculations. The formation of Al, Fe and Mg equilibrium phases is consistent with the changes in solution chemistry with increasing neutralization pH for KL-A solution data (Figure 3-4c) and what was reported by Gomez et al. (2013).

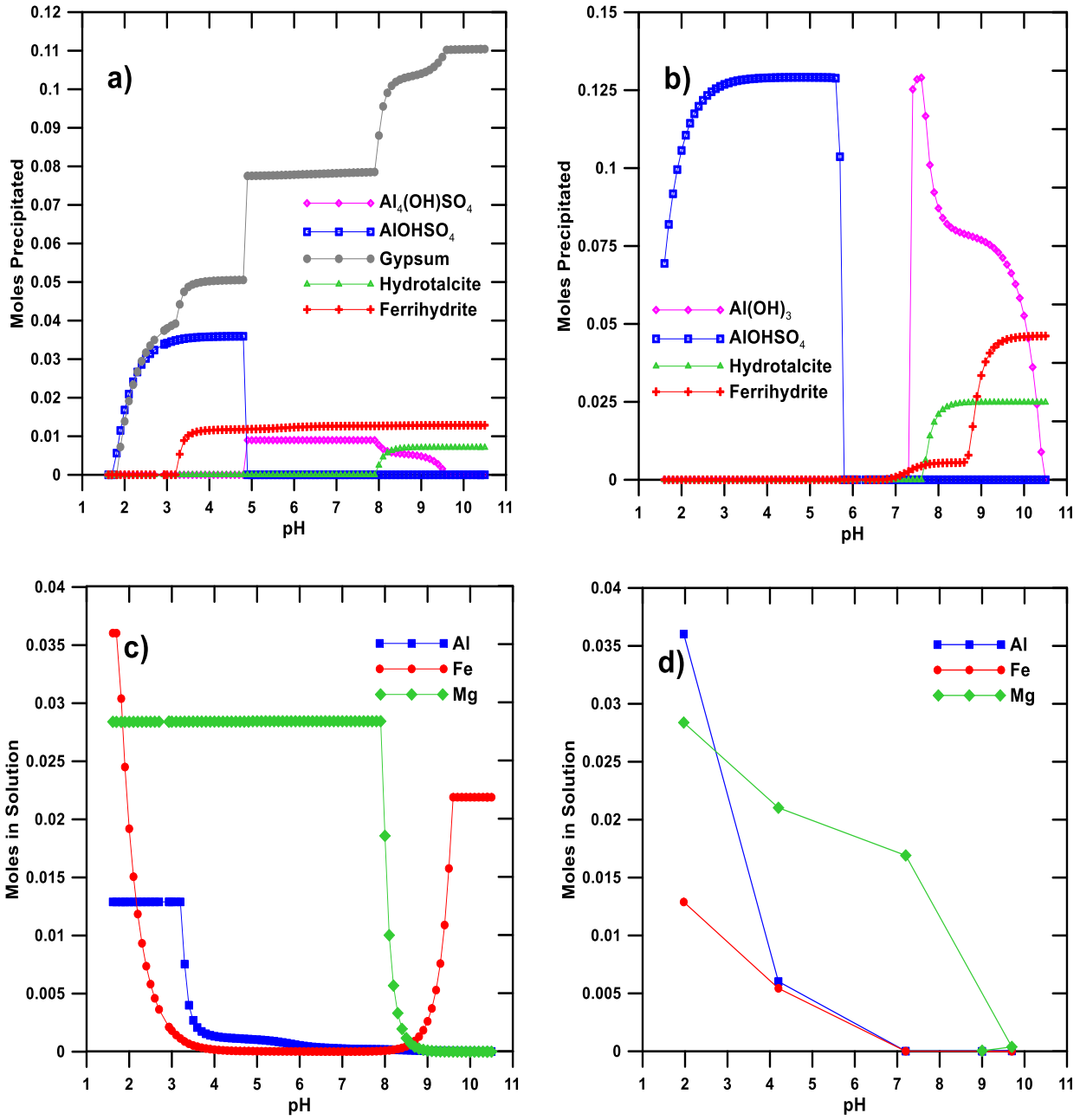

Figure 3-4. Thermodynamic modeling results (a-c) using the Lawrence Livermore National Laboratories (llnl) database for Al, Fe, Ca and Mg equilibrium phases in solution where the series represent a) mineral phases precipitated during neutralization b) mineral phases precipitated with gypsum and Al_4OHSO_4 suppressed c) calculated concentrations of Al, Fe and Mg in solution during neutralization and d) actual Key Lake mill data showing the removal of Al, Fe and Mg from solution.

3.5.2.2 The Fe-As System

Attempts to fit scorodite and ferric arsenate phases from the previous calculations were performed by adding the following phases presented in Table 3-5 to the llnl database using starting concentrations of raffinate solution for the Key Lake mill samples reacted stepwise with $Ca(OH)_2$ in 0.1 pH units.

Table 3-5. Aqueous species of As in the modified llnl database (Langmuir et al., 2006).

Reaction	**log K**	**deltaH**
As Aqueous Species		kJ/mol
$H_3AsO_4 = H_2AsO_4^- + H^+$	-2.24	-7.11
$H_3AsO_4 = HAsO_4^{2-} + 2H^+$	-9.20	-3.77
$H_3AsO_4 = AsO_4^{3-} + 3H^+$	-20.70	14.35
Ferric Arsenate		
$Fe^{3+} + H_2AsO_4^{3-} = FeH_2AsO_4^{2+}$	1.80	
$Fe^{3+} + HAsO_4^{3-} = FeHAsO_4^+$	0.66	
$Fe^{3+} + AsO_4^{3-} = FeAsO_4$	-1.80	

Using these species, a slight decrease in As concentration was calculated from pH 2.7 to pH 4.3, where scorodite was allowed to precipitate. The scorodite subsequently re-dissolved into solution from pH 3 to 4 (Figure 3-5 a). To determine the effect of scorodite and $FeAsO_4$ in the absence of other Fe mineral phases, measured pH and Eh values were used as inputs for a neutralization of raffinate solution with $Ca(OH)_2$ with only gypsum, $FeAsO_4$ and scorodite used as equilibrium phases (Figure 3-5b). Gypsum was saturated throughout the simulation. $FeAsO_4$ did not form during these calculations.

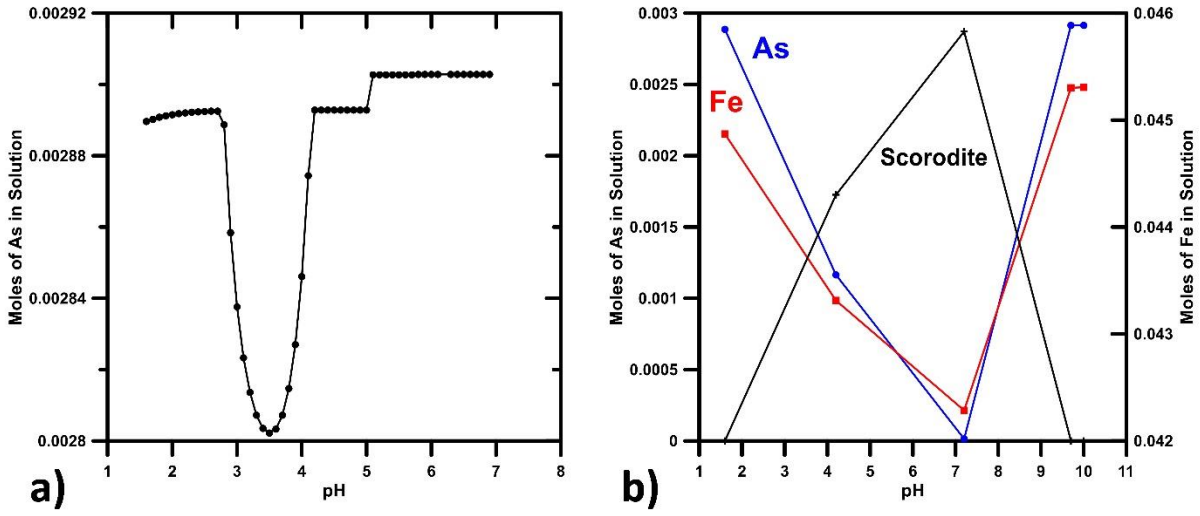

Figure 3-5. a) As solubility with $FeAsO_4$ phases considered and b) As and Fe solubility and scorodite ($FeAsO_4 \bullet 2H_2O$) precipitation in the absence of other Fe phases with the modified llnl database. Scorodite formation follows the Fe axis for moles of scorodite precipitated.

As and Fe solution data were consistent with the trend for scorodite by beginning to precipitate from of solution by pH 4.2 and continuing to precipitate to pH 7.2, after which scorodite dissolved and released As and Fe back into solution. Because the As and Fe continued to remain in solution during these calculations, it was determined that the llnl database did not adequately describe the scorodite phase. As such, the minteq.v4 database with modifications as per Robertson et al. (2014) was employed with equilibrium phases of $FeAsO_4$, scorodite ($FeAsO_4 \bullet 2H_2O$) and amorphous scorodite (Table 3-1). When all three were allowed to precipitate, the amorphous scorodite phase was favoured, and neither $FeAsO_4$ nor the more crystalline $FeAsO_4 \bullet 2H_2O$ formed (Figure 3-6a). In this case, As was effectively removed from solution while the Fe concentrations declined in solution but still remained in solution.

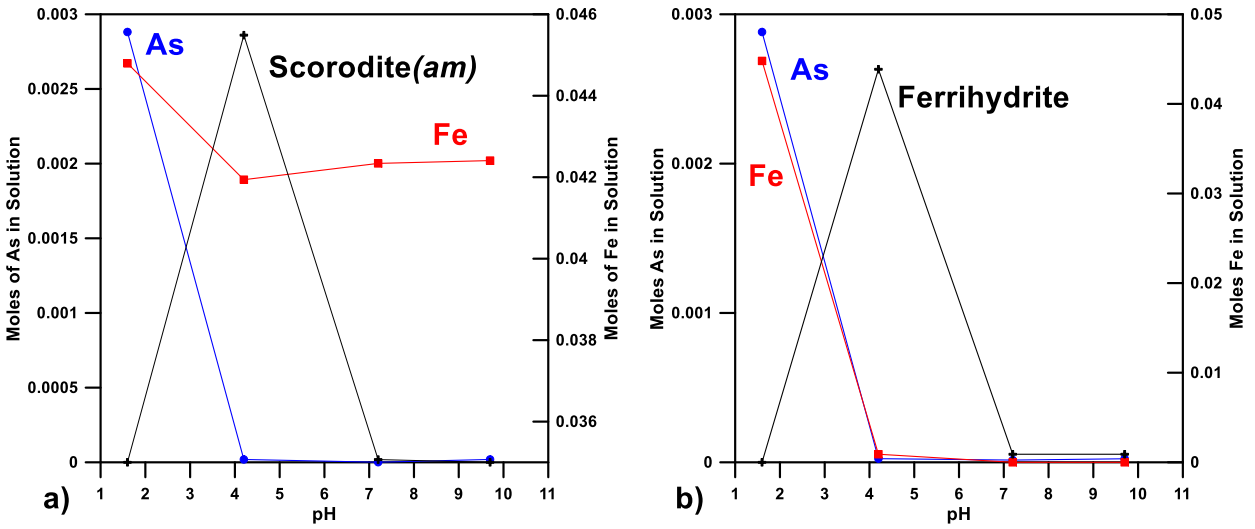

Figure 3-6. a) As and Fe solubility and amorphous scorodite precipitation in the absence of other Fe phases and b) As and Fe solubility with ferrihydrite precipitation with the modified minteq.v4 database. Amorphous scorodite formation follows the Fe axis for moles of scorodite precipitated.

The same input values were retained for a subsequent simulation, in which ferrihydrite was introduced as an equilibrium phase using the adsorption values presented in Table 3-2. When the ferrihydrite and adsorption phases were added to these calculations, Fe was more effectively removed from solution and no scorodite phases formed (Figure 3-6 b). This data suggests that although amorphous scorodite is predicted to form as a control on As concentration, it is a minor phase in the presence of ferrihydrite with a negligible affect on As solubility and adsorption of As to ferrihydrite is a dominant control on As for these types of solutions. Adsorption of arsenate to ferrihydrite was maximized at the pH 4.2 set point, consistent with the maximum for ferrihydrite formation in these calculations (data not shown).

3.5.2.3 The Fe-Al-Mo System

To determine the effect that Mo-bearing mineral phases has on Mo removal, measured pH and Eh values were used as inputs for neutralization of raffinate solution with $Ca(OH)_2$ with only a) $CaMoO_4$, b) $NiMoO_4$, c) $FeMoO_4$ and d) ferrihydrite adsorption considered according to surface

complexation reactions as per Table 3-2 (Figure 3-7). Gypsum was allowed to precipitate throughout each simulation.

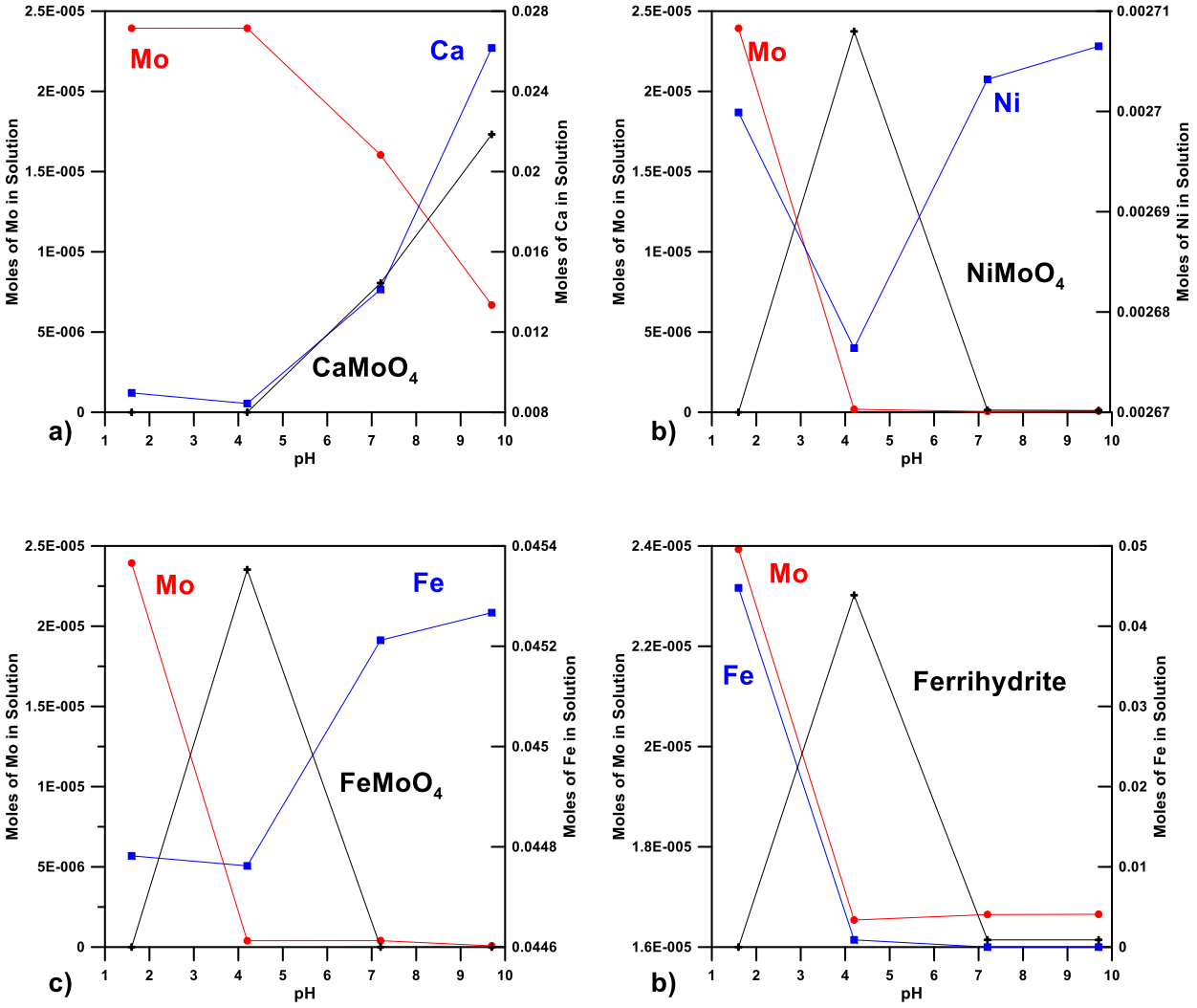

Figure 3-7. Thermodynamic modeling results (a-d) using the minteq.v4 database for Mo, Fe, Ni and Ca equilibrium phases in solution where the series represent: a) solution concentrations for $CaMoO_4$ precipitation, b) solution concentrations for $NiMoO_4$ precipitation, c) solution concentrations for $FeMoO_4$ precipitation, and d) solution concentrations for adsorption to ferrihydrite.

When only $CaMoO_4$ was added as an equilibrium phase, Mo was effectively removed from solution at high pH (> 7.5), with concentration decreasing at pH 4.2 as $CaMoO_4$ precipitated, then attaining the lowest concentration at pH 10 (Figure 3-7a). When only $NiMoO_4$ was added as an equilibrium phase, Mo was effectively removed from solution at pH 4.2 with Ni as $NiMoO_4$

precipitated, then as Ni re-dissolved back into solution, Mo did not redissolve suggesting the formation of a new mineral phase that was undefined in this model (Figure 3-7b). When only $FeMoO_4$ is used as an equilibrium phase with gypsum, Mo is effectively removed from solution at pH 4.2 but does not re-dissolve into solution over the pH range 4.3 to 10.0 (Figure 3-7c). When only ferrihydrite is considered, Fe is effectively removed from solution by pH 4.2, but Mo declines only to pH 4.2 and then begins to redissolve into solution with increasing pH as is expected from molybdate adsorption of ferrihydrite above the ZPC (pH 8.1) (Figure 3-7d). Above the ZPC, the surface of ferrihydrite has a net positive charge and anions adsorbed to the outer diffuse layer are expected to be released back into solution (Moldovan and Hendry, 2005; Dzombak and Morel, 1990). However, when $Al(OH)_3$ phases and Mg-Al-hydrotalcite phases are included in the model with adsorption to ferrihydrite, Mo in solution experiences a further decrease in concentration at high pH than when only ferrihydrite is considered (data not shown).

3.5.2.4 The Al-As System

The same input values as the previous Fe-As system calculations were used in the next simulation, as amorphous aluminum hydroxide was introduced as an equilibrium phase using the adsorption values in Table 3-2. The pH profile of Al follows the precipitation of amorphous $Al(OH)_3$ and the pH profile of As coincides with the adsorption of AsO_4^{2-} and $HAsO_4^{-}$ on amorphous alumina hydroxide (Figure 3-8).

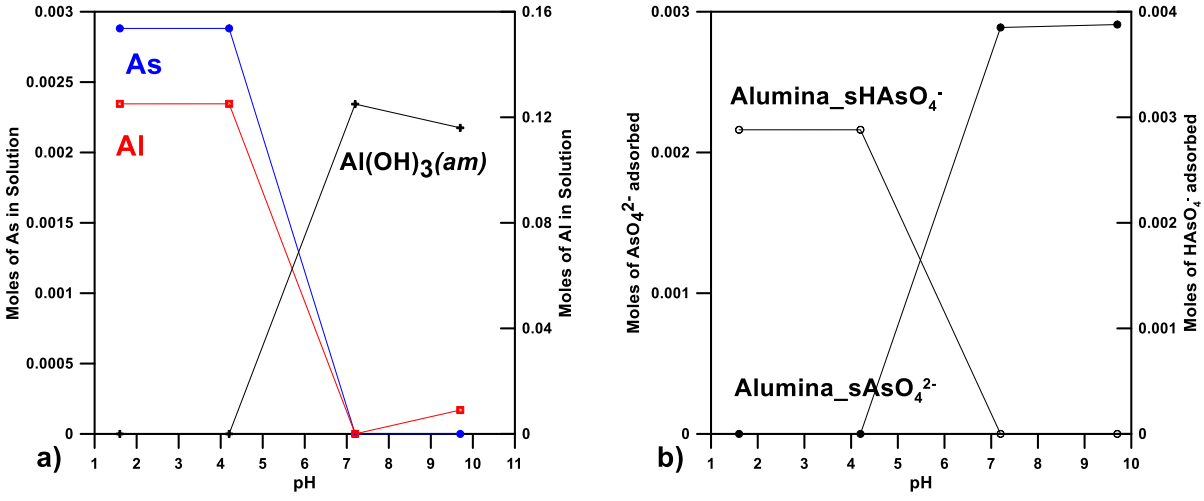

Figure 3-8. Thermodynamic modeling results (a-b) using the minteq.v4 database for a) solution concentrations for amorphous aluminum hydroxide precipitation and As adsorption and b) adsorption of selected arsenate species to amorphous aluminum hydroxide. Precipitation of aluminum hydroxide matches the As axis as moles of Al $(OH)_3$ precipitated.

Aluminum phases that could sequester As and Mo in the bulk neutralization circuits are a function of pH. In addition to adsorption to amorphous aluminum ($Al(OH)_3$) phases, amorphous $AlOHSO_4$, aluminous ferrihydrite and Mg-Al hydrotalcites can be associated with As and Mo in neutralized precipitates (Paikaray et al., 2013; Gomez et al., 2013; Robertson et al., 2014; Robertson et al., 2015). In the low pH stage (4.2) $AlOHSO_4$ and Al-ferrihydrite phases will precipitate together, while the high pH stage (9.5) precipitation is dominated by Mg-Al hydrotalcites (Robertson et al., 2015). When systems are precipitated in the absence of iron, As removal is consistent with Fe-rich systems, whereas Mo is only partially sequestered (43.7%) as compared to Fe-rich systems (98.2%) (Robertson et al., 2015). These observations indicate that As should be effectively removed in the presence of Al while in the absence of Fe, whereas Mo sequestration would be hindered without adsorption to Fe oxides (ferrihydrite) surfaces.

3.5.2.5 The Fe-Al-As-Mo System

With equilibrium phases described above included as inputs into the model, a best fit was obtained between calculated aqueous molalities of As and Mo and experimental data from LSP scenario 2 (S2) (Figure 3-9). Adsorption of As and Mo to both the Fe and Al systems were considered, along with gypsum, amorphous scorodite, calcium arsenates and hydrotalcites predicted to form in Section 3.5.2.1, as well as minor phases of $NiMoO_4$, $FeMoO_4$, and $AlOHSO_4$. S2 results were modelled because the measured pH values best represented the aqueous environment of the Key Lake mill samples (Table 3-3) and the blend included both McA and MLM ores starting materials (Appendix A). The solubility profiles were similar for all LSP and Key Lake mill sample calculations (data not shown). Though amorphous scorodite, $FeAsO_4$, and calcium arsenates were included they were under-saturated during these calculations. Gypsum remained saturated throughout the model.

The best fit described As solubility with 99.5% removal of As by pH 3.8, closely matched 99.9 % removal for actual S2 data (Figure 3-9), This is well explained by As precipitation as scorodite and adsorption to ferrihydrite phases from pH 2.2 to 4.2 that were collected in the SeMo thickener. The near identical pH profile for Al solubility also suggests the potential for $AlOHSO_4$ phases to participate in the removal of As at low pH (pH 2.4-6.2), before the formation of $Al(OH)_3$ was available for adsorption. This finding is consistent with linear combination fitting with As K-edge

XAS (Section 2.0) and suggests the arsenate anion was removed from solution by adsorption to the surface of ferrihydrite (majority) and to $AlOHSO_4$ (minority).

The model also predicts Mo phases begin to form above pH 2.8 as ferrihydrite and $FeMoO_4$ become available to sequester Mo from solution, measuring 98.6% removal in the model and 96.5% in actual LSP S2 data. The model predicts Mo will redissolve into solution above pH 8.0, and decreased from 99.6 % removal at pH 5.4 to 87.2% by pH 8.2. Similarly, Mo precipitation was highest in LSP S2 solution data at pH 5.4 with 99.0% removal in the SeMo thickener, then decreased to 95.1% removal at pH 8.2 in the Lamella thickener. The final tailings samples showed a rapid dissolution of Mo-bearing mineral phases of only 17.4 % removal at pH 9.4 indicating the most favourable pH range for Mo removal exists below pH 8. The high concentration of Mo in the final pH (tailings) samples could not be completely explained by the model, and suggests that the precipitation of $CaMoO_4$, $NiMoO_4$ and adsorption to ferrihydrite above pH > 8.2 does not fully control Mo in the tailings porewater. This finding suggests a high degree of association of Mo with ferrihydrite phases, over $CaMoO_4$, $NiMoO_4$ and $FeMoO_4$. Linear combination fitting of Mo K-edge XAS agreed with this distribution of Mo-bearing phases (Section 2.0). The XAS analysis indicated $CaMoO_4$, $NiMoO_4$ and $FeMoO_4$ played a minor role in defining Mo solubility, with the majority controlled by adsorption to ferrihydrite.

The model calculations predict Fe concentrations in solution will decrease dramatically at pH 2.6 with near complete (98.4 %) removal from solution by pH 3.8, whereas LSP S2 data indicated a lower percent removal (72.9%) at pH 3.8. This is the most favorable region for ferrihdyrite formation and agrees with results from As K-edge XAS (Section 2.4.2). The remaining Fe continues to decline from solution phases until pH 5.4 with the precipitation of $FeMoO_4$. The model predicted both Ni and Mg would remained in solution until pH 6.2 and 8.6, respectively, with the precipitation of brucite and theophrastite. Solution data from LSP S2 indicates Ni and Mg are each removed gradually from pH 4.2 to 8.2, likely associated with the precipitation of NiMoO4 and epsomite. Because these elements were not the focus of the current study, no additional comments were warranted.

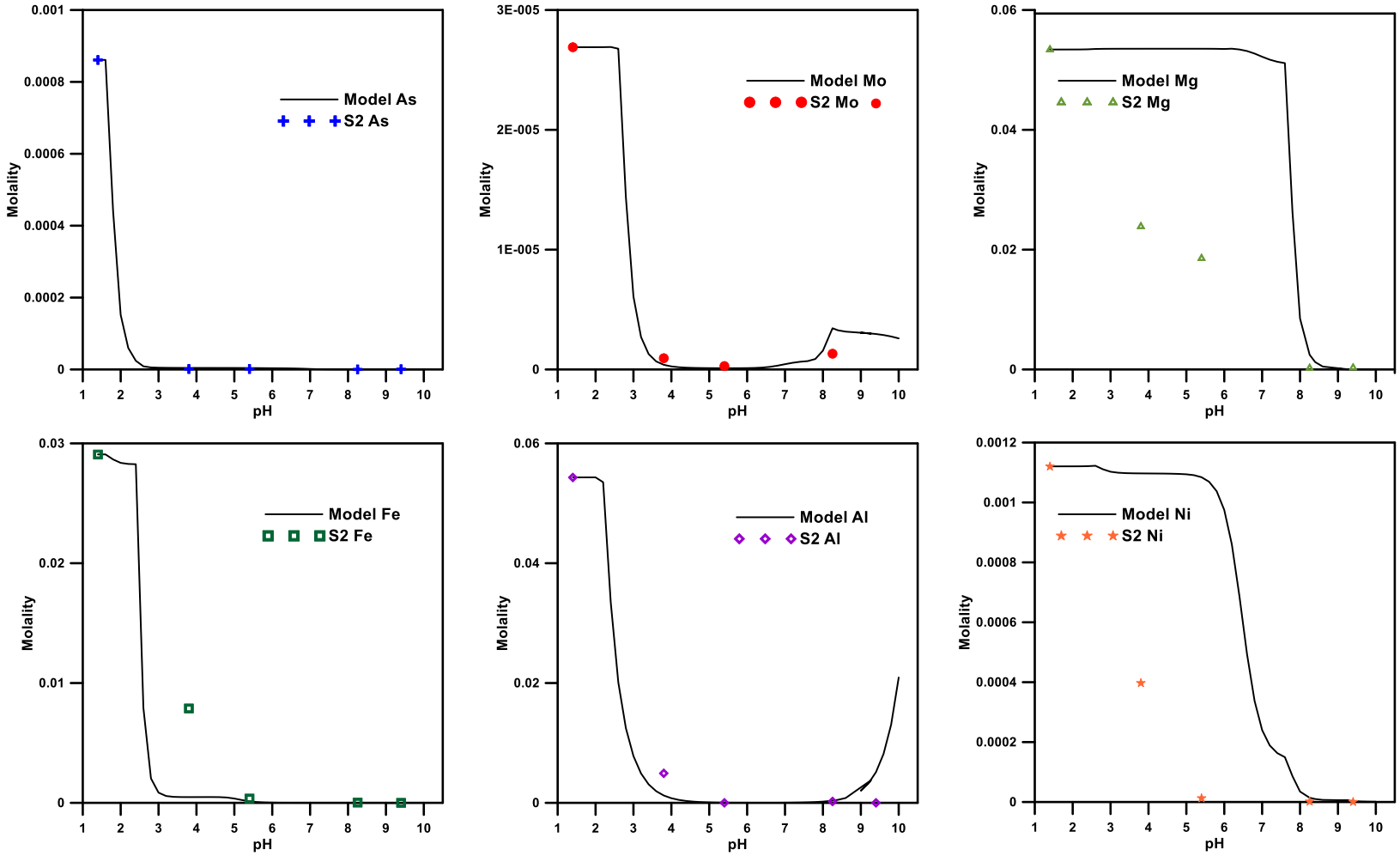

Figure 3-9. Solubility profiles of complete model for As, Mo, Mg, Fe and Al between pH 1.6-10.5 for LSP scenario 2 (S2).

3.6 Implications for the long-term stability of U mill tailings

Characterizing the As- and Mo-bearing mineral phases precipitated from the bulk neutralization circuit indicates that controls on solubility of As and Mo are present in U mill tailings facilities. The current research suggests that both As and Mo are controlled by adsorption to Fe and/or Al oxyhydroxide surfaces as well as by formation of secondary mineral phases such as $FeAsO_4$, $NiMoO_4$, $CaMoO_4$, $Fe_2(MoO_4)_3$. Overall, the dominant control on As and Mo was adsorption to ferrihydrite surfaces which resulted in their removal from solution by pH 4, regardless of sample blend tested. Since adsorption of anions (AsO_4^{2-}) to the surface of ferrihydrite has been shown to slow conversion to crystalline forms of Fe oxides (goethite and hematite) and sequestration of arsenate effectively control As solubility at high pH (pH >10), As-bearing mineral phases are expected to be stable for thousands of years (Ford, 2002; Das et al., 2011; Das et al., 2014b; Das et al., 2014a). With adsorption as well as direct precipitation considered, Mo phases though sequestered below pH 8, are released back into the tailings porewater (pH >10) regardless of sample blend tested. Historical data obtained from as-discharged tailings as well as previously published U mill tailings studies (Shaw et al., 2011; Essilfie-Dughan et al., 2011) support these findings.

3.7 References

APHA, AWWA, WEF, 2012a. Conductivity. Standard methods for the Examination of Water & Wastewater American Public Health Association, American Water Works Association, Water Environment Federation. pp. 2.52–2.55.

APHA, AWWA, WEF, 2012b. pH VALUE. Standard methods for the Examination of Water & Wastewater American Public Health Association, American Water Works Association, Water Environment Federation. pp. 4.91–4.96.

APHA, AWWA, WEF, 2012c. Standard methods for the Examination of Water & Wastewater., American Public Health Association, American Water Works Association, Water Environment Federation.

ASTM, 1995. Standard Practice for the Oxidation-Reduction Potential of Water, Volume 11.01 D1498-93.

Bethke, C. M., Yeakel, S., 2015. The Geochemist's Workbench. Release 10.0. Aqueous Solutions, LLC: Champaign. pp. 1-149.

CCME, 2007. Canadian Environmental Quality Guidelines, Canadian Council of Ministers of the Environment. Ottawa. URL http://www.ccme.ca/en/resources/canadian_environmental_quality_guidelines/index.html

CCME, 1999a. Canadian Sediment Quality Guidelines for the Protection of Aquatic Life - Arsenic. In: Canadian environmental quality guidelines, Canadian Council of Ministers of the Environment. Winnipeg.

CCME, 1999b. Water Quality Guidelines for the Protection of Aquatic Life - Molybdenum, Canadian Council of Ministers of the Environment. URL http://st-ts.ccme.ca/en/index.html (accessed 11-03-15)

CCME, 1997. Canadian Environmental Quality Guidelines: Arsenic. Canadian Council of Ministers of the Environment. URL http://st-ts.ccme.ca/en/index.html (accessed 11-03-15)

Charlton S. R. and Parkhurst D. L. (2002) PHREEQC I — A Graphical User Interface to the Geochemical Model PHREEQC. Water-Resource Investig. Rep. 95-4227, 1–2.

Chen, N., Jiang, D.T., Cutler, J., Kotzer, T., Jia, Y.F., Demopoulos, G.P., Rowson, J.W., 2009. Structural characterization of poorly-crystalline scorodite, iron(III)–arsenate co-precipitates and uranium mill neutralized raffinate solids using X-ray absorption fine structure spectroscopy. Geochim. Cosmochim. Acta 73, 3260–3276. doi:10.1016/j.gca.2009.02.019

Cloutier, J., Kyser, K., Olivo, G. R., Alexandre, P., Halaburda, J., 2009. The Millennium uranium deposit, Athabasca Basin, Saskatchewan, Canada: An atypical basement-hosted unconformity-related uranium deposit. Econ. Geol. 104, 815–840.

Cullen, W.R., Reimer, K.J., 1989. Arsenic speciation in the environment. Chem. Rev. 89, 713–764. doi:10.1021/cr00094a002

Das, A. K., Chakraborty, R., Cervera, M.L., de la Guardia, M., 2007. A review on molybdenum determination in solid geological samples. Talanta 71, 987–1000.

Das, S., Essilfie-Dughan, J., Hendry, M.J., 2014a. Arsenate adsorption onto hematite nanoparticles under alkaline conditions: effects of aging. J. Nanoparticle Res. 16, 1–12. doi:10.1007/s11051-014-2490-3

Das, S., Essilfie-Dughan, J., Hendry, M.J., 2014b. Arsenate partitioning from ferrihydrite to hematite : Spectroscopic evidence. Am. Mineral. 99, 749–754.

Das, S., Hendry, M.J., Essilfie-Dughan, J., 2011. Transformation of two-line ferrihydrite to goethite and hematite as a function of pH and temperature. Environ. Sci. Technol. 45, 268–275.

Dzombak, D.A., Morel, F.M., 1990. Surface Complexation Modeling: Hydrous Ferric Oxide. Wiley-Interscience, New York.

Eisler R., 1988. Arsenic hazards to fish, wildlife, and invertebrates: a synoptic review. U.S. Fish Wildl. Serv. Biological Report, Washington, Contaminant hazard reviews: I49.89/2:85 (1.5), pp 82-92.

Eisler R., 1989. Molybdenum hazards to fish, wildlife, and invertebrates: a synoptic review. U.S. Fish Wildl. Serv. Biological Report, Washington, Contaminant hazard reviews: I49.89/2:85(1.19), pp. 50-61.

Essilfie-Dughan, J., Hendry, M.J., Warner, J., Kotzer, T., 2013. Arsenic and iron speciation in uranium mine tailings using X-ray absorption spectroscopy. Appl. Geochemistry 28, 11–18. doi:10.1016/j.apgeochem.2012.10.022

Essilfie-Dughan, J., Hendry, M.J., Warner, J., Kotzer, T., 2012. Microscale mineralogical characterization of As, Fe, and Ni in uranium mine tailings. Geochim. Cosmochim. Acta 96, 336–352. doi:10.1016/j.gca.2012.08.005

Essilfie-Dughan, J., Pickering, I.J., Hendry, M.J., George, G.N., Kotzer, T., 2011. Molybdenum speciation in uranium mine tailings using X-ray absorption spectroscopy. Environ. Sci. Technol. 45, 455–60. doi:10.1021/es102954b

Ford, R.G., 2002. Rates of hydrous ferric oxide crystallization and the influence on coprecipitated arsenate. Environ. Sci. Technol. 36, 2459–2463.

Fritz, S.J., 1994. A survey of charge-balance errors in published analyses of potable ground and surface waters. Ground Water 32, 539–546.

Goldberg, S. 2002. Competitive adsorption of arsenate and arsenite on oxides and clay minerals. Soil Sci. Soc. Am. J. 66, 413. doi:10.2136/sssaj2002.0413

Gomez, M.A., Hendry, M.J., Koshinsky, J., Essilfie-Dughan, J., Paikaray, S., Chen, J., 2013. Mineralogical controls on aluminum and magnesium in uranium mill tailings: Key Lake, Saskatchewan, Canada. Environ. Sci. Technol. 47, 7883–91. doi:10.1021/es400658f

Harvey, C.F., Swartz, C.H., Badruzzaman, A.B.M., Keon-Blute, N., Yu, W., Ali, M.A., Jay, J., Beckie, R., Niedan, V., Brabander, D., Oates, P.M., Ashfaque, K.N., Islam, S., Hemond, H.F., Ahmed, M.F., 2002. Arsenic mobility and groundwater extraction in Bangladesh. Science 298, 1602–1606.

Hossain, M.A., 2014. Mineralogical Characterization of Uranium Ores, Blends and Resulting Leach Residues from Key Lake Pilot Plant, Saskatchewan, Canada. MSc Thesis, Department of Geological Sciences, University of Saskatchewan.

Jamieson, B.W., Frost, S.E., 1997. The McArthur River project: high grad uranium mining. In 22nd Annual International Symposium of the Uranium Institute. The Uranium Institute, London, England.

Korte, N.E., Fernando, Q., 1991. A review of arsenic (III) in groundwater. Crit. Rev. Environ. Control 21, 1–39.

Langmuir, D., Mahoney, J., Rowson, J., 2006. Solubility products of amorphous ferric arsenate and crystalline scorodite (FeAsO4·2H2O) and their application to arsenic behavior in buried mine tailings. Geochim. Cosmochim. Acta 70, 2942–2956. doi:10.1016/j.gca.2006.03.006

Liber, K., Doig, L.E., White-Sobey, S.L., 2011. Toxicity of uranium, molybdenum, nickel, and arsenic to Hyalella azteca and Chironomus dilutus in water-only and spiked-sediment toxicity tests. Ecotoxicol. Environ. Saf. 74, 1171–1179. doi:10.1016/j.ecoenv.2011.02.014

Lieu, A., Bissonnette, J., Hossain, A.M., Essilfie-Dughan, J., Moldovan, B.J., Hendry, M.J., 2015. Simulating the mineral process at the Key Lake uranium mill, northern Saskatchewan, Canada in a lab-scale plant. Submitted to Hydrometallurgy.

Mahoney, J., Slaughter, M., Langmuir, D., Rowson, J., 2007. Control of As and Ni releases from a uranium mill tailings neutralization circuit: Solution chemistry, mineralogy and geochemical modeling of laboratory study results. Appl. Geochemistry 22, 2758–2776. doi:10.1016/j.apgeochem.2007.06.021

Masscheleyn, P.H., Delaune, R.D., Patrick W.H.Jr., 1991. Effect of redox potential and pH on arsenic speciation and solubility in a contaminated soil. Environ. Sci. Technol. 25(8) 1414–1419.

Moldovan, B.J., Hendry, M.J., 2005. Characterizing and quantilying controls on arsenic solubility over a pH range of 1-11 in a uranium mill-scale experiment. Environ. Sci. Technol. 39, 4913–4920.

Ngai, T.K.K., 2002. Arsenic Speciation and Evaluation of an Adsorption Media in Rupandehi and Nawalparasi Districts of Nepal. Massachusetts Institute of Technology.

Paikaray, S., Hendry, M.J., Essilfie-Dughan, J., 2013. Controls on arsenate, molybdate, and selenate uptake by hydrotalcite-like layered double hydroxides. Chem. Geol. 345, 130–138. doi:10.1016/j.chemgeo.2013.02.015

Paktunc, D., Bruggeman, K., 2010. Solubility of nanocrystalline scorodite and amorphous ferric arsenate: Implications for stabilization of arsenic in mine wastes. Appl. Geochem. 25, 674–683. doi:10.1016/j.apgeochem.2010.01.021

Parkhurst, D.L., Appelo, C.A.J., 2013. Description of input and examples for PHREEQC version 3–A computer program for speciation, batch-reaction, one-dimensional transport, and inverse geochemical calculations: U.S. Geological Survey Techniques and Methods, book 6, chap. A43, 497p., available only at http://pubs.usgs.gov/tm/06/a43/.

Parkhurst, D.L., Appelo, C.A.J., 1999. User's guide to PHREEQC (Version 2) - A computer program for speciation, batch-reaction, one-dimensional transport, and inverse geochemical calulations. Water-Resource Investig. Rep. 99-4259.

Pierce, M.L., Moore, C.B., 1982. Adsorption of arsenite and arsenate on amorphous iron hydroxide. Water Resour. 16, 1247–1253.

Robertson, J., Hendry, M.J., Essilfie-Dughan, J., Chen, J., 2015. Precipitation of aluminum and magnesium secondary minerals from uranium mill raffinate (pH 1.0-10.5) and their controls on aqueous contaminants. Appl. Geochem. *in press*. doi:10.1016/j.apgeochem.2015.09.002

Robertson, J., Shacklock, K., Frey, R., Gomez, M.A., Essilfie-Dughan, J., Hendry, M.J., 2014. Modeling the Key Lake uranium mill's bulk neutralization process using a pilot-scale model. Hydrometallurgy 149, 210–219. doi:10.1016/j.hydromet.2014.08.010

Rozov, K., Berner, U., Taviot-Gueho, C., Leroux, F., Renaudin, G., Kulik, D., Diamond, L.W., 2010. Synthesis and characterization of the LDH hydrotalcite-pyroaurite solid-solution series. Cem. Concr. Res. 40, 1248–1254. doi:10.1016/j.cemconres.2009.08.031.

Shaw, S.A., Hendry, M.J., Wallschläger, D., Kotzer, T., Essilfie-Dughan, J., 2011. Distribution, characterization, and geochemical controls of elements of concern in uranium mine tailings, Key Lake, Saskatchewan, Canada. Appl. Geochem. 26, 2044–2056. doi:10.1016/j.apgeochem.2011.07.002

US EPA (1998) Research Plan for Arsenic in Drinking Water: EPA/600/R-98/042. U.S. Environmental Protection Agency Office of Research and Development: National Centre for Environmental Assessment, Cincinnati.

US EPA, 1987. Standards for Remedial Actions at Inactive Uranium Processing Sites, Federal Register, 40 CFR Part 192. U.S. Environmental Protection Agency.

US EPA, 1995. Aquatic Life Criteria Table: National Recommended Water Quality Criteria [WWW Document]. Sect. 304(a) Clean Water Act. URL http://water.epa.gov/scitech/swguidance/standards/criteria/current/index.cfm (accessed 6.1.15).

Wang, S., Mulligan, C.N., 2006. Occurrence of arsenic contamination in Canada: sources, behavior and distribution. Sci. Total Environ. 366, 701–21.

4.0 Summary and Conclusions

The As- and Mo- bearing secondary mineral phases formed during the neutralization of uranium mill wastes were studied for the current ore blend and two potential future ore blends at the Key Lake mill, northern Saskatchewan, Canada. A lab-scale plant was used to characterize secondary mineral phases in the precipitates from the three ore blends during the uranium mill bulk neutralization process. Slurry samples (n = 12) were collected from the precipitates formed at pH points 4.2, 6.5 and 9.2 during the neutralization of mill wastes (raffinate) with $Ca(OH)_2$ (slaked lime) from pH 1.5 to 10.5. Synchrotron based X-ray absorption spectroscopic analysis of mill and lab-scale plant precipitates showed that arsenate adsorbed to ferrihydrite was the dominant As mineral phase regardless of pH or sample blend (53-77%), with fractional contribution from ferric arsenates, and adsorption to aluminum phases (basaluminite, aluminum hydroxide and hydrotalcite). Molybdate adsorbed to ferrihydrite was the dominant Mo mineral phase, regardless of pH or sample blend, with fractional contribution decreasing with increasing pH, and minor contributions from calcium molybdate, ferric molybdate and nickel molybdate. Comparison of X-ray absorption near edge structures (XANES) of samples to model compounds indicated As and Mo were stable as the oxidized +5 and +6 states for all samples in scenarios tested.

The mineralogical data was successful in verifying the source terms for these mineral phases in tailings facilities when used as inputs into geochemical models. Models confirmed the stable oxidation state for As and Mo were +5 and +6, during neutralization regardless of sample blend. Sequestration of As and Mo in the geochemical model showed solubility was controlled by adsorption to both Fe and Al oxyhydroxide surfaces as well as formation of secondary mineral phases such as $FeAsO_4$, $NiMoO_4$, $CaMoO_4$, $Fe_2(MoO_4)_3$. The models developed solubility profiles of mineral phase precipitation for As, Mo, Fe, Al, Mg and Ni during sequestration from pH 1.5 to 10.5 that were consistent regardless of ore blend used in simulations. Because adsorption of anions to the surface of ferrihydrite has been shown to slow conversion to crystalline forms of Fe oxides (goethite and hematite) and the sequestration of arsenate effectively control As solubility at high pH (pH >10), As-bearing ferrihydrite is expected to be stable for thousands of years. With adsorption as well as direct precipitation considered, Mo phases though effectively sequestering below pH 8, became unstable and released Mo back into the tailings porewater (pH >10). Historical

data obtained from as-discharged tailings from the Key Lake mill as well as previously published U mill tailings studies support these findings.

Based on this understanding, the impact of altering the hydrometallurgical processes and chemical parameters (i.e. ore used) on the removal of As and Mo by precipitation with lime from raffinate solutions was determined. The geochemistry of the ore does not alter the removal of either As or Mo during the bulk neutralization of mill wastes at Key Lake mill and precipitates generated are comparable to those currently observed in the U mill process. Lastly the findings of this study were used to predict the long-term stability of the formed secondary mineral phases once deposited in the tailings facility. The As-bearing mineral phases observed are expected to remain stable in the tailings for thousands of years, whereas the Mo-bearing mineral phases are observed to be soluble at the conditions present at the Key Lake Deilmann Tailings Management Facility.

5.0 Recommendations for Future Work

Based on the research conducted in this study, the following suggestions are made for further work in uranium mill neutralization studies and other As and Mo rich tailings facilities.

1. Continue monitoring the concentrations of As and Mo in as-discharged tailings porewater, as well as, in the groundwater monitoring programs at the Key Lake milling operation to verify the stability of solubility profiles described by the models and geochemical phases identified in this study.
2. Conclusion made in this study regarding the long-term stability of As in the tailings were based on arsenate and molybdate adsorbed to 2-line ferrihydrite being the dominant control on the solubility of both anions, but recent work in water bodies impacted by acid mine drainage have observed ferrihydrite dominated sediments will also include substitution of aluminum for iron ions creating aluminum-doped ferrihydrite structures that aide in stabilizing the final mineral phases. Further synchrotron-based mineralogical analysis of the bulk neutralization precipitates and the impact of aluminum substitution on the long-term stability of arsenic and molybdenum in the precipitates is warranted, based on comparable bond lengths found for arsenic adsorption to aluminum-substituted ferrihydrite to those found in this study.
3. The thermodynamic stability of ferric arsenate and amorphous scorodite phases during the pH adjustment process remain debatable. Though the solubility of limed (< pH 4) scorodite-like phases have been extensively studied, the kinetics of the transition from amorphous scorodite phases found at low pH in this study (pH 4) to the absence of such phases in the final tailings (pH 10) has not been determined. Aging tests of freshly precipitated neutralization precipitates would aide in determining the stability of these phases and the fate of arsenic released during dissolution.
4. The role of process and chemical parameters such as final pH, retention times and alternative reagents on the solubility of the As- and Mo-bearing mineral phases though touched upon in the thesis, were not investigated for alternative mill neutralization methods. It was evident from analysis that Mo sequestration would benefit from a lower final pH set point (pH <8.0) in preventing the dissolution of molybdenum adsorption

from ferrihydrite surfaces. Further work is recommended to determine if changing process parameters (i.e., pH) would have an adverse effect on solubility profiles for elements (i.e., Ni, Mg) that are controlled at higher pH values (pH >5).

5. Nickel, selenium, and silicon mineral phases were included in geochemical modelling, but the mineralogical controls on their solubility were not investigated. Wulfenite ($PbMoO_4$) though a potential sink for molybdenum, was not included in modeling or phase identification. Future work in this regard is recommended to develop a more holistic picture of the interactions of elements of concern within the Deilmann tailings management facility at Key Lake operation.
6. Further work is recommended to determine if the same mineralogical controls exist in other mine waste neutralization circuits under similar conditions to that of the Key Lake mill, as well as, those with differing Fe/As and Mo/As ratios in mill waste solutions. The fate and mobility of As and Mo in other in-pit uranium mill tailings facilities that exist in northern Saskatchewan (e.g. Rabbit Lake in-pit tailings management facility and the McClain Lake JEB tailings management facility) have been studied, however the precipitates originating from each pH step in the neutralization circuits have not been studied.

APPENDIX A
Construction of the Lab Scale Plant model

Introduction

The focus of this study was to characterize mineral phases formed during neutralization of waste materials in the Key Lake bulk neutralization (BN) circuit that was part of a lab-scale plant (LSP) model of the full mill. The BN circuit utilized the ore milled through a replication of the entire milling process from grinding, counter-current decantation, solvent extraction for neutralization into precipitates that would contribute to the final tailings. The following briefly describes the set-up of each stage in the LSP model as has been previously validated as replication the Key Lake mill by comparison of performance indicators and effluent quality (Lieu et al., 2015). Mineralogy of the ore blends and leach residues have also been previously characterized (Hossain, 2014; Lieu et al., 2015).

Modeling the LSP model after the Key Lake Process

An overview of the LSP process that was constructed is presented in Figure A1 (Lieu et al., 2015). Three ore blends were created from McArthur River ore as well as representative core material from the Millennium deposit; a potential future ore source for the Key Lake mill. Ores were processed through the grinding circuit with low grade materials to the desired head grade (Table A-1). The purpose of making adjustments to the mill feed was to determine if changes to the mill feed blend would have any effect on the mill effluent and geochemical stability of precipitates formed during the bulk neutralization and subsequently the final tailings.

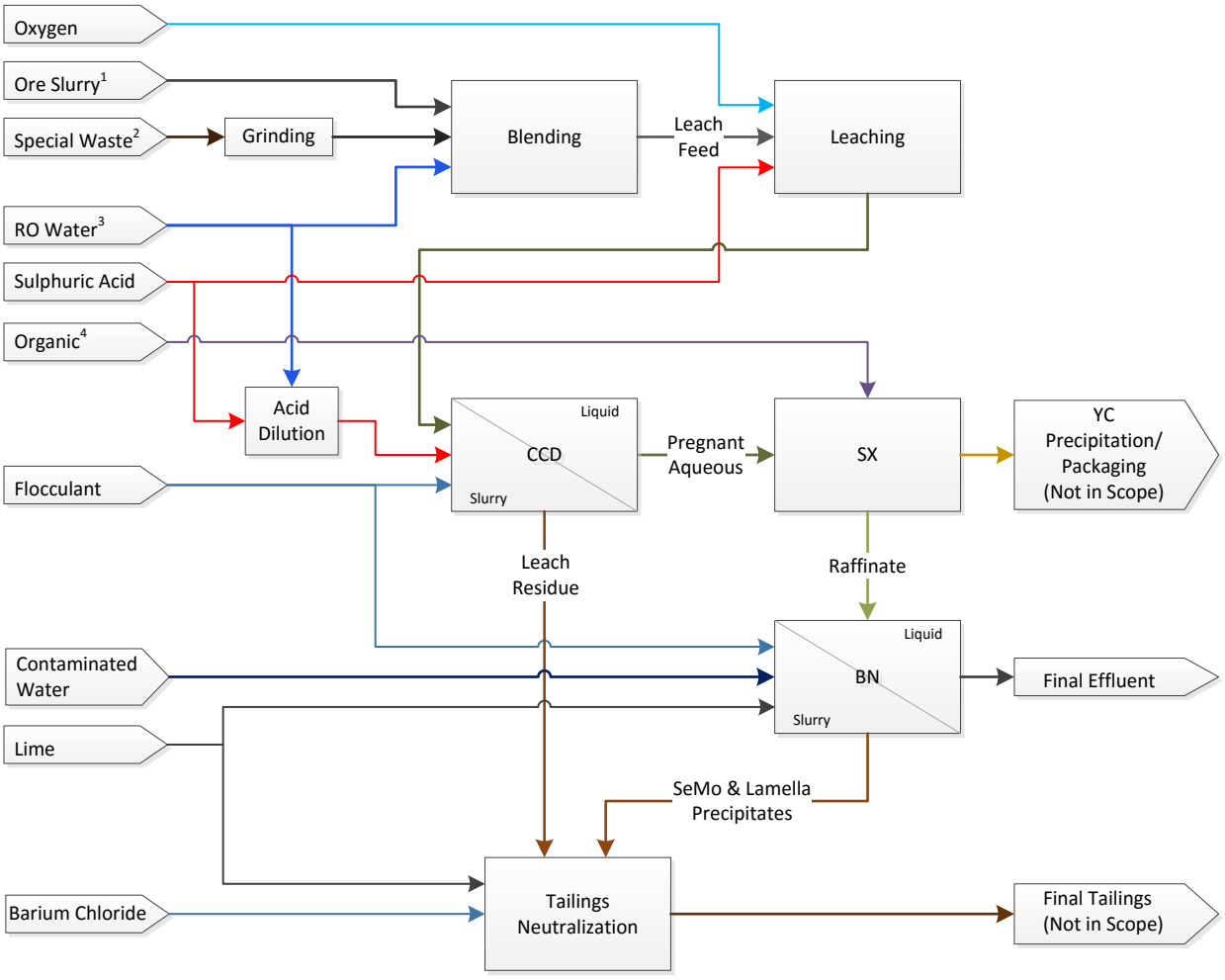

[1] McArthur River Slurry

[2] Deilmann, Gaertner, McArthur River special waste

[3] Reverse Osmosis Water

[4] 85% kerosene, 5% isodecanol, and 10% tertiary amine

1(b)

Figure A1. Overview of Lab-scale plant (LSP), used with permission from Lieu et al., 2015.

Grinding

Current ore is at Key Lake taken from McArthur River mining operation and blended with various low grade materials to achieve a leach feed concentration of approximately 4% U_3O_8. Future ore blends may include ore from the Millennium deposit that have lower total concentrations of uranium, and will result in different blend ratios. To create the three blend scenarios for processing in the LSP study, the following ores were collected: McArthur composite slurry (McA) and Millennium core samples (MLM). Low grade materials, Deilmann (DSW), Gaertner (GSW)

special wastes, and McArthur River mineralized waste (McW), are also collected for the following blending instructions (Table A1).

Table A-1. Blending instruction for the LSP scenarios.

Scenario	Blending Instruction
1	5% grade with McA ore, DSW: GSW: McW = 45:45:10 (Current Key Lake Ore Blend)
2	5% grade with McA:MLM = 75:25 & DSW: GSW: McW = 30:50:20
3	2% grade with MLM ore, DSW: GSW: McW = 30:50:20 (Worst case when no ore from McA)

A 43-kg composite sample of high-grade ore from the McArthur River mine was collected between March and May 2012 using 250 mL daily sub-samples of the slurry from the ore storage tanks in the KL ore receiving facility. Core samples (N = 94) were taken from defined intervals (every 4th sample of increasing depth from 364 samples at 7 drill holes) of Millennium ore and crushed using a laboratory jaw crusher in the same was as composite samples (50 kg) of mineralized DSW and GSW that were collected. The crushed materials were screened at using #6 Tyler mesh (3.35 mm). The +6 mesh (>3.35 mm) materials were then crushed and screened again. This step was repeated several times until all oversize material passed through the mesh. The -6 mesh (<3.35 mm) material was saved for grinding as described by (Bwalya et al., 2014; Lee et al., 2012).

Individual -6 mesh (<3.35 mm) samples of DSW, GSW, and McW were processed though the lab-scale grinding mill using two 2.5 kg rod mills (Fig. A2). The rod mill consisted of a cylindrical carbon steel container with 24 mild steel rod charges of various sizes that rotated along the same axis on a mechanical roller. Due to the variation of hardness of these mineralized wastes, grinding time was determined for each to ensure the optimal grain sizes were achieved for maximum U recovery during leaching by grinding sets of sample mixed with reverse osmosis water at 50% solids (Lieu et al., 2015).

Figure A2. Grinding circuit showing two carbon steel grinding mills.

Leaching

The leaching process was carried out using a custom-designed stir tank reactor (STR) that was scaled down (1:13,490) based on the STRs in the KL mill. This vessel (Fig. A3) was made of a 27-inch (686 mm) long section of 8-inch (203 mm) outside diameter Schedule 80 316 stainless steel pipe with welded flanges on both ends. Four baffle plates that were one-twelfth the diameter of the pipe were welded along and inside the pipe at 90° from each other to enhance mixing of the slurry. A 0.5 HP variable speed overhead mixer and 36-inch (915 mm) long 316 stainless steel duo impellers were installed on an adjustable mount.

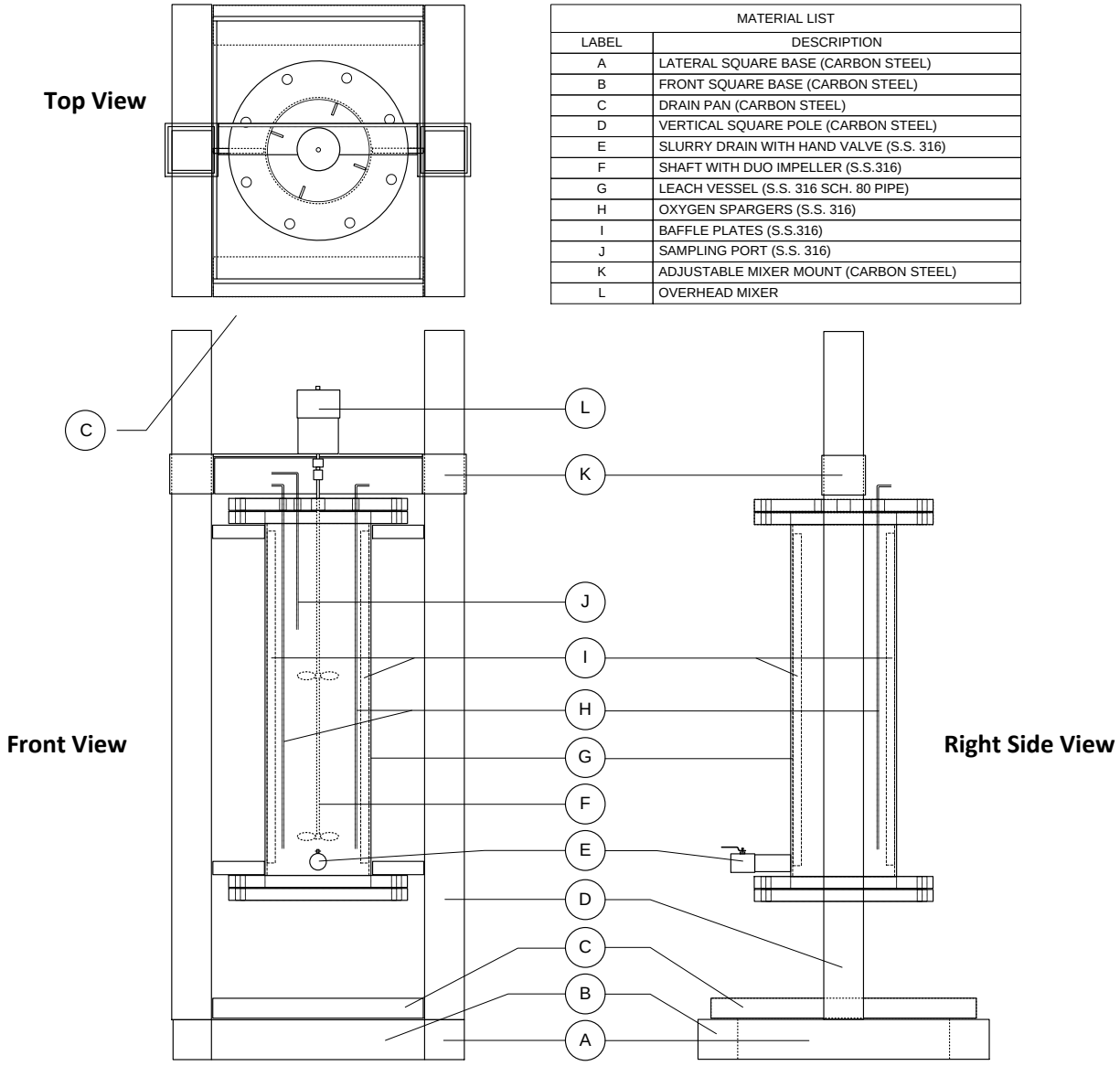

MATERIAL LIST	
LABEL	DESCRIPTION
A	LATERAL SQUARE BASE (CARBON STEEL)
B	FRONT SQUARE BASE (CARBON STEEL)
C	DRAIN PAN (CARBON STEEL)
D	VERTICAL SQUARE POLE (CARBON STEEL)
E	SLURRY DRAIN WITH HAND VALVE (S.S. 316)
F	SHAFT WITH DUO IMPELLER (S.S.316)
G	LEACH VESSEL (S.S. 316 SCH. 80 PIPE)
H	OXYGEN SPARGERS (S.S. 316)
I	BAFFLE PLATES (S.S.316)
J	SAMPLING PORT (S.S. 316)
K	ADJUSTABLE MIXER MOUNT (CARBON STEEL)
L	OVERHEAD MIXER

Figure A3. Schematic of leaching vessel, used with permission from Lieu et al., 2015.

During leaching (Fig. A4), the temperature of the slurry was maintained at 60° C with a 508 × 406 mm silicon heat blanket wrapped around the vessel and controlled by a rheostat. An external heat source was used to avoid direct contact between the materials of the heat source and the leach slurry to prevent subsequent contamination during the acid-leach process. Three oxygen spargers made from 1/4 inch (6.35 mm) 316 stainless steel tubing were installed to allow compressed oxygen to be discharged inside and at the bottom of the vessel. At start of the leaching test,

sulphuric acid (94% w/w) was added at a concentration of 140 g acid/kg ore to the slurry. Industrial grade O_2 was injected continuously at a constant feed pressure of 344 kPa into the slurry over the 24 h test period.

Figure A4. Leaching simulation in progress.

Counter-Current Decantation (CCD)

CCD was carried out using a 50 L cone-shaped bottom high density polyethylene (HDPE) vessel (Fig. A5), where the leach-residue slurry was mixed with flocculant (0.1% w/w) and wash solution (10% H_2SO_4 vol/vol in reverse osmosis water). After the slurry was allowed to settle, the supernatant was decanted from the vessel. Additional flocculant and wash water were mixed with the leach-residue slurry, each time combining with the supernatant that was previously decanted. This procedure was repeated for several cycles until a final concentration of uranium in the supernatant was between 12 and 14 g/L U_3O_8. This resulting solution was referred to as pregnant aqueous solution (PAS).

Figure A5. Counter-current decantation vessel with stirring.

Solvent Extraction (SX)

The extraction of U from the PAS was conducted using a 50 L cone-shaped bottom HDPE tank (Fig. A6). To avoid cross contamination from reagents used in the plant, fresh SX organic reagents were prepared using 85% kerosene, 5% isodecanol, and 10% tertiary amine. The SX organic solution was protonated with 360 g/L H_2SO_4 by contacting with the acid solution for 10 min. The protonated organic solution and the PAS were both maintained at 40°C in a water bath regulated by a PolyScience Standard Immersion Circulator. The PAS was added to the SX organic at a ratio of 1:1.5 (v/v), then mixed with an overhead mixer at 1,000 rpm for 15 min with the impeller blade set just above the solution interphase. After mixing and phase separation, the aqueous solution was drained and the organic collected. The aqueous solution was reacted a second time with fresh SX organic to ensure 100% extraction of U from the PAS, combined and then used as the waste solution (raffinate) treated through the bulk neutralization circuit.

Figure A6. Solvent extraction vessel with stirring.

Bulk Neutralization (BN)

The raffinate solution was mixed with two other mill waste streams (reservoir 1 and 2) to create the raffinate feed before reporting to the BN process. Variable-speed peristaltic pumps were used to deliver the raffinate feed and flocculant solutions through 3.1 mm internal diameter Tygon® lab tubing during neutralization. Each reaction vessel (Pachuca) was fitted with an overhead mechanical mixer, at 950 rpm, with polypropylene swing-out paddle assembly equipped with 8 mm × 350 mm length × 60 mm diameter paddles. $Ca(OH)_2$ addition (slaked lime) was monitored by pH/Eh pump control systems capable of 1 L/h and 15 bar max pressure to ensure pH set points were reached at each Pachuca. Dilute sulphuric acid was added to the reactors if the pH drifted higher than the target. Final pH and Eh values were recorded immediately after the thickeners were sampled.

The details of the operation of the LSP bulk neutralization circuit are as follows (Fig. A7). The raffinate feed solution (A) was created using 7.6 L raffinate and 19.7 L of reservoir 1 and 2. This feed was pumped into the first reaction vessel (B) where pH control pumps delivered slaked lime in batch mode until the target set point of pH 3.5 was achieved. Continuous mode began as B

overflowed to the SeMo thickener (C) at a raffinate feed flow rate of 14.5 mL/min. Flocculant was added to enhance settling with overhead stirring. Solids were collected in the first thickener while the overflow from C was directed to the second reaction vessel (D), controlled with slaked lime addition to a target of pH 6.5. D overflowed to the final reaction vessel (E) controlled with slaked lime to a target of pH 9.5, where the overflow was collected into the Lamella thickener (F). The overflow of the Lamella thickener was collected as final effluent as the solids settled. Samples of secondary precipitates were collected from each thickener, C (SeMo) and F (Lamella), as well as the reaction vessel D (Pachuca 3) and processed further for analysis. The underflows for each thickener were then combined into the tailings sampling campaign described following.

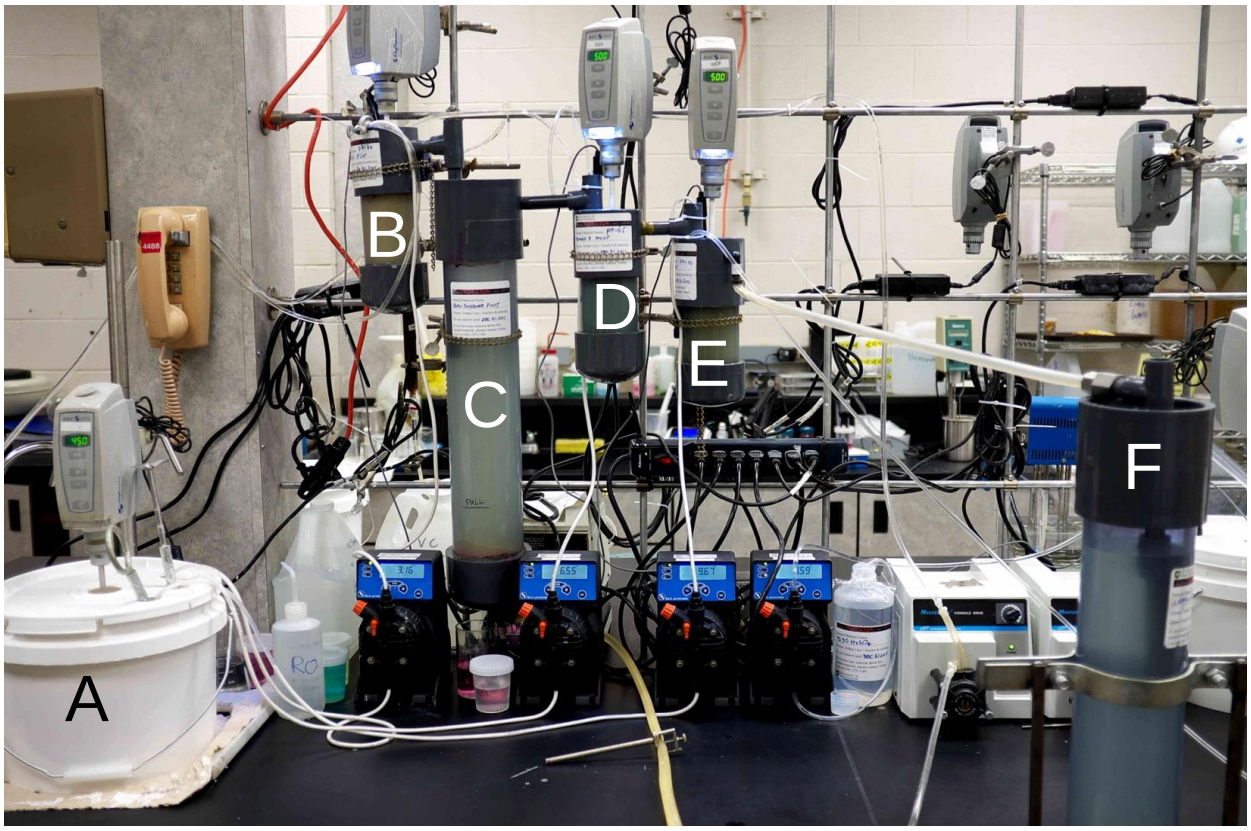

Figure A7. Bulk neutralization circuit with sample locations A) raffinate feed solution B) Pachuca 2 (pH 3.5) C) SeMo thickener (pH 3.5-4.2) D) Pachuca 3 (pH 6.5) E) Pachuca 4 (pH 9.5) F) Lamella thickener (pH 9.2-9.5)

Tailings and Final Effluent

The supernatant from the Lamella thickener collected as final effluent was treated with 5% H_2SO_4 to the target pH of 7.5. The precipitated solids from each thickener were combined with leach residues from CCD and further adjusted in two stages with $Ca(OH)_2$ to pH 8.0 and then finally 10.5 for tailings studies. During the first stage of pH adjustment, $BaCl_2$ was added to co-precipitate dissolved Ra with barite in a complex form ($Ra–BaSO_4$). While $BaCl_2$ is continuously added in the KL mill, its addition exclusively at the terminal pH set point for tailings was determined to be adequate in controlling Ra precipitation in this study (unpublished data); this alteration was necessary to eliminate interferences from the barite by-product that forms as a result of reactions between $Ca(OH)_2$ and $BaCl_2$ in the BN process (Gomez et al., 2013).

Conclusions

The LSP was modeled to replicate the Key Lake process from grinding, leaching, counter-current decantation, bulk neutralization and tailing. The ore blends processed through the full LSP provided secondary precipitates for the purpose of this study.

References

Bwalya, M.M., Moys, M.H., Finnie, G.J., Mulenga, F.K., 2014. Exploring ball size distribution in coal grinding mills. Power Technol. 257, 68–73.

Hossain, M.A., 2014. Mineralogical Characterization of Uranium Ores, Blends and Resulting Leach Residues from Key Lake Pilot Plant, Saskatchewan, Canada. MSc Thesis, Department of Geological Sciences, University of Saskatchewan.

Lee, H., Klima, M.S., Saylor, P., 2012. Evaluatio of a laboratory rod mill when grinding bituminous coal. Fuel 92, 116–121.

Lieu, A., Bissonnette, J., Hossain, A.M., Essilfie-Dughan, J., Moldovan, B.J., Hendry, M.J., 2015. Simulating the mineral process at the Key Lake uranium mill, northern Saskatchewan, Canada in a lab-scale plant. Submitted to Hydrometallurgy.

APPENDIX B

Total Chemical Profiles for Lab Scale Plant (LSP) and Key Lake (KL) Models

Table B1. Chemical analysis of samples collected from Scenario 1 of current mill conditions [5% grade with McA ore, DSW:GSW:McW = 45:45:10] in August 2012 of the LSP (Figure 3-1) study.

	Raffinate[a]	SeMo Thickener[b]		Pachuca 3 Reactor[c]		Lamella Thickener[d]		Final Tailings[e]	
Parameter	Solution	Solution	Solids	Solution	Solids	Solution	Solids	Solution	Solids
As	195	0.129	2630	0.005	482	0.018	556	0.144	193
Se	0.376	0.019	3.90	0.010	1.25	0.010	1.39	0.056	4.75
Mo	3.08	0.043	152	0.009	30.4	0.363	16.3	0.223	64.8
Ni	295	40.6	491	6.09	1610	0.024	2260	0.178	396
Cu	52.2	4.86	73.2	0.030	301	0.095	333	0.024	308
Co	15.0	4.10	12.0	0.798	146	0.005	238	0.005	59.8
Zn	27.4	5.42	24.2	0.373	300	0.093	302	0.018	74.0
U	2.83	0.984	43.3	1.74	109	1.27	272	1.50	847
Fe	4062	367	49250	70.8	27315	0.106	37236	2.08	18577
Al	3167	390	28382	0.041	50106	3.67	52455	6.66	79788
Na	68.1	78.9	23563	74.3	39230	72.6	24880	48.8	52556
Mg	2792	434	1498	346	3897	9.42	26600	6.72	13651
Ca	1267	447	144849	632	121240	583	134808	554	26401
K	502	69.5	4855	64.4	505	60.6	5690	21.5	19517
HCO_3		< 0.1		< 0.1		58.8		68.1	
Cl		48.7		na		39.0		80.3	
$NO_{2/3}$		6.04		na		< 0.01		9.60	
SO_4	17938[f]	7080		na		1630		1310	
pH	1.59	3.90		4.35		8.90		9.20	
Cond (mS/cm)	58.1	6.43		4.79		2.89		2.36	
Eh (mV)	635	489		543		457		382	
Charge Balance	3.30	-7.77		na		-0.503		-0.014	
Fe/As (M)	27.9	3810	25.1	18967	75.9	7.89	89.7	19.3	129
Fe/Mo (M)	2262	14639	556	13493	1541	0.50	3918	16.0	492
Mg/Al (M)	0.98	1.24	0.06	9368	0.09	2.85	0.56	1.12	0.19

[a] Sample point A on figure 3-1, [b] Sample point C on figure 3-1, [c] Sample point D on figure 3-1, [d] Sample point F on figure 3-1, [e] Sample point G on figure 3-1, [f] Calculated value from pH and free acid (average = 13 g/L), na = not available due to insufficient sample

Table B2. Chemical analysis of samples collected from Scenario 2 of ore blend [5% grade with McA:Me 25:75, DSW:GSW:McW = 30:50:20] in August 2012 of the LSP (Figure 3-1) study.

	Raffinate[a]	SeMo Thickener[b]		Pachuca 3 Reactor[c]		Lamella Thickener[d]		Final Tailings[e]	
Parameter	Solution	Solution	Solids	Solution	Solids	Solution	Solids	Solution	Solids
As	223	0.093	1950	0.006	232	0.011	119	0.056	128
Se	0.450	0.026	3.07	0.008	2.01	0.010	1.28	0.044	8.82
Mo	6.10	0.090	146	0.027	36.8	0.126	13.1	2.13	98.6
Ni	222	23.3	482	0.740	2059	0.082	1550	0.020	232
Cu	47.4	0.945	199	0.012	387	0.015	270	0.023	269
Co	36.1	3.74	29.5	0.228	259	0.012	214	0.005	52.9
Zn	18.8	2.00	35.2	0.045	235	0.007	251	0.005	40.4
U	2.18	0.824	208	0.058	256	0.039	616	0.023	256
Fe	5628	440	35028	20.0	44152	1.14	31997	0.051	12689
Al	5076	133	51039	0.110	61538	6.27	56704	0.061	72463
Na	49.5	84.7	25843	77.4	68139	73.3	21577	46.0	1077
Mg	4438	580	2065	451	6651	5.35	39597	7.10	12464
Ca	1286	513	136006	776	126621	561	124028	706	20469
K	177	68.6	5440	75.3	13793	73.5	5005	22.0	9025
HCO_3		< 0.1		9.2		57.8		94.7	
Cl		51.3		48.4		46.7		78.5	
$NO_{2/3}$		5.14		4.44		4.24		3.10	
SO_4	26292	6230		4030		1660		1880	
pH	1.16	3.85		5.36		8.22		9.3	
Cond (mS/cm)	63.3	6.52		5.32		3.00		3.83	
Eh (mV)	610	573		513		426		349	
Charge Balance	3.25	-3.93		-0.550		-1.21		2.68	
Fe/As (M)	33.8	6337	24.1	4465	255	138	360	1.22	132
Fe/Mo (M)	1582	8385	412	1271	2058	15.5	4190	0.04	221
Mg/Al (M)	0.97	4.84	0.04	4551	0.12	0.95	0.78	129	0.19

[a] Sample point A on figure 3-1, [b] Sample point C on figure 3-1, [c] Sample point D on figure 3-1, [d] Sample point F on figure 3-1, [e] Sample point G on figure 3-1, [f] Calculated value from pH and free acid (average = 13 g/L)

Table B3. Chemical analysis of samples collected from Scenario 3 of worst case [2% grade with Millennium ore, DSW:GSW:McW = 30:50:20] in August 2012 of the LSP (Figure 3-1) study.

	Raffinate[a]	SeMo Thickener[b]		Pachuca 3 Reactor[c]		Lamella Thickener[d]		Final Tailings[e]	
Parameter	Solution	Solution	Solids	Solution	Solids	Solution	Solids	Solution	Solids
As	47.7	0.101	2690	0.049	332	0.047	393	0.090	131
Se	0.127	0.014	5.61	0.013	1.43	0.012	1.42	0.082	14.2
Mo	1.34	0.015	331	0.026	58.2	0.133	25.6	2.62	133
Ni	63.6	19.2	883	5.12	2110	0.129	4090	0.017	365
Cu	14.4	2.87	141	0.036	678	0.020	823	0.013	208
Co	4.51	1.56	26.6	0.439	148	0.012	293	0.005	30.8
Zn	5.20	1.42	1331	0.095	457	0.017	339	0.005	46.5
U	1.07	0.437	160	0.069	232	0.023	176	0.017	634
Fe	1311	76.7	56410	4.12	26268	1.04	32456	0.014	13135
Al	1108	164	34406	1.65	89122	1.13	79654	0.032	78942
Na	29.8	69.0	38187	74.5	68934	63.9	32509	41.0	45306
Mg	553	161	989	139	2408	20.8	32880	4.00	12089
Ca	504	508	151973	878	150239	780	101166	744	14689
K	212	85.9	8374	85.8	13620	78.8	6661	15.5	22895
HCO_3		<0.1		< 0.1		10.1		117	
Cl		51.9		na		48.7		59.6	
$NO_{2/3}$		5.87		na		5.84		6.11	
SO_4	19662	4230		na		1980		1910	
pH	1.46	3.88		3.68		5.53		9.97	
Cond (mS/cm)	58.2	4.17		4.49		3.11		2.79	
Eh (mV)	629	503		548		507		297	
Charge Balance	-10.8	-7.69		na		0.713		-1.22	
Fe/As (M)	36.8	1017	28.1	112	106	2.96	111	0.21	134
Fe/Mo (M)	1678	8770	292	272	775	13.4	2180	<0.01	169
Mg/Al (M)	0.55	1.09	0.03	93.5	0.03	20.4	0.46	138	3.83

[a] Sample point A on figure 3-1, [b] Sample point C on figure 3-1, [c] Sample point D on figure 3-1, [d] Sample point F on figure 3-1, [e] Sample point G on figure 3-1, [f] Calculated value from pH and free acid (average = 13 g/L), na = not available due to insufficient sample

Table B4. Chemical analysis of samples collected from Key Lake bulk neutralization circuit (Figure 3-2) in August 2013.

	Raffinate[a]	SeMo Thickener[b]		Pachuca 3 Reactor[c]		Lamella Thickener[d]		Final Tailings[e]	
Parameter	Solution	Solution	Solids	Solution	Solids	Solution	Solids	Solution	Solids
As	210	0.253	3014	0.006	133	0.010	81.6	0.280	541
Se	0.257	0.029	3.84	0.017	2.67	0.014	2.08	0.033	3.95
Mo	2.23	0.079	219	0.052	19.2	0.090	11.8	8.81	61.3
Ni	154	37.0	755	0.191	4373	0.019	3447	0.087	694
Cu	21.1	3.41	104	0.010	426	0.014	325	0.015	176
Co	14.5	3.24	40.6	0.028	484	0.005	383	0.005	81.8
Zn	12.9	1.88	44.8	0.010	424	0.008	321	0.014	92.6
U	2.87	1.52	77.1	0.010	336	0.009	210	0.074	720
Fe	2429	304	29550	0.320	52697	0.032	40719	0.017	19249
Al	3277	163	63914	0.421	48812	0.937	40588	0.068	82899
Na	81.9	83.2	30606	116.4	36122	117.6	32182	102.9	35997
Mg	2270	511	2289	411	16224	9.25	50767	1.15	19599
Ca	797	478	154015	688	152803	612	136134	470	79919
K	132	60.1	6893	64.1	6603	64.1	6004	44.8	16376
pH	1.60	4.20		7.20		9.70		9.00	
Eh (mV)	596	475		446		411		412	
Cond (mS/cm)	41.0	6.12		4.95		3.09		2.73	
Fe/As (M)	15.5	1610	13.1	71.4	531	4.29	669	0.08	47.6
Fe/Mo (M)	1868	6600	231	10.6	4708	0.610	5919	<0.01	539
Mg/Al (M)	0.769	3.48	0.04	1083	0.37	11.0	1.39	1.15	0.26
Mg/Fe (M)	2.15	3.87	0.18	2956	0.71	665	2.87	0.07	2.34

[a] Sample point A on figure 3-2, [b] Sample point C on figure 3-2, [c] Sample point D on figure 3-2, [d] Sample point F on figure 3-2, [e] Sample point G on figure 3-2, [f] Calculated value from pH and free acid (average = 13 g/L), na = not available due to insufficient sample

APPENDIX C
Additional Solid Sample Characterization

Introduction

Additional analysis was performed on solid precipitate samples collected from the bulk neutralization circuit at the Key Lake (KL) mill and the lab-scale plant (LSP) model. The following describes the results of these analysis.

Materials and Methods

ICP-MS

Bulk elemental analysis by inductively coupled plasma mass spectrometry (ICP-MS) was performed at the Key Lake chemistry lab, performed on an Agilent 7500cx and 7700 equipped with an ASX–500 series sample changer, using 1500 W and 1550 W RF power, respectively. Instruments were tuned daily with a 10 ppb tuning solution of Ce, Co, Li, Tl, and Y to achieve maximum counts with minimum interferences from oxides and doubly-charged species. Samples (n = 12) were digested in a four acid leach (HCl, HNO_3, $HClO_4$, HF) before analysis on the instrument with a relative standard deviation (RSD) of ±10% (Donallson, 1981). The analysis for every 10^{th} sample were submitted to the Aqueous and Environmental Laboratory (AEL) in the Department of Geological Sciences, University of Saskatchewan for comparison. Samples sent to AEL were analyzed using a Perkin-Elmer NexION 300D (RSD ±10%) and similar acid digestion techniques for solid sample preparation (Longerich et al., 1990; Stefanova et al., 2003).

XRD

X-ray diffraction (XRD) analysis were conducted on washed solid samples (n = 12) using a PANanalytical Empyrean X-ray diffractometer equipped with a Spellman generator and Co target (λ Co K_α = 1.7902 A), operating at 40 kV and 45 mA. The samples were mounted on glass substrates as methanol slurries, and scanned in continuous mode using a spinning reflection/transmission stage. Spectra were acquired from 8 to 80° 2θ with a step size of 0.0167° and a scan speed of 1.2°/min. Detection limits for phases defined by lab-based XRD are reported as 1-5 wt% (Bish and Chipera, 1995; Gomez et al., 2014).

SEM

Scanning electron microscopy (SEM) imaging was performed using a JEOL JSM 840A. Samples (n = 4) were dry mounted, one particle thick, on double sided adhesive tape and coated with approximately 200 angstroms of gold using an Edwards S150B sputter coater. Images were acquired at x1,000, x25,000 and x50,000 magnification.

Results and Discussion

Characterization of BN precipitates

Total elemental concentrations in solid precipitates from pH set point 4.2 (SeMo thickener), 6.5 (Pachuca 3) and 9.2 (Lamella thickener) are compared in Figure C1. The first pH stage of the neutralization circuit (pH 4.2) contained the highest concentrations of As and Mo where the solids were allowed to settle in the SeMo thickener. These concentrations range from 2630 to 3010 ug/g and 152 to 331 ug/g, of As and Mo respectively, containing the highest concentrations regardless of ore blend in the first pH stage of neutralization (Appendix B).

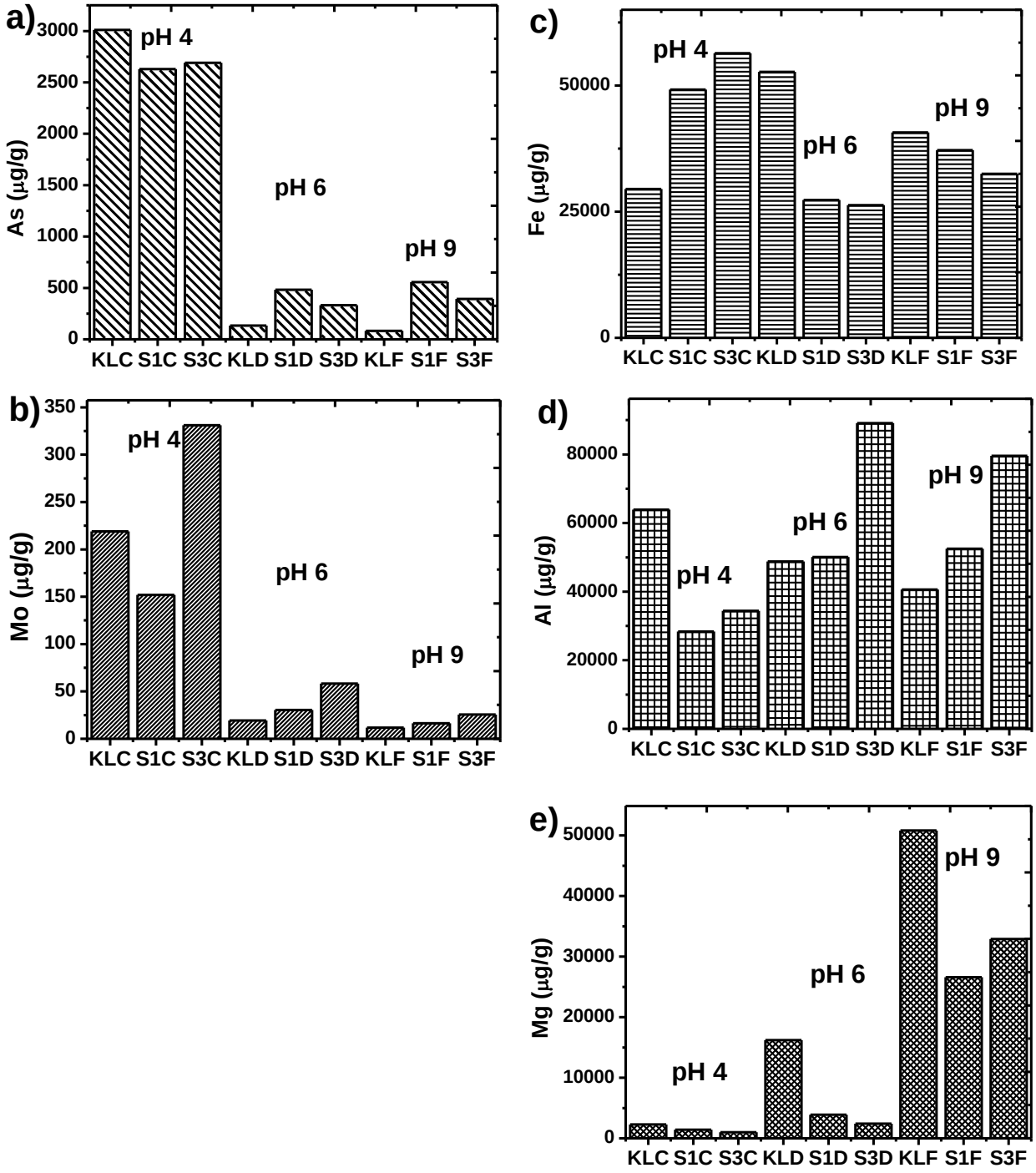

Figure C1. Bulk elemental concentration of a) As b) Mo c) Fe d) Al and e) Mg (µg/g) in the secondary precipitates by IPC-MS.

The high concentrations of As and Mo in the solid phases of the first pH set point (pH 4) indicate that both elements predominantly precipitate at this early stage of the neutralization process and agrees with earlier studies that found complete As removal (99.9 - 100.0 %) and near complete Mo removal (95.5 – 99.6 %) by pH 4 (Lieu et al., 2015; Robertson et al., 2014). Scenario 3 had the highest concentration of Mo at the first pH stage, but this was likely due to higher concentrations of Mo in the ore material and raffinate than the other sample blends (Appendix B). This trend of highest removal of As and Mo in the low pH thickener (pH 4.2) confirms previous publications on U mill bulk neutralization circuits (Mahoney et al., 2007; Moldovan and Hendry, 2005; Robertson et al., 2014).

Arsenic concentrations ranged from 133 to 482 ug/g in the Pachuca 3 sample point (pH 6.5) and 81.6 to 556 ug/g in the final Lamella thickener (pH 9.2) stage (Appendix B). The highest concentrations of As are found in scenario 1 solids at these two pH stages due to the higher concentration of As in the raffinate solution (Table B1). The lower concentrations of As in the Key Lake samples for pH 6.5 and pH 9.2 stages may be due to more efficient removal from the circuit with respect to the lab-scale mill. Mo concentrations ranged from 19.2 to 58.2 ug/g in the Pachuca 3 sample point (pH 6.5) and 11.8 to 25.6 ug/g in the final Lamella thickener (pH 9.2) stage. The highest concentrations of Mo are found in all scenario 3 samples due to the higher concentration of Mo in the raffinate for this blend (Table B3).

The concentration profiles of Fe and Al did not follow the same progression with pH for all scenarios (Figure C1 c-d). The Key Lake samples contained the highest concentrations of Fe in the mid pH range (pH 6.5) and the highest concentrations of Al at the low pH stage (pH 4.2), agreeing with the formation of ferrihydrite at pH values between 3 and 8 (Jia et al., 2006) and basaluminites between pH 3 and 6 (Robertson et al., 2015, 2014). Both LSP sample blends (S1 and S3) had higher concentrations of Fe in the low pH range and higher Al concentrations in the final pH stages (pH 6.5 and pH 9.2). This again agrees with ferrihydrite formation, but instead of basaluminite formation, amorphous aluminum hydroxide and Al-bearing hydrotalcites above pH 7 would be favoured (Gomez et al., 2013; Paikaray and Hendry, 2014; Paikaray et al., 2014; Robertson et al., 2015, 2014). Mg concentrations are greatest in the higher pH sample points, indicating the most removal occurred at high pH (Figure C1e). This agrees with the formation of Mg-Al hydrotalcite (HTLC) at pH values above 8 where low crystalline type HTLC have been

reported to form at pH 8 to 9, which increase in crystallinity with increasing pH (Robertson et al., 2014; Paikaray and Hendry, 2014).

The Fe/As and Fe/Mo molar ratios range from 13.1 to 688 and 231 to 5970 respectively, with an increase in molar ratio with increasing pH for all scenarios tested (Appendix B). A previous study on As adsorption to Fe oxides indicate at higher Fe/As molar ratios, the co-precipitation and loss of transformation to more crystalline forms of Fe oxides is favoured (Das and Hendry, 2014). Similarly, As co-precipitation with Fe is most favourable in molar ratios from 3 to 5 and higher in raffinate solutions, (DeKlerk, 2008; Langmuir et al., 1999; Moldovan et al., 2003). For Fe/As ratios near 2 in the raffinate, mixtures of poorly crystalline ferric arsenate and ferrihydrite are reported to co-exist, but as the molar ratios increase above 4-8, the major phase becomes ferrihydrite with arsenate adsorbed to the surface (Jia et al., 2006). Tables B1 to B4 indicate all samples are well above these ratios, regardless of sample blend. Previous studies have found tailings samples with high Fe/Mo molar ratios (>708) are dominated by molybdate adsorbed onto ferrihydrite (Essilfie-Dughan et al., 2011). Similarly, Mo adsorption to Fe oxides is most favourable at the high Fe/Mo molar ratios for all samples in this study.

The ratio of Al to Mg is closest to the molar ratio required to form (hydrotalcites) HTLC in in the final pH stage (Lamella thickener, pH 9.2) for all scenarios tested (Appendix B). The divalent (M^{2+}) to trivalent (M^{3+}) cationic ratios, mainly Mg^{2+} ratios to Fe^{3+} or Al^{3+}, temperature and pH of precipitating solutions will dictate which HTLC compounds will form (Paikaray and Hendry, 2014). Formation of Mg-Al-Fe HTLCs are most often reported at M^{2+}/M^{3+} ratios between two to five, though some formation is reported at ratios less than two (Paikaray and Hendry, 2014). Since HTLC formation is more favourable at higher Mg/Al or Mg/Fe ratios,(Gomez et al., 2013; Robertson et al., 2014) the solid phases in the final sample point (pH 9.2) with Mg/Al ratios ranging from 0.46 to 1.39 and Mg/Fe ratios ranging from 1.65 to 2.87 would favour formation of Mg-Al-Fe HTLCs over Mg-Al HTLCs.

XRD Analysis

X-ray diffraction measurements though unable to give indication of As- and Mo- bearing mineral phases, were successful in predicting dominant Fe and Al phases. Gypsum and calcite were the dominant mineral phases in un-washed samples (Figure C2).

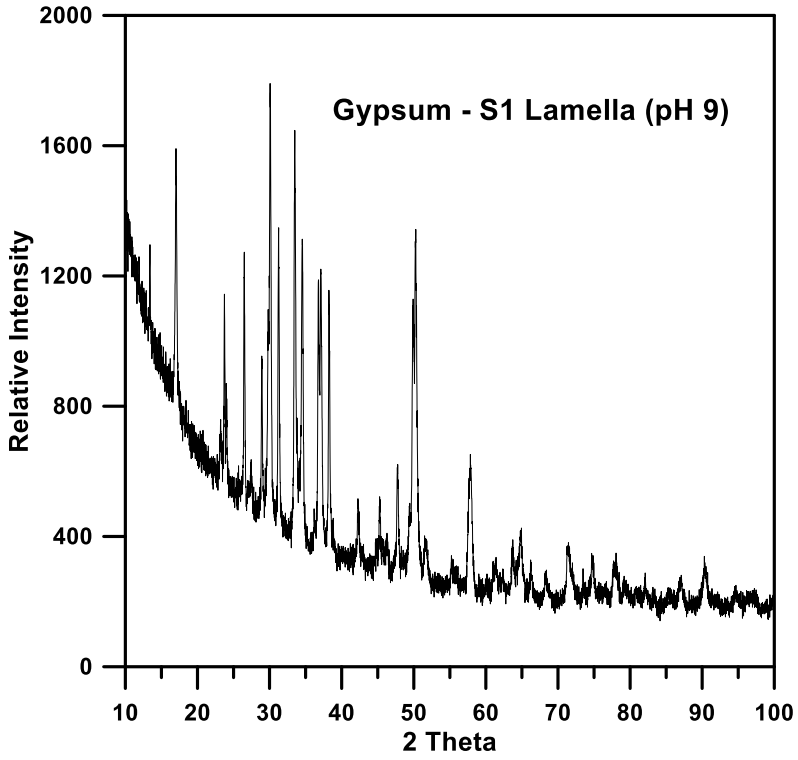

Figure C2. XRD of unwashed solids featuring gypsum ($CaSO_4 \bullet 2H_2O$) peaks in S1 Lamella thickener (pH 9) sample.

XRD spectra were obtained on washed samples to remove interferences with major phases, mainly gypsum, as was reported previously (Gomez et al., 2013; Robertson et al., 2014) though peaks from gypsum and calcite are still apparent (Figure C3).

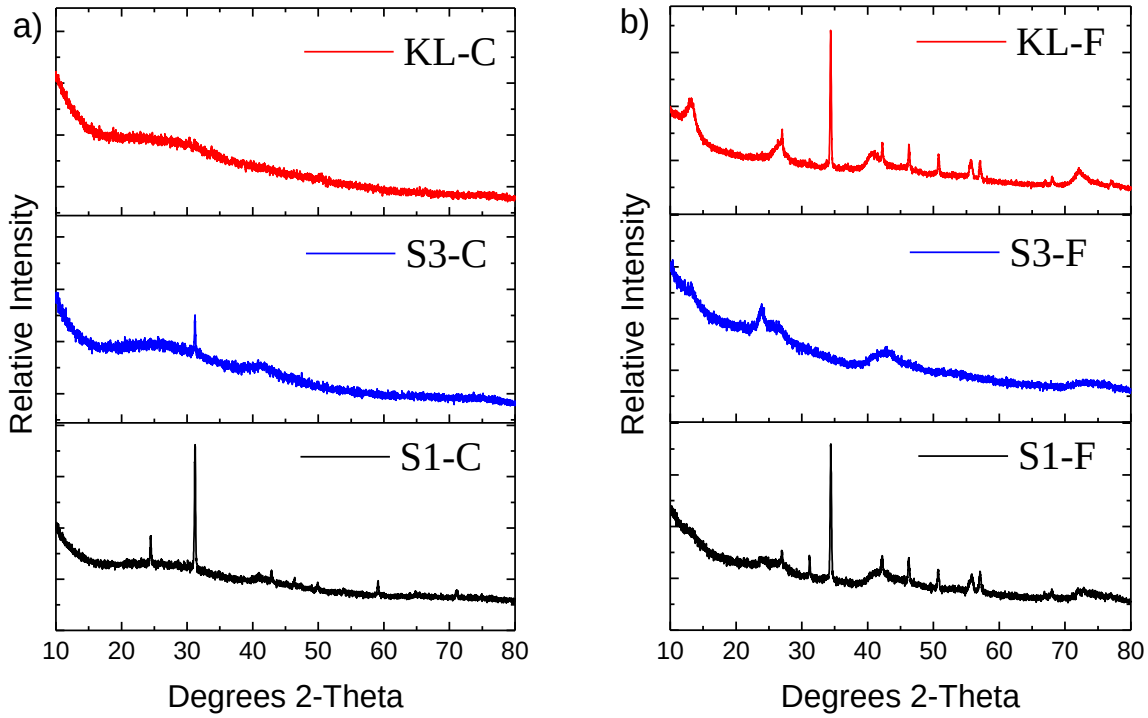

Figure C3. XRD of washed solids from scenarios 1 (S1) and 3 (S3) and Key Lake (KL) sample points: a) SeMo thickener (C - pH 4.2) and b) Lamella thickener (F - pH 9.5).

The solids in the LSP SeMo thickener samples (S3C and S1C) feature the amorphous pattern with two broad peaks approximately at 30° and 70° 2θ indicate the presence ferrihydrite, though the peak shift could indicated ferric arsenate or As adsorbed to ferrihydrite, along with sharp peaks remaining from un-washed gypsum (Fig. C3). Ferric arsenate is characterized by two broad peaks centred at 2θ values ~28° and ~58° in the XRD spectrum (Jia et al., 2006; Paktunc and Bruggeman, 2010) and ferrihydrite is characterized by two broad peaks centred at 2θ values of ~34° and ~61° (Das and Hendry, 2011; Jia et al., 2006). Measurements of the ferrihydrite standard synthesized in this study obtained at 2θ values of ~40° and ~74° (Appendix D) similar to what was seen in Das et al., (2014a, 2014b) indicating there is some variation between XRD measurements reported in literature, mostly from the XRD source used (Co or Cu). The broadness of peaks from these amorphous iron solids is of similar size and shape, but those of ferric arsenate tend to be shifted to lower 2θ values. These broad peaks are slightly more apparent in S3C, though the broadness of the amorphous patterns makes them hard to distinguish from the band between 20° to 30° 2θ in the

spectrum for KLC. This broad band has also been attributed to the presence of amorphous $Al(OH)_3$ or an $Al(OH)\text{-}SO_4$ complex which is more thermodynamically favourable in solutions with concentrations of sulfate (SO_4^{2-}) as high as the solutions from which these precipitates formed (Appendix B) (Martin et al., 2009; Robertson et al., 2015, 2014). Typically minerals such as gibbsite ($Al(OH)_3$) would be predicted to precipitate at this pH stage (pH 4.2), however, the presence of SO_4 alters the geochemistry of these phases and instead insoluble aluminum hydroxysulfates ($Al(OH)\text{-}SO_4$) become more stable (Bigham and Nordstrom, 2000). It is therefore not clear from the XRD features if the precipitates include $Al(OH)_3$ phases or $Al\text{-}OH\text{-}SO_4$ or Al-doped ferrihydrite, but it is clear that there are not significant differences between scenarios by this method.

The washed Lamella solids (S1-F, S3-F and KL-F) at pH 9.2 contain sharp peaks from residual gypsum and the bands characteristic of amorphous Mg-Al and/or Mg-Al-Fe containing SO_4/CO_3 hydrotalcite-like (HTLC) compounds previously described, though these are difficult to identify solely based on XRD (Fig. C3) (Gomez et al., 2014, 2013; Paikaray and Hendry, 2014; Robertson et al., 2014). HTLC peaks at ~13, ~27 and ~40° and first peak of the doublet at ~70-72° belong to a more crystalline structure of hexagonal system with 3R symmetry (Paikaray and Hendry, 2014). Both the pH and molar ratios of solids sampled from the Lamella thickener are favourable for HTLC formation, most likely the Mg-Fe-HTLC type of mineral phases (Appendix B). The diffraction patterns of KLF and S1F are nearly identical, with differences in S3F mainly from the absence of gypsum or calcite peaks. Therefore, the XRD spectrums indicate there are no significant differences between scenarios of sample blends with respect to main mineral phase in the Lamella thickener (pH 9.2). Based on the XRD spectrum for samples tested, the dominant mineral forms at pH 4 (SeMo Thickener) are a mixture of ferric arsenate and ferrihydrite, with some evidence of an $Al(OH)\text{-}SO_4$ complex. At pH 9 (Lamella Thickener) the dominant mineral phases is Mg-Fe HTLCs.

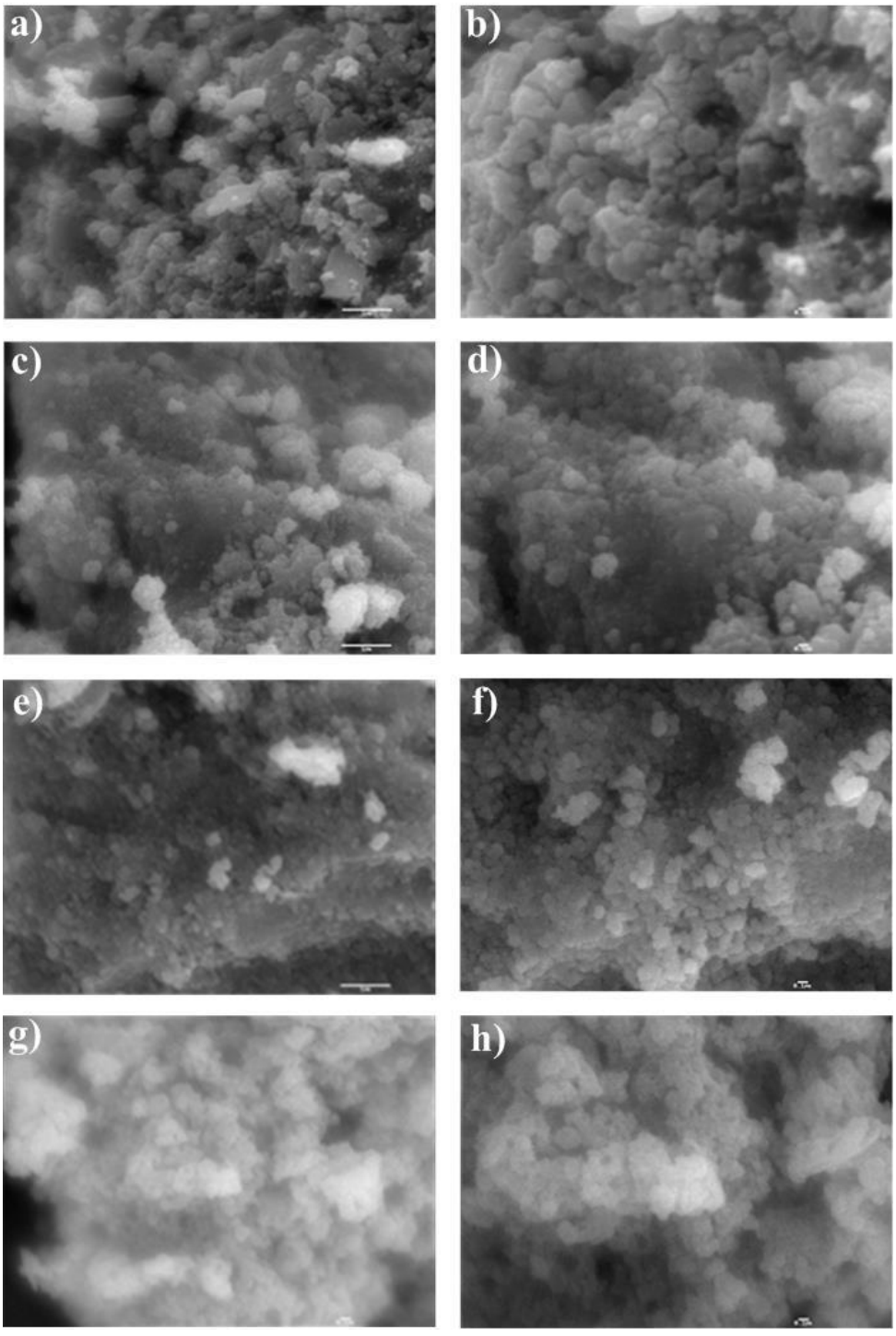

Figure C4. SEM of washed solids and standards prepared via hydrolysis of $FeCl_3$ as described previously and obtained from Robertson, et al., 2015 a) Ferrihydrite scale bar = 1 µm b) scale bar = 0.1 µm c) MgAlFe-Hydrotalcite scale bar = 1 µm d) scale bar = 0.1 µm e) Key Lake SeMo thickener (KL5) scale bar = 1 µm f) scale bar = 0.1 µm g) Key Lake Lamella thickener (KL6) scale bar = 0.1 µm h) scale bar = 0.1 µm.

SEM Analysis

Amorphous crystal features can be difficult to characterize by scanning electron microscope due to their tendency to become electrically charged and their aggregated nature (Das and Hendry, 2014.) Likewise in this study, the exact shape and size could not be determined from this method due to the aggregated nature of the particles. Similarities in morphology between model compounds (MgAlFe-HTLC and ferrihydrite) chosen based on XRD results and samples, were evident between pH stages (Fig. C4). Ferric arsenate ($FeAsO_4$) has been reported to occur as small particles aggregated into clusters with rounded outlines measuring 50-100nm (Paktunc and Bruggeman, 2010) similar to those seen in the SeMo samples (Fig. C4f) Literature indicates HTLC particles are prone to strong agglomeration leading to the formation of cohesive smooth spheroidal masses, with crystal sizes ranging from 12.1 to 88.5 nm with increases in cation ratios (Paikaray and Hendry, 2014) as is observed in the Lamella samples (Fig C4g).

The morphologies of ferrihydrite in (a) and (b) resemble those of the SeMo Thickener (KL-C, pH 4.2) in (e) and (f) with an approximate particle size of 0.2 to 0.5 μm (Fig. C4). The optimal pH for MgAlFe-HTLC formation is ~ 10, as lower pH (acidic solutions) do not favor formation and there has never been reported formation of HLTC at < pH 4 (Paikaray and Hendry, 2014). The SEM results match well with this as MgAlFe-HTLC in (c) and (d) resemble the solids more closely to solids from the Lamella thickener (KL-F, pH 9.2) samples in (g) and (h) with an average particle size approximately 0.1 to 0.2 μm (Fig. C5). This indicates SEM aligns with XRD analysis placing a more visible presence of ferrihydrite in the lower pH solids and more visible MgAlFe-HTLC in the higher pH solids, though this method is best used for confirmation than qualitative analysis.

Conclusion

Elemental analysis by ICP-MS indicate the majority of solids are precipitated in the first pH stage (SeMo thickener, pH 4.2) of both the LSP and Key Lake samples. XRD indicate a mixture of either $AlOHSO_4$ and ferrihdyrite phases or Al-doped ferrihydrite at pH 4.2 (SeMo thickener) and hydrotalcite phases at pH 9.2 (Lamella thickener). These results agree well with SEM analysis, though confirmation through additional methods is required.

References

Bigham, J.M., Nordstrom, D.K., 2000. Iron and Aluminum Hydroxysulfates from Acid Sulfate Waters, in: Jambor, J.L. (Ed.), Sulfate Minerals: Crystallography, Geochemistry and Environmental Significance. Mineralogical Society of America, pp. 351–403. doi:10.2138/rmg.2000.40.7

Bish, D.L., Chipera, S.J., 1995. Accuracy in quantitative X-ray powder diffraction analysis, in: P. Predecki, et al. (Ed.), Advances in X-Ray Analysis. Vol 38. Plenum Pub Co., pp. 47–57.

Das, S., Essilfie-Dughan, J., Hendry, M.J., 2014a. Arsenate partitioning from ferrihydrite to hematite : Spectroscopic evidence. Am. Mineral. 99, 749–754.

Das, S., Essilfie-Dughan, J., Hendry, M.J., 2014b. Arsenate adsorption onto hematite nanoparticles under alkaline conditions: effects of aging. J. Nanoparticle Res. 16, 1–12. doi:10.1007/s11051-014-2490-3

Das, S., Hendry, M.J., 2014. Characterization of hematite nanoparticles synthesized via two different pathways. J. Nanoparticle Res. 16, 1–16.

Das, S., Hendry, M.J., 2011. Application of Raman spectroscopy to identify iron minerals commonly found in mine wastes. Chem. Geol. 290, 101–108. doi:10.1016/j.chemgeo.2011.09.001

DeKlerk, R.J. 2008. Investigating the Continuous Circuit Coprecipitation of Arsenic (V) with Ferric Iron in Suphate Media. M.Eng. Thesis, Department o fMining and Materials, McGill Univeristy, Montreal, QC.

Donallson, E.M., 1981. Methods for the Analysis of Ores, Rocks and Related Minerals, 2nd ed. CANMET: Mines Branch, Department of Energy, Mines and Resources.

Essilfie-Dughan, J., Pickering, I.J., Hendry, M.J., George, G.N., Kotzer, T., 2011. Molybdenum speciation in uranium mine tailings using X-ray absorption spectroscopy. Environ. Sci. Technol. 45, 455–60. doi:10.1021/es102954b

Gomez, M.A., Hendry, M.J., Elouatik, S., Essilfie-Dughan, J., Paikaray, S., 2014. Fe(II) (aq) uptake of Mg(II)–Al(III)/Fe(III)–SO4/CO3 HTLCs under alkaline conditions: adsorption and solid state transformation mechanisms. RSC Adv. 4, 54973–54988. doi:10.1039/C4RA08802F

Gomez, M.A., Hendry, M.J., Koshinsky, J., Essilfie-Dughan, J., Paikaray, S., Chen, J., 2013. Mineralogical controls on aluminum and magnesium in uranium mill tailings: Key Lake, Saskatchewan, Canada. Environ. Sci. Technol. 47, 7883–91. doi:10.1021/es400658f

Jia, Y., Xu, L., Fang, Z., Demopoulos, G.P., 2006. Observation of surface precipitation of arsenate on ferrihydrite. Environ. Sci. Technol. 40, 3248–53.

Langmuir, D., Mahoney, J., MacDonald, A., Rowson, J., 1999. Predicting arsenic concentrations in the porewaters of buried uranium mill tailings. Geochim. Cosmochim. Acta 63, 3379–3394. doi:10.1016/S0016-7037(99)00259-8

Lieu, A., Bissonnette, J., Hossain, A.M., Essilfie-Dughan, J., Moldovan, B.J., Hendry, M.J., 2015. Simulating the mineral process at the Key Lake uranium mill, northern Saskatchewan, Canada in a lab-scale plant. Submitted to Hydrometallurgy.

Longerich, H., Jenner, G., Fryer, B., Jackson, S., 1990. Inductively coupled plasma-mass spectrometric analysis of geological samples: A critical evaluation based on case studies. Chem. Geol. 83, 105–118. doi:10.1016/0009-2541(90)90143-U

Mahoney, J., Slaughter, M., Langmuir, D., Rowson, J., 2007. Control of As and Ni releases from a uranium mill tailings neutralization circuit: Solution chemistry, mineralogy and geochemical modeling of laboratory study results. Appl. Geochemistry 22, 2758–2776. doi:10.1016/j.apgeochem.2007.06.021

Martin, M., Yu, G., Barberis, E., Violante, A., Kozak, L.M., Huang, P.M., 2009. Impact of structural perturbation of aluminum hydroxides by tannate on arsenate adsorption. Soil Sci. Soc. Am. J. 73, 1664–1675.

Moldovan, B.I., Hendry, M.J., 2005. Characterizing and quantilying controls on arsenic solubility over a pH range of 1-11 in a uranium mill-scale experiment. Environ. Sci. Technol. 39, 4913–20.

Moldovan, B.J., Jiang, D.T., Hendry, M.J., 2003. Mineralogical characterization of arsenic in uranium mine tailings precipitated from iron-rich hydrometallurgical solutions. Environ. Sci. Technol. 37, 873–9.

Paikaray, S., Gomez, M. a., Hendry, M.J., Essilfie-Dughan, J., 2014. Formation Mechanism of Layered Double Hydroxides in Mg2+-, Al3+-, and Fe3+-rich Aqueous Media: Implications for Neutralization in Acid Leach Ore Milling. J. Mater. Chem. A 101, 579–590. doi:10.1016/j.clay.2014.09.022

Paikaray, S., Hendry, M.J., 2014. Formation and crystallization of Mg(2+)-Fe(3+)-SO4(2−)-CO3(2−)-type anionic clays. Appl. Clay Sci. 88-89, 111–122. doi:10.1016/j.clay.2013.11.034

Paktunc, D., Bruggeman, K., 2010. Solubility of nanocrystalline scorodite and amorphous ferric arsenate: Implications for stabilization of arsenic in mine wastes. Appl. Geochemistry 25, 674–683. doi:10.1016/j.apgeochem.2010.01.021

Robertson, J., Hendry, M.J., Essilfie-Dughan, J., Chen, J., 2015. Precipitation of aluminum and magnesium secondary minerals from uranium mill raffinate (pH 1.0-10.5) and their controls on aqueous contaminants. Appl. Geochem. *in press*. doi:10.1016/j.apgeochem.2015.09.002

Robertson, J., Shacklock, K., Frey, R., Gomez, M. a., Essilfie-Dughan, J., Hendry, M.J., 2014. Modeling the Key Lake uranium mill's bulk neutralization process using a pilot-scale model. Hydrometallurgy 149, 210–219. doi:10.1016/j.hydromet.2014.08.010

Stefanova, V., Kmetov, V., Canals, a., 2003. Application of internal standardization in ICP-QMS through discrete sample introduction methodologies. J. Anal. At. Spectrom. 18, 1171. doi:10.1039/b301809a

APPENDIX D

XAS Reference Compound Synthesis

Introduction

Reference compounds of arsenate, arsenite and molybdate adsorbed to ferrihydrite were required for XAS analysis at the Canadian Light Source in Saskatoon, Saskatchewan, Canada (Section 2.0). Samples of ferrihydrite were synthesized by the following methods, confirmed by XRD and BET, and then used in adsorption experiments for XAS reference compounds.

Materials and Methods

Ferrihydrite Synthesis

2-line ferrihydrite was prepared at the University of Saskatchewan according to the methods of Schwertmann & Cornell (1991) with slight modification as per Jia et al. (2007) & Das et al. (2014) where $FeCl_3$ was dissolved in Millipore water (instead of ferric nitrate) with 1 M NaOH utilized (instead of 1 M KOH) to bring the solution to a pH of 7-8. The pH meter was calibrated daily with 4.01, 7.00, and 10.00 buffers +/- 0.002 pH. The solution was stabilized for 1 hour to ensure final pH values did not drift. The solution was then decanted and rinsed in 50 mL centrifuge tubes, run at 1500 rpm for 5 min, until decanted solution measured a conductivity < 0.05 mS/cm indicating the majority of unreacted salts had been removed. Conductivity meter was calibrated daily with 1412 uS/cm quality control standard. XRD and BET analysis was used to confirm that 2-line ferrihydrite was synthesized.

Sorption Standard Preparation

As and Mo sorbed to 2-line ferrihydrite were prepared using 0.1 M NaCl as electrolyte, according to (Dixit and Hering, 2003; Raven et al., 1998). Three standards were prepared, at different pH values with reagents as indicated to achieve target molar ratios (Table D1). Only one standard of As (III) was prepared at pH 7, for use as oxidation state reference for XANES analysis. Final solids were freeze dried and stored at -17 ºC until further preparation for CLS standards.

Solutions were stirred and brought to final pH with NaOH and HCl, then left for 1 hour to ensure pH stabilization. Sample vials were then shaken for 24 hours to allow metalloids to adsorb to surface of ferrihydrite, then centrifuged at 4000 rpm for 30 minutes and decanted five times. First and final decanted wash were collected and submitted for ICP-MS analysis to determine concentration of un-reacted standard. Solids were freeze dried directly into centrifuge tubes.

BET

Specific surface area measurement of the freeze dried synthesized ferrihydrite (n = 2) was accomplished using 11-pt BET-nitrogen isotherms using a Quantachrome NOVA 2200e Surface Area and Pore Size Analyzer. The sample was degassed at 80°C for 24 h prior to analysis, with the multi-point BET surface area of the sample measured at atmospheric pressure. The adsorption isotherms achieved a p/p_o range of 0.05-0.35.

XRD

X-ray diffraction (XRD) analysis were conducted on freeze dried solid samples (n = 2) using a PANanalytical Empyrean X-ray diffractometer equipped with a Spellman generator and Co target (λ Co K_α = 1.7902 A), operating at 40 kV and 45 mA. The samples were mounted on glass substrates as methanol slurries, and scanned in continuous mode using a spinning reflection/transmission stage. Spectra were acquired from 8 to 80° 2θ with a step size of 0.0167° and a scan speed of 1.2°/min. Detection limits for phases defined by lab-based XRD are reported as 1-5 wt% (Bish and Chipera, 1995; Gomez et al., 2014).

ICP-MS

Bulk elemental analysis by inductively coupled plasma mass spectrometry (ICP-MS) was performed at the University of Saskatchewan using a Perkin-Elmer NexION 300D (RSD ±10%) on HNO_3 treated aqueous samples (n = 19) from centrifuge wash solutions.

Results and Discussion

The first round of ferrihydrite synthesis produced a sample that was a mixture of 2-line and 6-line ferrihydrite, shown in Figure D1. This was likely due to increased filtration time required for the large batch (80 g of $FeCl_3$) of sample in the first trial. The second batch used a smaller mass (40 g) of starting material and produced the desired compound.

XRD confirmed synthesis of the reference compounds. 2-line ferrihydrite is characterized by two broad peaks centred at 2θ values of ~34° and ~61° (Das and Hendry, 2011; Jia et al., 2006). Measurements of the ferrihydrite standard synthesized in this study measured 2θ values of ~40° and ~74° (Fig. D1) as was previously reported (Das et al., 2014a, 2014b). The broadness of peaks

from these standards are due to the amorphous nature of the iron oxide solids. Spectrums for 6-line ferrihydrite and the amorphous solids at pH 10 in the Key Lake solids are shown for comparison (Fig. D1).

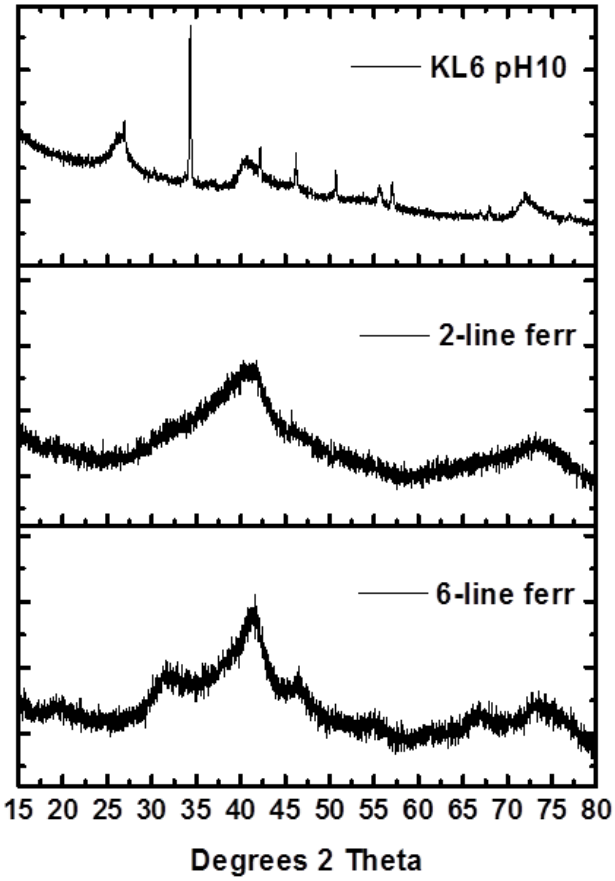

Figure D1. – XRD of synthesized ferrihydrite (2-line and 6-line) and Key Lake Lamella thickener solids (KL6 pH 9.8).

BET measured similar surface areas with 264.4 m^2/g for 6-line and 287.6 m^2/g for 2-line ferrihydrite (Table D1). The samples were freeze dried and then reacted with arsenate, arsenite and molybdate according to methods described. Concentrations of reagents in rinse water and total elemental concentration in adsorbed standards were determined by ICP-MS to calculate final molar ration of Fe:As and Fe:Mo in synthesized reference compounds from unreacted reagents (Table D1).

Table D1. Reagents and measured results of synthesized reference compounds.

Compounds	Reagent	Supplier	Measured Result
Sorption Standard			
6-line Ferrihydrite	$FeCl_3$	Sigma-Aldrich	264.4 m^2/g
2-line Ferrihydrite	$FeCl_3$	Sigma-Aldrich	287.6 m^2/g
Sorbed Standards pH 3			
As(V)_Ferrihydrite	$HAsNa_2O_4{:}7H_2O$	Sigma-Aldrich	41:1 M (Fe:As)
Mo(VI)_Ferrihydrite	Na_2MoO_4 :$2H_2O$	Sigma-Aldrich	33:1 M (Fe:Mo)
Sorbed Standards pH 10			
As(V)_Ferrihydrite	$HAsNa_2O_4{:}7H_2O$	Sigma-Aldrich	39:1 M (Fe:As)
Mo(VI)_Ferrihydrite	Na_2MoO_4 :$2H_2O$	Sigma-Aldrich	32:1 M (Fe:Mo)
Sorbed Standard pH 7			
As(III)_Ferrihydrite	$NaAsO_2$	J.T. Baker	38:1 M (Fe:As)

Source: Molar ratios are from concentration profiles by ICP-MS, surface areas were from BET analysis.

Conclusion

Synthesis of reference compounds were determined successful by characterization by ICP-MS, XRD and BET analysis. These reference compounds were further characterized by XAS and compared to literature values (Section 2.0).

References

Bish, D.L., Chipera, S.J., 1995. Accuracy in quantitative X-ray powder diffraction analysis, in: P. Predecki, et al. (Ed.), Advances in X-Ray Analysis. Vol 38. Plenum Pub Co., pp. 47–57.

Das, S., Essilfie-Dughan, J., Hendry, M.J., 2014. Arsenate partitioning from ferrihydrite to hematite : Spectroscopic evidence. Am. Mineral. 99, 749–754.

Das, S., Hendry, M.J., 2011. Application of Raman spectroscopy to identify iron minerals commonly found in mine wastes. Chem. Geol. 290, 101–108. doi:10.1016/j.chemgeo.2011.09.001

Dixit, S., Hering, J.G., 2003. Comparison of arsenic(V) and arsenic(III) sorption onto iron oxide minerals: implications for arsenic mobility. Environ. Sci. Technol. 37, 4182–9.

Gomez, M.A., Hendry, M.J., Elouatik, S., Essilfie-Dughan, J., Paikaray, S., 2014. Fe(II) (aq) uptake of Mg(II)–Al(III)/Fe(III)–SO4/CO3 HTLCs under alkaline conditions: adsorption and solid state transformation mechanisms. RSC Adv. 4, 54973–54988. doi:10.1039/C4RA08802F

Jia, Y., Xu, L., Fang, Z., Demopoulos, G.P., 2006. Observation of surface precipitation of arsenate on ferrihydrite. Environ. Sci. Technol. 40, 3248–53.

Jia, Y., Xu, L., Wang, X., Demopoulos, G.P., 2007. Infrared spectroscopic and X-ray diffraction characterization of the nature of adsorbed arsenate on ferrihydrite. Geochim. Cosmochim. Acta 71, 1643–1654.

Raven, K.P., Jain, A., Loeppert, R.H., 1998. Arsenite and Arsenate Adsorption on Ferrihydrite: Kinetics, Equilibrium, and Adsorption Envelopes. Environ. Sci. Technol. 32, 344–349. doi:10.1021/es970421p

Schwertmann, U., Cornell, R.M., 1991. Iron Oxides in the Laboratory. VCH Verlagsgesellschaft mbH & VCH Publishers, Inc, Weinheim.